NONLINEAR VISCOELASTIC MATERIAL MODELING USING NESTED LINKAGE MECHANISMS

by
Mustafa Umut Özcan
B.S., Mechanical Engineering, Marmara University, 2007
M.S., Mechanical Engineering, Koç University, 2009

Submitted to the Institute for Graduate Studies in
Science and Engineering in partial fulfillment of
the requirements for the degree of
Doctor of Philosophy

Graduate Program in Mechanical Engineering
Boğaziçi University
2022

This study is dedicated to three special persons, my mother Nursel Özcan, my father Prof.Cemil Özcan and, meaning of my life, Buse Aynuru. You have made me stronger and better than I could have ever imagined. I love you to the moon and back.

ACKNOWLEDGEMENTS

Firstly, I would like to express my sincere gratitude to my advisor Prof. Çetin Yılmaz and Co-advisor Prof. Fazıl Önder Sönmez for the continuous support of my Ph.D. study and related research, for their patience, motivation, and immense knowledge. Their guidance helped me in all the time of research and writing of this thesis.

I could not have imagined having a better advisors and mentors for my Ph.D. study.

My sincere thanks also go to Prof. Serdar Soyöz, Prof. Erdem Alaca, Assist. Prof. Polat Şendur and Prof. Günay Anlaş, for their insightful comments and encouragement, but also for the vital guidance which incent me to widen my research from various perspectives.

ABSTRACT

NONLINEAR VISCOELASTIC MATERIAL MODELING USING NESTED LINKAGE MECHANISMS

In this study, basic linear lumped elements such as springs and dashpots are used in nested linkage mechanisms in order to simulate and predict the mechanical behaviour of nonlinear viscoelastic materials. The proposed mechanism model containing two nested linkages can show initial softening followed by hardening response under quasi-static loading, which is commonly displayed by hyperelastic materials. Hence, material nonlinearity is simulated by geometric nonlinearity of the linkage mechanism. The mechanism also displays relaxation, hysteresis, and dynamic stiffness responses of viscoelastic materials with the help of dashpot elements. By tuning the geometric parameters of the mechanism, and the stiffness and damping parameters in the system, desired viscoelastic response can be obtained. Most of the previous experimental studies in the literature considered just two of different possible test scenarios. Comparisons with the experimental results in the literature show that the nested linkage mechanism with linear springs and dashpots can successfully simulate the material response in the tests for different double combinations of quasi-static loading, ramp-and-hold loading, hysteresis, and dynamic stiffness tests. When the experimental studies in the literature are investigated, it is seen that studies investigating three different test scenarios are rare. In this thesis, these four testing scenarios are considered in the same study for model validation for the first time. These four tests are conducted on three rubber samples with different stiffness and damping characteristics. It is shown that the nested linkage mechanism model can accurately mimic the material behaviour in these four different tests with a single set of values for the design parameters. In order to evaluate the prediction capability of the nested linkage mechanism model, optimization is conducted using only two test scenarios and the responses in the other two test scenarios are validated. To further assess the prediction capability of the model, parameter values are obtained for a sample and the responses of a sample from the same material with a different size is estimated for the four test scenarios. Finally, considering the hardening behaviour of the samples, the number of parameters in the model is reduced from 8 to 5 and it is shown that the reduced model also gives quite satisfactory results.

ÖZET

İÇİÇE KONUMLANDIRILMIŞ ÇUBUK MEKANİZMALARI İLE LİNEER OLMAYAN VİSKOELASTİK MALZEME MODELLEMESİ

Bu çalışmada, içiçe konumlandırılmış bağlantı mekanizmalarına eklenmiş doğrusal yay ve sönüm elemanları gibi basit parçalar kullanılarak, lineer olmayan viskoelastik malzemelerin mekanik davranışları taklit ve tahmin edilmiştir. Hiperelastik malzemelerde sıklıkla gözlemlenen yarı-statik yükleme altında ilk başta yumuşama ve arkasından gelen sertleşme eğilimi, önerilen mekanizma model ile taklit edilmiştir. Bu şekilde doğrusal olmayan malzeme davranışı, bağlantı mekanizması modelinin doğrusal olmayan geometrik özelliği ile taklit edilmiştir. Aynı zamanda, mekanizma modeli barındırdığı sönüm elemanları sayesinde viskoelastik malzemelerin gevşeme, histerezis ve dinamik sertlik tepkilerini de göstermektedir. Literatürde bulunan önceki çalışmalar çoğunlukla iki ayrı test senaryosuna odaklanmıştır. Literatürdeki deneysel çalışmalar ile, mekanizma modeli kıyaslandığında, yarı-statik yükleme, gevşeme, histerezis ve dinamik sertlik testlerinin farklı ikili kombinasyonları altında model tahmin sonuçları malzeme tepkisini başarılı bir şekilde tahmin edebilmiştir. Literatürdeki deneysel çalışmalar incelendiğinde, üç farklı test koşulunu aynı anda değerlendiren çalışma sayısının çok az olduğu gözlemlenmektedir. Model doğrulaması amacıyla bahsi geçen dört farklı test senaryosu ilk defa, bu tez ile aynı anda değerlendirilmiştir. Bu dört farklı test senaryosu, farklı sertlik ve sönüm özelliğine sahip üç farklı kauçuk numune üzerine uygulanmıştır. Mekanizma modelinin bu dört test senaryosu altında malzeme davranışını, tek bir parametre değer seti ile doğru bir şekilde taklit edebildiği gösterilmiştir. Mekanizma modelinin tahmin yetkinliğini test etmek için, bahsedilen dört test senaryosundan sadece iki tanesine eniyileme yapılmış ve belirlenen değişkenler ile geriye kalan diğer iki test senaryosu için malzeme tepkisi tahmin edilmiştir. Bunun ötesinde, modelin tahmin yetkinliğini değerlendirmek adına, değişken değerleri tek bir numune üzerinden eniyileme yöntemiyle belirlenmiş ve büyüklüğü farklı olan ama aynı malzemeden yapılmış farklı bir numunenin tepkilerini tahmin etmek için kullanılmıştır. Son olarak, model parametreleri malzemenin sertleşme eğilimi göz önüne alınarak 8'den 5'e düşürülmüş ve bu sadeleştirilmiş modelin dahi tüm senaryolarını tatminkar şekilde taklit ettiği gösterilmiştir.

TABLE OF CONTENTS

ACKNOWLEDGEMENTS iv
ABSTRACT v
ÖZET vi
LIST OF FIGURES ix
LIST OF TABLES xvi
LIST OF SYMBOLS xvii
LIST OF ACRONYMS / ABBREVIATIONS xix
1. INTRODUCTION 1
1.1. General Information 1
1.2. Literature Review 2
1.3. Aim of the Thesis 5
1.4. Contributions of This Ph.D. Thesis 7
1.5. Organization of Thesis 8
2. MODELING 10
2.1. Capabilities of Well-Known Spring-Dashpot Based Models 10
2.2. Mechanism Model 17
2.2.1. Analytical Model of the Nested Linkage Mechanism 17
2.2.2. Numerical Model of the Nested Linkage Mechanism 22
2.2.3. Comparison of Analytical and Numerical Models 23
2.3. Parametric Studies 36
3. COMPARISON OF TEST DATA AND MODEL RESPONSE 47
3.1. Double Combinations of Literature Test Data 47
3.2. Material Samples and Experiments 51
3.2.1. Material Samples 52
3.2.2. Experiments 53
3.3. Model Calibration Using Four Different Test Results 59
3.4. Comparison of Nested Linkage Mechanism Model with the Well-Known Spring-Dashpot Based Models 63

3.5. Material Response Prediction by Using the Model Calibrated with Two Test Results 66
3.6. Material Response Prediction for Different Size Samples 74
3.7. Calibration of a Reduced Model with Five Parameteres Using Four Different Test Results 77
4. CONCLUSIONS 82
REFERENCES 84
APPENDIX A: RUBBERS, POLYMERS AND ELASTOMERS 91
A.1. General Information 91
A.2. Copyright Details 97

LIST OF FIGURES

Figure 2.1. Common spring-dashpot based models. (a) Maxwell, (b) Kelvin-Voigt and (c) Standard Linear Solid. 10

Figure 2.2. Maxwell model with the spring coefficient of k = 10N/mm and dashpot coefficient of c = 10Ns/mm under (a) 10mm quasi-static loading, (b) 10mm ramp-and-hold loading with 0.25sec loading and 100sec holding, (c) 10mm hysteresis loading and (d) 1mm dynamical loading 0-100Hz. 13

Figure 2.3. Kelvin-Voigt model with the spring coefficient of k = 10N/mm and dashpot coefficient of c = 10Ns/mm under (a) 10mm quasi-static loading, (b) 10mm ramp-and-hold loading with 0.25sec loading and 100sec holding, (c) 10mm hysteresis loading and (d) 1mm dynamical loading 0-100Hz..... 15

Figure 2.4. Standard Linear Solid model with the both spring coefficients of k = 10N/mm and dashpot coefficient of c = 10Ns/mm under (a) 10mm quasi-static loading, (b) 10mm ramp-and-hold loading with 0.25sec loading and 100sec holding, (c) 10mm hysteresis loading and (d) 1mm dynamical loading 0-100Hz. . 16

Figure 2.5. The proposed mechanism model that mimics the mechanical behavior of nonlinear viscoelastic materials. 18

Figure 2.6. The proposed mechanism model created in ADAMS software that mimics the mechanical behavior of nonlinear viscoelastic materials..... 23

Figure 2.7. Inner mechanism's horizontal (a) displacement, (b) horizontal velocity, (c) vertical displacement and (d) vertical velocity responses under quasi-static loading. 25

Figure 2.8. Inner mechanism's horizontal (a) displacement, (b) horizontal velocity, (c) vertical displacement and (d) vertical velocity responses under ramp-and-hold loading. 26

Figure 2.9. Inner mechanism's horizontal (a) displacement, (b) horizontal velocity, (c) vertical displacement and (d) vertical velocity responses under hysteresis loading. 27

Figure 2.10. Inner mechanism's horizontal (a) displacement, (b) horizontal velocity, (c) vertical displacement and (d) vertical velocity responses under dynamic loading. 28

Figure 2.11. Responses of MATLAB and ADAMS model results under quasi-static loading. 29

Figure 2.12. Responses of MATLAB and ADAMS model results under slow ramp-and-hold loading. 30

Figure 2.13. Responses of MATLAB and ADAMS model results under fast ramp-and-hold loading. 31

Figure 2.14. Responses of MATLAB and ADAMS model results under slow hysteresis loading. 32

Figure 2.15. Responses of MATLAB and ADAMS model results under fast hysteresis loading. 33

Figure 2.16. Responses of MATLAB and ADAMS model results under slow dynamic loading. 34

Figure 2.17. Responses of MATLAB and ADAMS model results under fast dynamic loading. 35

Figure 2.18. (a) Vertical spring and outer four-bar linkage, (b) horizontal spring, inner and outer four-bar linkages, (c) Horizontal and vertical springs, inner and outer four-bar linkages. (d) Effect of vertical spring as softening response, (e) effect of horizontal spring as hardening response, (f) combined effect of horizontal and vertical springs as initial softening and later hardening response. Response is obtained for 10 mm compression with parameter values given in Table 2.3. 37

Figure 2.19. The effects of (a) k_{vs}, (b) k_{hs}, (c) α_0, and (d) L_i on the response of the mechanism under quasi-static loading. The blue dashed-dotted line represents the response of the reference configuration. 38

Figure 2.20. (a) Single SLS element in the mechanism, (b) double SLS elements in the mechanism. 39

Figure 2.21. The effect of different SLS configurations on relaxation response after 8 mm compression applied in 0.05sec. The parameter values are given in Table 2.4. 40

Figure 2.22. The effects of (a) k_{hs}, (b) k_{vs}, (c) k_h, (d) k_v, (e) c_h, (f) c_v, (g) L_i, and (h) α_0 on the relaxation response of the mechanism under ramp-and-hold loading. The blue dashed-dotted line represents the response of the reference configuration. 42

Figure 2.23. The effects of (a) k_{hs}, (b) k_{vs}, (c) k_h, (d) k_v, (e) c_h, (f) c_v, (g) L_i, and (h) α_0 on the hysteresis behavior of the mechanism. The blue dashed-dotted line represents the response of the reference configuration. 44

Figure 2.24. The effects of (a) k_{hs}, (b) k_{vs}, (c) k_h, (d) k_v, (e) c_h, (f) c_v, (g) L_i, and (h) α_0 on the dynamic stiffness response of the mechanism under dynamic loading. k_h is taken as 100 N/mm, k_v is taken as 3 N/mm and c_v is taken as 0.3 Ns/mm for better comparison. Other values are from Table 2.3. The blue dashed-dotted line represents the response of the reference configuration. 46

Figure 3.1. Comparison of the mechanism response and the material response reported by Bergstrom and Boyce (Bergstrom and Boyce, 2000) for (a) quasi-static loading and (b) hysteresis loading. 48

Figure 3.2. Comparison of the mechanism response and the material response reported by Ciambella et.al. (Ciambella et al., 2010) for (a) ramp-and-hold loading and (b) hysteresis loading. 49

Figure 3.3. Comparison of the mechanism response and the material response reported by Oman and Nagode (Oman and Nagode, 2014) for (a) quasi-static loading and (b) ramp-and-hold loading. 50

Figure 3.4. Comparison of the mechanism response and the material response reported by Tarrago and Leif (Garcia Tarrago et al., 2007) for (a) hysteresis loading and (b) dynamic loading. 51

Figure 3.5. Samples used in four different test scenarios: (a) Long sample (L_0 = 60mm, 36 Shore A hardness), (b) Medium sample (L_0 = 45mm, 38 Shore A hardness), (c) Short sample (L_0 = 30mm, 40 Shore A hardness). 52

Figure 3.6. X-ray image of the (a) long sample (L_0 = 60mm, 36 Shore A hardness), (b) medium sample (L_0 = 45mm, 38 Shore A hardness) and (c) short sample (L_0 = 30mm, 40 Shore A hardness). 53

Figure 3.7. Test setup components (a) Zwick / Roell Z010, (b) compression tools and sample and (c) computer. 55

Figure 3.8. Long sample (a) initial condition without any compression and (b) after 20mm compression during quasi-static loading test. 56

Figure 3.9. Dynamic stiffness test set-up with electromagnetic shaker, the proof mass and the accelerometers. 57

Figure 3.10. Real and imaginary parts of transmissibility for the (a) long sample real part, (b) medium sample real part, (c) short sample real part, (d) long sample imaginary part, (e) medium sample imaginary part, (f) short sample imaginary part. 58

Figure 3.11. Dynamic stiffness original test data with trend line used in optimization process for the (a) long sample, (b) medium sample and (c) short sample. 59

Figure 3.12. Long sample (L_0 = 60mm, 36 Shore A hardness) experimental and mechanism model response comparison. (a) quasi-static loading, (b) ramp-and-hold loading, (c) hysteresis and (d) dynamic stiffness. 60

Figure 3.13. Medium sample (L_0 = 45mm, 38 Shore A hardness) experimental and mechanism model response comparison. (a) quasi-static loading, (b) ramp-and-hold loading, (c) hysteresis and (d) dynamic stiffness. 61

Figure 3.14. Short sample (L_0 = 30mm, 40 Shore A hardness) experimental and mechanism model response comparison. (a) quasi-static loading, (b) ramp-and-hold loading, (c) hysteresis and (d) dynamic stiffness. 62

Figure 3.15. Medium sample experimental response comparison with the mechanism, Maxwell, Kelvin-Voigt and Standard Linear Solid model responses. (a) quasi-static loading, (b) ramp-and-hold loading, (c) hysteresis and (d) dynamic stiffness. 64

Figure 3.16. Long sample experimental and mechanism model response comparison. (a) quasi-static loading, (b) ramp-and-hold loading, (c) hysteresis and (d) dynamic stiffness. Model is tuned using ramp-and-hold and dynamic stiffness responses only. 68

Figure 3.17. Medium sample experimental and mechanism model response comparison. (a) quasi-static loading, (b) ramp-and-hold loading, (c) hysteresis and (d) dynamic stiffness. Model is tuned using ramp-and-hold and dynamic stiffness responses only. 69

Figure 3.18. Short sample experimental and mechanism model response comparison. (a) quasi-static loading, (b) ramp-and-hold loading, (c) hysteresis and (d) dynamic stiffness. Model is tuned using ramp-and-hold and dynamic stiffness responses only. 70

Figure 3.19. Long sample experimental and mechanism model response comparison. (a) quasi-static loading, (b) ramp-and-hold loading, (c) hysteresis and (d) dynamic stiffness. Model is tuned using hysteresis and dynamic stiffness responses only. 71

Figure 3.20. Medium sample experimental and mechanism model response comparison. (a) quasi-static loading, (b) ramp-and-hold loading, (c) hysteresis and (d) dynamic stiffness. Model is tuned using hysteresis and dynamic stiffness responses only. 72

Figure 3.21. Short sample experimental and mechanism model response comparison. (a) quasi-static loading, (b) ramp-and-hold loading, (c) hysteresis and (d) dynamic stiffness. Model is tuned using hysteresis and dynamic stiffness responses only. 73

Figure 3.22. Double medium sample experimental test setup. Samples are under 9mm compression state. 74

Figure 3.23. Double medium sample experimental response, its mechanism model fit and predicted model response comparison. (a) quasi-static loading, (b) ramp-and-hold loading, (c) hysteresis and (d) dynamic stiffness. 76

Figure 3.24. Nested linkage mechanism without vertical SLS element. 77

Figure 3.25. Long sample experimental and reduced mechanism model (w/o vertical SLS element) response comparison. (a) quasi-static loading, (b) ramp-and-hold loading, (c) hysteresis and (d) dynamic stiffness. 78

Figure 3.26. Medium sample experimental and reduced mechanism model (w/o vertical SLS element) response comparison. (a) quasi-static loading, (b) ramp-and-hold loading, (c) hysteresis and (d) dynamic stiffness. 79

Figure 3.27. Short sample experimental and reduced mechanism model (w/o vertical SLS element) response comparison. (a) quasi-static loading, (b) ramp-and-hold loading, (c) hysteresis and (d) dynamic stiffness. 80

Figure A.1. Chain molecules of Different Polymers. (a) plastomers, (b) elastomers, (c) thermoplastic elastomers, and (d) thermosets (duromers). 93

LIST OF TABLES

Table 2.1. Parameters used in Figure 2.2, Figure 2.3 and Figure 2.4. 12

Table 2.2. Displacements and displacement rates applied for quasi-static, ramp-and-hold and hysteresis tests for Maxwell, Kelvin-Voigt and Standard Linear Solid models. 12

Table 2.3. The reference configuration for the proposed model. 36

Table 2.4. Parameters used in Figure 2.21. 40

Table 3.1. Displacements and displacement rates applied for quasi-static, ramp-and-hold and hysteresis tests. 54

Table 3.2. Optimally tuned parameter values for the long, medium and short samples. 63

Table 3.3. Optimally tuned parameter values of the Maxwell, Kelvin-Voigt and Standard Linear Solid models considering the medium sample test results in Figure 3.13. 63

Table 3.4. Optimally tuned parameter values obtained by only using ramp-and-hold & dynamic stiffness or hysteresis & dynamic stiffness test results of the long, medium and short samples. 67

Table 3.5. Optimally tuned parameter values of the reduced model (w/o vertical SLS element) for the long, medium and short samples. 81

LIST OF SYMBOLS

c_h	Horizontal SLS element serial dashpot
c_v	Vertical SLS element serial dashpot
f	Frequency
F_d	Resistive force of the dashpot
F_s	Resistive force of the spring
F_t	Total force on the left side of the mechanism
$Im(T)$	Imaginary part of the transmissibility
k_{dyn}	Dynamic stiffness
k_h	Horizontal SLS element serial spring
k_{hs}	Horizontal SLS element parallel spring
k_v	Vertical SLS element serial spring
k_{vs}	Vertical SLS element parallel spring
ℓ	Horizontal length of the system
ℓ_i	Initial values of the horizontal length of the system
L_i	Length of the inner links
L_o	Length of the outer links
m_p	Proof mass
R_{1i}	Data points on the first response curve obtained from two different test scenarios
R_{2i}	Data points on the second response curve obtained from two different test scenarios
R_{3i}	Data points on the third response curve obtained from two different test scenarios
R_{4i}	Data points on the fourth response curve obtained from two different test scenarios
$Re(T)$	Real part of the transmissibility
T_{1i}	Data points of the first target curve
T_{2i}	Data points of the second target curve
T_{3i}	Data points of the third target curve

T_{4i}	Data points of the fourth target curve
u	Horizontal displacement of the left side of the nested mechanism
u_1	Horizontal displacements of the inner link left joint
u_2	Horizontal displacements of the inner link right joint
u_d	Extensions of the dashpot
u_p	Horizontal displacements of horizontal SLS element serial spring and dashpot mid-point
u_s	Extensions of the spring
u_t	Total extension in the horizontal Maxwell arm
v_1	Vertical displacements of the inner link upper joint
v_2	Vertical displacements of the inner link lower joint
v_p	Vertical displacements of vertical SLS element serial spring and dashpot mid-point
x_1	Positions of the inner link left joint
x_2	Positions of the inner link right joint
y_1	Position of the inner link upper joint
y_2	Position of the inner link lower joint
α	Angle of the outer links
β	Angle of the inner links

LIST OF ACRONYMS / ABBREVIATIONS

2D	Two dimensional
DOE	Design of Experiment
LDS	Ling Dynamic Systems
SLS	Standard Linear Solid

1. INTRODUCTION

1.1. General Information

The theory and experimental studies regarding viscoelastic materials are first investigated in the 19th century. Famous physicists Maxwell, Boltzmann, and Kelvin studied on suspensions in electric measuring devices for recovery and creep response. These suspensions were silk, metals, glass, and natural rubber. Later in 20th century, synthetic polymers and elastomers are vastly used in engineering. As a result of this, viscoelasticity became one of the most interested subjects. Viscoelasticity and the viscoelastic characteristics of materials are designed and used for specific purposes, so controlling it and designing it became an important engineering need for building better products. For more information on rubbers, polymers and elastomers please see Appendix A.

Quantification of viscoelasticity is a major issue. For example, elastic modulus is a quantifier of the elastic response of an elastic solid, but it is not straightforward to quantify the response of a nonlinear viscoelastic solid. For this purpose, different test scenarios and their results are investigated and used for quantifying the properties accordingly. Creep is considered one of the main measurement and quantifying method for viscoelastic materials. During creep, constant stress is applied and the time dependent changes in strain are evaluated. An alternative step function loading scenario is stress relaxation. In stress relaxation loading, constant strain is applied whereas the time dependent changes in stress is observed. Since the mechanical damping is one of the most important characteristics of viscoelasticity, harmonic loading tests are important for quantifying it. Since the force response of the viscoelastic damping increases as the velocity of the applied strain increases, dynamic loading is applied as a cyclic loading and unloading loops following each other in different frequencies. (McCrum et al., 1988)

The strain-stress curves of these testing scenarios depend on the test type. Compression, tension, shear, and flexural tests give different responses of the same material. The flaws in the material and microscopic cracks act largely in tension. In compression, the cracks tend to close rather than opening. As a result of this, quantifying pure polymer

characteristics is better with compression experiment. Tension experiments are better for quantifying flaws in the material characteristics. During the flexural tests, combination of tension and compression occurs, since one part of the sample is under tension whereas other parts in under compression. (Lawrence, 1974)

1.2. Literature Review

Nonlinear viscoelastic materials are widely used in various industrial areas from automotive to medical applications. Passive vibration isolators and absorbers, and most of the damping components are made of elastomers, rubbers, or other nonlinear viscoelastic materials. In surgical training organs, and in some other medical applications, nonlinear viscoelastic materials are used. As these materials possess both viscoelastic and hyperelastic features, their response under different loading conditions is complex. In order to fully describe the structural response of a material, different loading scenarios need to be considered. These tests may vary from quasi-static to dynamic loading scenarios. Nonlinear viscoelastic materials display nonlinear response when subject to large displacement quasi-static loading. Initially they soften and after some point, they start to harden as strain increases. Also due to the presence of damping, they exhibit hysteresis response, which is the difference in the loading and unloading paths as the material is compressed or extended in cyclic loading. Stress relaxation is also seen in these materials after a relatively fast loading followed by a long steady state period. Force response peaks in the fast-loading phase and it gradually relaxes to a specific value after holding in the same strain. Under dynamic loading, nonlinear viscoelastic materials exhibit increasing stiffness values as the frequency increases. These four different testing scenarios are generally used to characterize nonlinear viscoelastic materials.

Hyperelastic materials are widely investigated under quasi-static and hysteresis loading scenarios, since the nonlinear response of the material characteristics can be clearly seen in these two loading scenarios. Hyperelastic materials exhibit different stiffness responses during loading and unloading. Because the stress-strain curves during loading and unloading are different, thus, the area under the curve is different. The material absorbs energy in each load cycle, which is called “hysteresis”. Damping of vibrations in viscoelastic material systems occurs due to hysteresis. Many researchers (Abe et al., 2004; Agoras et al.,

2009; Bergstrom and Boyce, 1998; Buhan et al., 2015; Khajehsaeid et al., 2013; Mansouri and Darijani, 2014; Rey et al., 2014; Vieira et al., 2014) studied hyperelastic structural response as well as hysteresis behaviour of nonlinear viscoelastic materials under quasi-static loading. Constitutive equations and analytical formulations were developed to describe nonlinear hyperelastic response. In these studies, material nonlinearities were accounted for by defining nonlinear material properties in constitutive models or using nonlinear elements in rheological models like nonlinear springs and dashpots.

Stress relaxation response of viscoelastic materials under ramp-and-hold loading was also extensively studied in the literature (Bergstrom and Boyce, 2000; Bhuiyan et al., 2009; Drozdov, 1997; Feng and Gan, 2002; Muliana et al., 2016; Pellicer and Morales, 2004; Saitoh, 2012; Tam et al., 2015; Wang and Han, 2013). In this loading scenario, following a quickly applied compressive strain, the specimen is kept at constant strain. The magnitude of the stress drops with a decreasing rate and reaches a steady value in the long run. Relaxation behaviour varies with material type, sample geometry, loading rate, applied strain, temperature, humidity, and composition (Wang and Han, 2013). The analytical rheological models and the numerical models based on linear springs and dashpots can mimic relaxation response as well as dynamic stiffness response, but not nonlinear hyperelastic response. Only by using nonlinear springs and dashpots, a few models (Bergstrom and Boyce, 2000; Bhuiyan et al. 2009; Drozdov, 1997; Tam, 2015) account for nonlinear viscoelastic material response in both quasi-static and ramp-and-hold test scenarios.

Nonlinear viscoelastic materials under dynamic loading exhibit increasing stiffness response with an increase in frequency due to material damping. Dynamic stiffness response of nonlinear viscoelastic materials was investigated usually via constitutive models or rheological models using linear elements. (Carleo et al., 2017; Iniguez-Macedo et al., 2019; Renaud et al., 2011; Wollscheid and Lion, 2013; Zoffoli et al., 2017) In some studies (Bhuiyan et al., 2009; Lewandowski and Chorazyczewski, 2010; Osterlof et al., 2014; Xu et al., 2018) complex elements such as frequency dependent springs and dashpots are used to capture the dynamic response more closely.

For double test scenarios quasi-static and creep recovery are investigated by (Muliana et al., 2016). Some researchers focused on stress relaxation and hysteresis (Bergstrom and Boyce, 1998; Drozdov, 1997; Vandenbroucke et al., 2010). (Martinez et al., 2011) created a statistical approach on filled elastomer modelling with stress relaxation and hysteresis. (Rendek and Lion, 2010) investigated dynamic-stiffness and hysteresis scenarios. (Zhang et al., 2020) worked on stress relaxation and dynamic loading. For triple test scenarios quasi-static, stress relaxation and hysteresis are investigated at the same time by (Zrida et al., 2009; Liao et al., 2020). Quasi-static, stress relaxation and dynamic stiffness responses of nonlinear viscoelastic materials investigated at the same time by (Kamaruddin et al., 2017). However, to the authors' knowledge, not all four testing scenarios are considered at the same time in a single study.

Linkage mechanisms are used in the literature for investigating modal responses of structures rather than considering nonlinear viscoelastic materials (Acar and Yilmaz, 2013; Hegde and Ananthasuresh, 2012; Kim et al., 2014; Yilmaz et al., 2007; Yilmaz and Hulbert, 2010; Yuksel and Yilmaz, 2015). Single test scenarios for nonlinear viscoelastic materials are attempted to be modelled with lattice structures containing linear springs and dashpots. Nonlinearity is obtained with the geometric relation between the deformed and undeformed geometry of the lattice structure (Holecek and Moravec, 2006; Natsupakpong and Cavusoglu, 2010; Noborio and Oohara, 2009; San-Vicente et al., 2012).

In this study, a mechanism-based model is developed using a small number of parameters to represent the complex mechanical behaviour of nonlinear viscoelastic materials. In the proposed model, the mechanism contains only rigid links and linear lumped elements, i.e., springs and dashpots. Material nonlinearity is simulated by geometric nonlinearity of the linkage mechanism, while in the previous models this is mostly achieved by defining nonlinear material properties or using nonlinear spring or dashpot elements. In the literature, different models were proposed for different loading conditions to simulate the response of nonlinear viscoelastic materials. For instance, the commonly used Maxwell, Generalized Maxwell, Kelvin-Voigt, Standard Linear Solid (SLS) and Burgers models are capable of displaying relaxation response and/or dynamic stiffness response, but they cannot show nonlinear softening-hardening behaviour in quasi-static loading. In contrast, the mechanism-based model proposed in this study can mimic the nonlinear force-displacement,

stress relaxation, hysteresis, and dynamic stiffness characteristics of nonlinear viscoelastic materials with the same parameter values. As far as the authors know, there is no mechanical model in the literature that can mimic the response of nonlinear viscoelastic materials under these four loading scenarios.

In this thesis, literature test data of various elastomers are used to validate the simulation capability of the proposed model. Since double combinations of the aforementioned four test scenarios were present in different studies, the model parameters are tuned for two tests at a time. In order to fully evaluate the simulation capability of the proposed nested linkage mechanism model, the aforementioned four test scenarios are conducted on three different rubber samples. These three samples are selected with different damping and stiffness characteristics for extending the material variety. Moreover, the parameters of the nested linkage mechanism model are optimized using only two test scenarios and the responses in the other two test scenarios are predicted. To further evaluate the prediction capability of the model, parameters are obtained for a sample and the responses of a sample with double cross-sectional area is estimated for the four test scenarios. Finally, the number of parameters in the linkage mechanism model is reduced considering the hardening behaviour of the samples and the response of the reduced model is compared with the full model.

1.3. Aim of the Thesis

The aim of this study is to find a representation for the mechanical response of nonlinear viscoelastic materials under various loading scenarios via using mechanical structures and relations between multibody systems. Multibody dynamics-based approach provides an advantage for easy modification and tuning of the desired system responses by changing the basic system parameters for predicting and characterizing the complex nonlinear viscoelastic behaviours of real-life materials under various testing scenarios.

Proposed system can be considered as a combined mechanisms working for one purpose. Two nested linkage parallelogram mechanisms are attached to each other at the input and output joints. With this combination, the ability of different extension capabilities and their combined effects are obtained for the desired outcomes. Linear springs and

dashpots are used for tuning the response of the system. With this approach, nonlinearity is obtained and modulated as it is desired for modelling nonlinear viscoelastic material behaviour.

Modelling nonlinear viscoelastic materials is essential for many engineering applications. Nonlinear viscoelastic materials are used in many sectors such as automotive industry, aerospace industry, construction industry and medical applications. In many cases, rubber like materials are chosen from catalogues to satisfy some vibration isolation, damping or absorption demand.

Predicting nonlinear viscoelastic material response is important for vibration isolation, damping and absorption applications. These materials are needed to be tuned for the desired scenarios of the applications. Most common material models are based on springs and dashpots (lumped element models). These spring dashpot systems are vastly accepted by the researchers due to their easy applicability, optimization capability and direct analogy of the viscoelastic and nonlinear material characters. Most of these studies use nonlinear springs and dashpots since material nonlinearity prediction is not easy when linear elements are used.

Viscoelasticity of a system or material can be described as the delay in shape reformation to the original state after exposed to a forced deformation. Ramp and hold behaviour after deformation can be thought as a characteristic behaviour of the material. Viscoelasticity has advantageous uses in vibration isolation and damping. In case of resonance, damping provides a means to limit the maximum deformation in the system and hence prevent failure.

Hyperelasticity of a system or material can be described as the stress-strain relationship derives from a strain energy density function. When large strains are considered, hyperelastic materials show nonlinear strain-stress behaviour. When elastomeric samples are subject to large deformations, due to their hyperelasticity, they display nonlinear force-displacement response. In general, when a hyperelastic sample is subject to large deformation its stiffness increases, i.e., it shows hardening response. This property is used to prevent excessive movements in mechanical systems. For example, automotive manufacturers always desire

rock solid engine mounts if the power-train starts to move excessively. For this purpose, they use rubber materials especially in roll-restrictors. Also, when the rubber mount characteristics are not satisfactory to reach high stiffness at desired deformation level, they add secondary rubber contact surfaces to increase the effective stiffness of the mount.

It is shown that viscoelasticity and nonlinear force-displacement characteristics of elastomeric samples have important uses in engineering applications. If one can introduce an easily tuneable mechanical system that is used for both predicting and characterizing viscoelastic and nonlinear material responses, then it can have major implications for many engineering applications.

The main aim in this thesis to come up with a mechanical model that can display nonlinear viscoelastic material response. The model should be able to mimic the response of elastomeric samples under various test scenarios such as large strain quasi-static testing, ramp-and-hold testing, dynamic stiffness testing and hysteresis response in cyclic loading. The proposed model will not be just a mathematical model, but it will be a physical model, which can easily be manufactured. Moreover, it will provide tuning capability of the nonlinear force-displacement characteristics, such as softening and/or hardening response, and it will also provide tuning for the viscoelastic characteristics. Proposed method will differ from the studies in the literature for the nonlinear characteristics. Most of the studies provide non-linear behaviour via using serial and/or parallel combinations of nonlinear springs and dashpots. Our proposed model will obtain nonlinear response by exploiting the geometrical nonlinearity of linkage mechanisms. Hence, by using linear springs and dashpots, the mechanism model will show both hardening and softening behaviour in large strain quasi-static testing, and also mimic viscoelastic material response in ramp-and-hold, dynamic stiffness and hysteresis loading scenarios.

1.4. Contributions of This Ph.D. Thesis

Nonlinear viscoelastic materials are vastly investigated in the literature. For this purpose, generally two but rarely three different test scenarios are used for modelling and predicting material response. Also, the models in literature are either composed of analytical formulations, which cannot be built in real life by using mechanical elements or they are composed of mechanical systems that contain nonlinear springs and dashpots which are

complicated and not easy to physically realize. The proposed model is composed of two nested linkage mechanisms combined with simple linear springs and dashpots. This model can be built in real life and tuned to simulate various nonlinear viscoelastic components such as engine mounts or tuned mass dampers. The proposed model provides accurate response of nonlinear viscoelastic materials under four different test scenarios, namely, quasi-static, ramp-and-hold, hysteresis and dynamic loading scenarios. These four test scenarios are selected since they are commonly used in evaluating both nonlinear and viscoelastic material responses. However, in the literature, these four tests are not considered at the same time for model validation. Hence, this thesis is the first study that considers these four important test scenarios at the same time for model validation. Among these four test scenarios, double combinations of literature test data are predicted. Moreover, experiments are conducted for verifying the model under four test scenarios at the same time. In order to evaluate the prediction capability of the proposed model, only two test scenarios are used for tuning the model parameters and then, the responses in other two test scenarios are predicted. It is shown that the proposed model with 8 parameters is very successful in predicting nonlinear viscoelastic material response. Furthermore, model parameters are reduced from 8 to 5 in order to compare the prediction capability of the reduced model with the original model. The model is also used for predicting different sample sizes. Model parameters are tuned according to one sample and the four test responses of a double cross sectional area sample is predicted successfully. Two journal papers are written within the framework of this thesis. One article is published in International Journal of Solids and Structures in 2020 and another one is submitted to European Journal of Mechanics / A Solids recently.

1.5. Organization of Thesis

The aim of this study is to design a mechanical model by using linear elements that can predict nonlinear viscoelastic material response under four different loading scenarios, i.e., quasi-static, ramp-and-hold, hysteresis, and dynamic loading. In Chapter 2, both well-known spring-dashpot models in the literature are considered and the proposed nested linkage mechanism model is introduced. Analytical derivations regarding the force-displacement characteristics are provided and the response of the analytical model of the system is compared with the numerical model generated using multi-body dynamics simulation software (MSC ADAMS). Parametric studies are conducted in order to see how

the individual parameters of the proposed mechanism model affect the response in four different testing scenarios and how they contribute to the simulation of nonlinear viscoelastic material behaviour. In Chapter 3, test data and model response comparisons are given. Double combinations of the literature test data are provided. Moreover, the experimental setup and the samples used in this thesis are explained. Model parameters are tuned by optimization so that accurate prediction of test results is achieved. In Chapter 4, conclusions and summary of the main contributions are given.

2. MODELING

2.1. Capabilities of Well-Known Spring-Dashpot Based Models

Material models composed of linear or non-linear springs and dashpots are used in literature for nonlinear viscoelastic material prediction. The most common models are Maxwell, Kelvin-Voigt and Standard Linear Solid. These models can predict non-linear viscoelastic material responses under some loading scenarios, but none of them is capable of predicting all four test scenarios (quasi-static, ramp-and-hold, hysteresis and dynamic) at the same time. Figure 2.1 shows the common spring-dashpot based models. (a) Maxwell, (b) Kelvin-Voigt and (c) Standard Linear Solid.

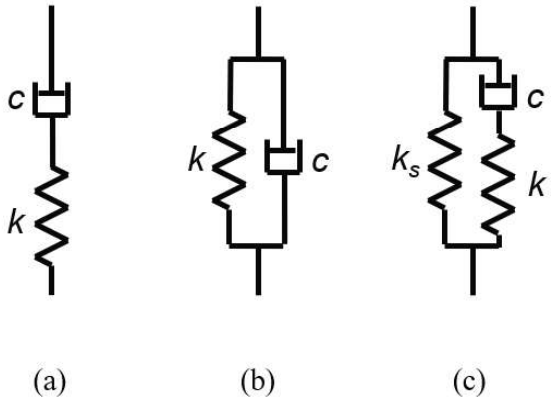


Figure 2.1. Common spring-dashpot based models. (a) Maxwell, (b) Kelvin-Voigt and (c) Standard Linear Solid.

Maxwell and Kelvin-Voigt models are considered as the simple viscoelastic models. Whereas Standard Linear Solid model is considered as a more realistic and complex model for material prediction. Similar to real viscoelastic materials, Standard Linear Solid model reacts rapidly and recovers completely after unloading. The constitutive equation for Maxwell model is given as

$$\sigma + \frac{c}{k}\dot{\sigma} = c\dot{\varepsilon} \tag{2.1}$$

where σ is stress at both ends and ε is the total strain of spring and dashpot element. The constitutive equation for Kelvin-Voigt model is given as

$$\sigma = k\varepsilon + c\dot{\varepsilon} \tag{2.2}$$

where σ is stress at both ends, $\varepsilon = \frac{1}{k}\sigma_1$, $\dot{\varepsilon} = \frac{1}{c}\sigma_2$, $\sigma = \sigma_1 + \sigma_2$, σ_1 is the stress on spring element and σ_2 is the stress on dashpot element. The constitutive equation for Standard Linear Solid model is given as

$$\sigma + \frac{c}{k}\dot{\sigma} = k_s\varepsilon + \frac{c(k_s + k)}{k}\dot{\varepsilon} \tag{2.3}$$

where ε is the total strain on both ends.

For understanding the capabilities of these models, all three of them are investigated under four different loading scenarios and their behaviours are evaluated considering nonlinear viscoelastic material response. Figure 2.2 shows Maxwell model composed of serially attached spring k and a dashpot element c with the coefficients summarized in Table 2.1 under (a) quasi-static loading, (b) ramp-and-hold loading (c) hysteresis loading and (d) dynamical loading. Displacements and displacement rates are given in Table 2.2. As seen in Figure 2.2a, there is no response under quasi-static loading. Therefore, the dashpot element absorbs all the displacement and generates no force due to quasi-static loading speed. On the other hand, nonlinear viscoelastic materials exhibit initial softening and later hardening response under quasi-static-loading scenario. Ramp-and-hold response of Maxwell model in Figure 2.2b has a relaxation response but the steady-state response value is zero. Therefore, the dashpot element absorbs all the displacement gradually as the loading stops after 0.25 second. Nonlinear viscoelastic materials exhibit a similar relaxation trend, but the steady state response should converge to a non-zero value according to the material properties. In Figure 2.2c and Figure 2.2d hysteresis and dynamical responses are similar to nonlinear viscoelastic material responses.

Table 2.1. Parameters used in Figure 2.2, Figure 2.3 and Figure 2.4.

	k_s (N/mm)	k (N/mm)	c (Ns/mm)
Maxwell	-	10	10
Kelvin-Voigt	-	10	10
Standard Linear Solid	10	10	10

Table 2.2. Displacements and displacement rates applied for quasi-static, ramp-and-hold and hysteresis tests for Maxwell, Kelvin-Voigt and Standard Linear Solid models.

		Maxwell	Kelvin-Voigt	Standard Linear Solid
Quasi-static	Disp	10mm	10mm	10mm
	Disp rate	$1x10^{-12}$mm/sec	$1x10^{-12}$mm/sec	$1x10^{-12}$mm/sec
Ramp-and-Hold	Disp	10mm	10mm	10mm
	Disp Rate	40mm/sec for 0.25sec	40mm/sec for 0.25sec	40mm/sec for 0.25sec
		0mm/min for 100sec	0mm/min for 100sec	0mm/min for 100sec
Hysteresis	Disp	10mm	10mm	10mm
	Disp rate	1mm/sec	1mm/sec	1mm/sec
Dynamic Stiffness	Disp	1mm	1mm	1mm
	Frequency	0-100Hz	0-100Hz	0-100Hz

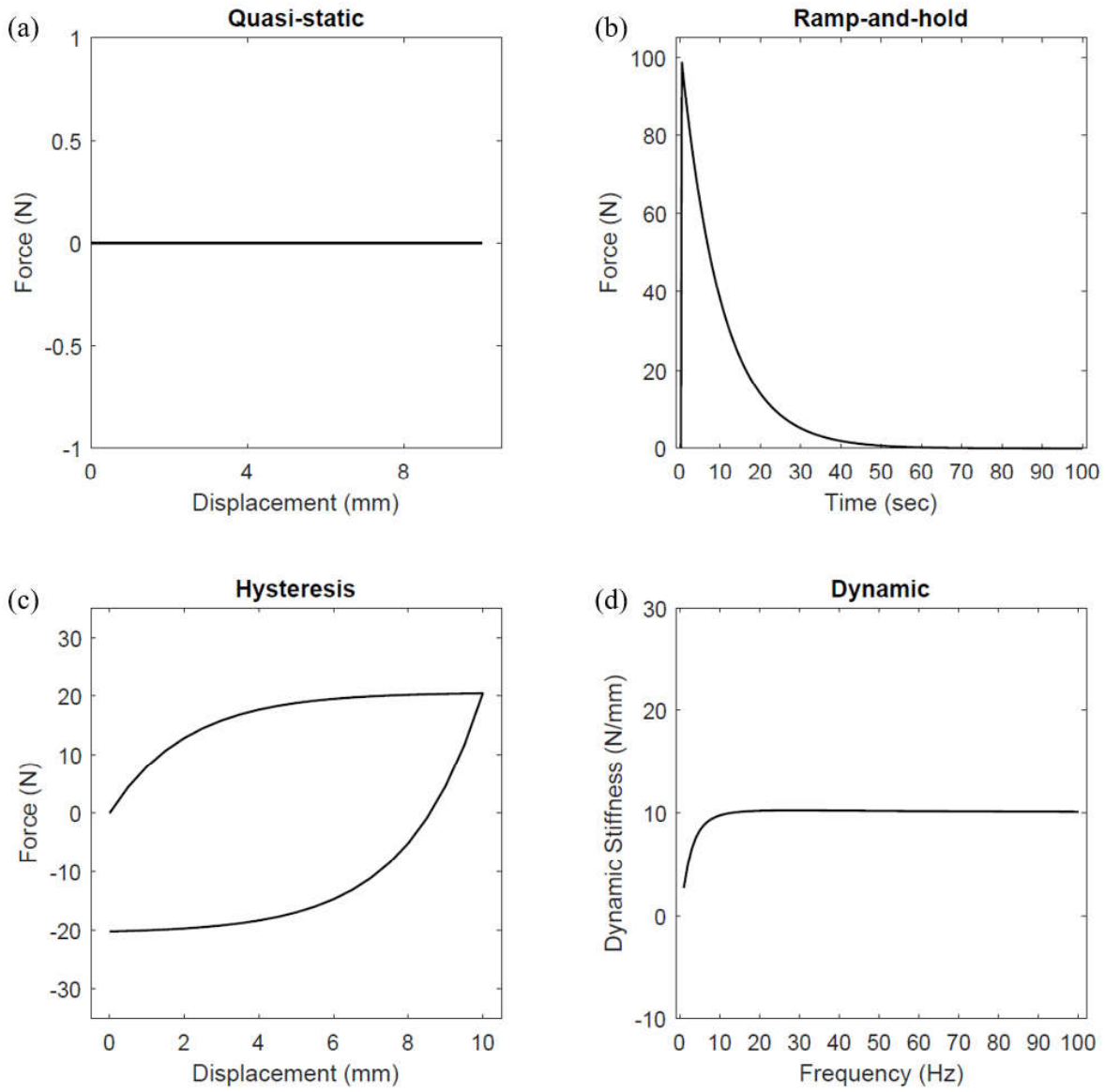


Figure 2.2. Maxwell model with the spring coefficient of k = 10N/mm and dashpot coefficient of c = 10Ns/mm under (a) 10mm quasi-static loading, (b) 10mm ramp-and-hold loading with 0.25sec loading and 100sec holding, (c) 10mm hysteresis loading and (d) 1mm dynamical loading 0-100Hz.

Figure 2.3 shows Kelvin-Voigt model composed of parallel attached spring k and a dashpot element c with the coefficients summarized in Table 2.1 for (a) quasi-static loading, (b) ramp-and-hold loading, (c) hysteresis loading and (d) dynamical loading. Displacements and displacement rates are given in Table 2.2. As seen in Figure 2.3a, quasi-static loading exhibits a linear response since only the linear spring element is confronting the loading due to quasi-static speed, whereas it is expected to be nonlinear with an initial softening and later

hardening as it is observed in nonlinear viscoelastic materials. Figure 2.3b shows the Kelvin-Voigt model response under ramp-and-hold loading. Since the spring and dashpot element are attached in parallel, the initial fast loading response is resulted with a high force response on the dashpot element, but after the loading stops, this force value decreases to zero. Only the spring element static force is remains in steady-state condition. So, there is no relaxation response observed in this scenario. In Figure 2.3c there is a difference in loading and unloading cycles, but the parallel attached dashpot element increases the force response rapidly as the loading starts and decreases as the loading changes direction at maximum deflection. This results an initial fast hardening and later linear response up to maximum deflection and unloading cycle has an offset but the trend is similar and parallel to the loading cycle. Whereas nonlinear viscoelastic materials exhibit curved loading and unloading cycles. The dynamic loading response in Figure 2.3d exhibit force response in increasing trend since the parallel attached dashpot element provides an increasing force response as the frequency (so the velocity) increases. This behavior is similar to the natural response of nonlinear viscoelastic materials under dynamic loading.

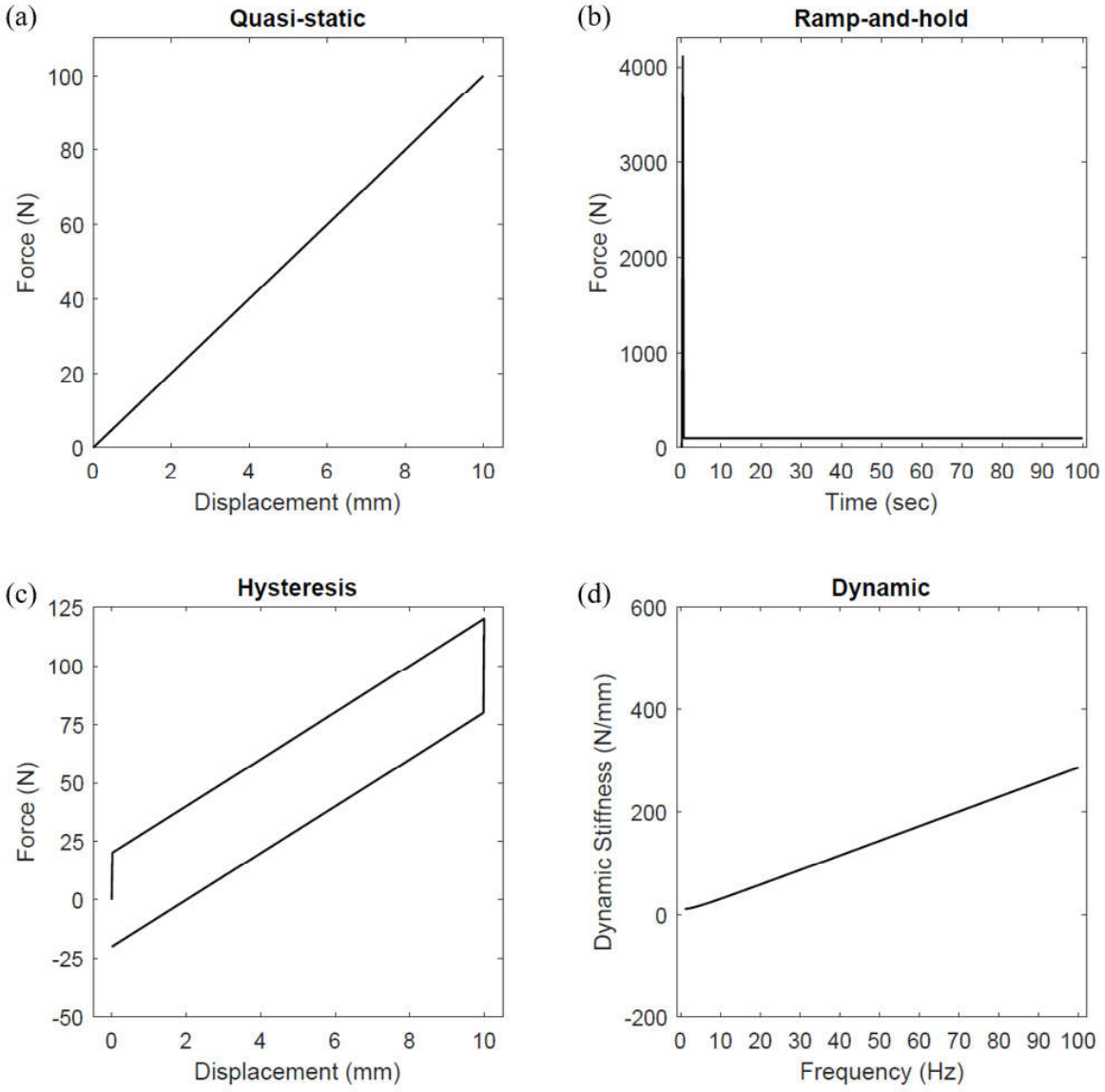


Figure 2.3. Kelvin-Voigt model with the spring coefficient of k = 10N/mm and dashpot coefficient of c = 10Ns/mm under (a) 10mm quasi-static loading, (b) 10mm ramp-and-hold loading with 0.25sec loading and 100sec holding, (c) 10mm hysteresis loading and (d) 1mm dynamical loading 0-100Hz.

Figure 2.4 shows Standard Linear Solid model composed of parallel attached spring k_s and a serially attached spring k and dashpot element c with the coefficients summarized in Table 2.1 (a) quasi-static loading, (b) ramp-and-hold loading, (c) hysteresis loading and (d) dynamical loading. Displacements and displacement rates are given in Table 2.2. As seen in Figure 2.4a, quasi-static loading exhibits a linear response since only the spring elements k_s is confronting the loading due to quasi-static speed, whereas it is expected to be nonlinear

with an initial softening and later hardening for a nonlinear viscoelastic material. In Figure 2.4b, Figure 2.4c and Figure 2.4d the response characteristics are similar to nonlinear viscoelastic material responses.

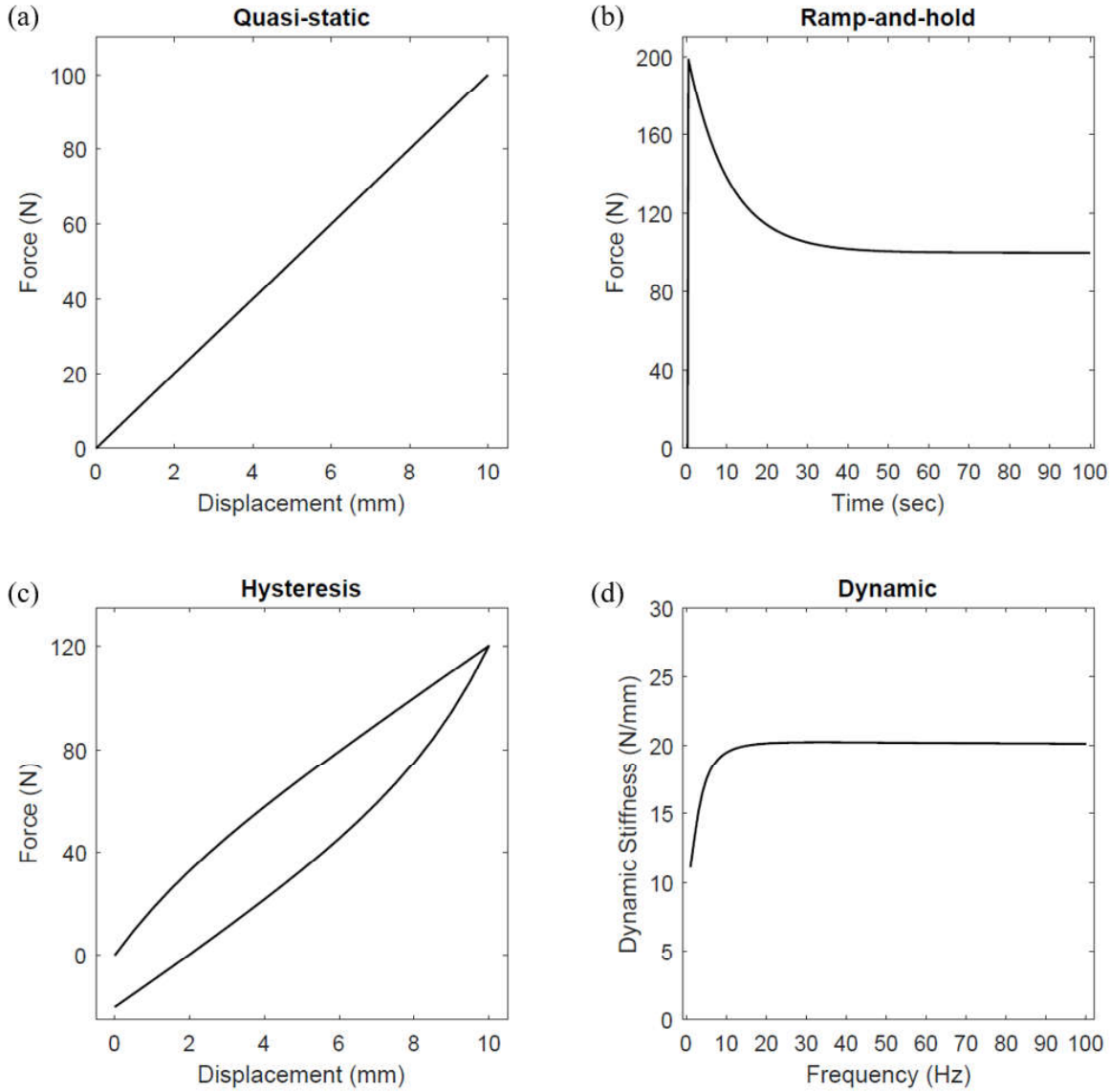


Figure 2.4. Standard Linear Solid model with the both spring coefficients of k = 10N/mm and dashpot coefficient of c = 10Ns/mm under (a) 10mm quasi-static loading, (b) 10mm ramp-and-hold loading with 0.25sec loading and 100sec holding, (c) 10mm hysteresis loading and (d) 1mm dynamical loading 0-100Hz.

These well-known material models are good for some loading scenarios, but they cannot accurately represent all four test scenarios mentioned above. Only Standard Linear

Solid model can predict 3 of 4 loading scenarios. Since the motivation of this thesis is to predict the material response under these four test scenarios at the same time, nested mechanism extenders are combined with two Standard Linear Solid models. With this approach, all responses of nonlinear viscoelastic materials are mimicked successfully. In next section, the details of the nested linkage mechanism model are described.

2.2. Mechanism Model

2.2.1. Analytical Model of the Nested Linkage Mechanism

The mechanism model that will be used to mimic the mechanical behaviour of nonlinear viscoelastic materials includes two nested parallelogram linkages as shown in Figure 2.5. The inner and outer loops are connected by two pin joints. The opposite joints of the inner loop are connected by springs having stiffness k_{hs} and k_{vs}. Additionally, parallel to these springs (k_{hs} and k_{vs}), serially connected springs and dashpots are used with stiffness and damping coefficients k_h, c_h and k_v, c_v respectively. k_{hs}, k_h and c_h form a Standard Linear Solid model arm in horizontal direction, whereas k_{vs}, k_v and c_v form another one in vertical direction. These two SLS model arms are displaced at different rates due to the nonlinear geometry of the mechanism. The movement of the right-most joint is restrained and load is applied to the left-most joint along the *x*-direction. The inner mechanism loop has shorter links ($L_i < L_o$). Consequently, $\beta(t)$ is always greater than $\alpha(t)$ for any value of the input displacement $u(t)$. Moreover, the mechanism has one degree of freedom. Given the displacement of the left joint ($u(t)$) and the initial configuration of the mechanism, its mechanical response can be completely determined.

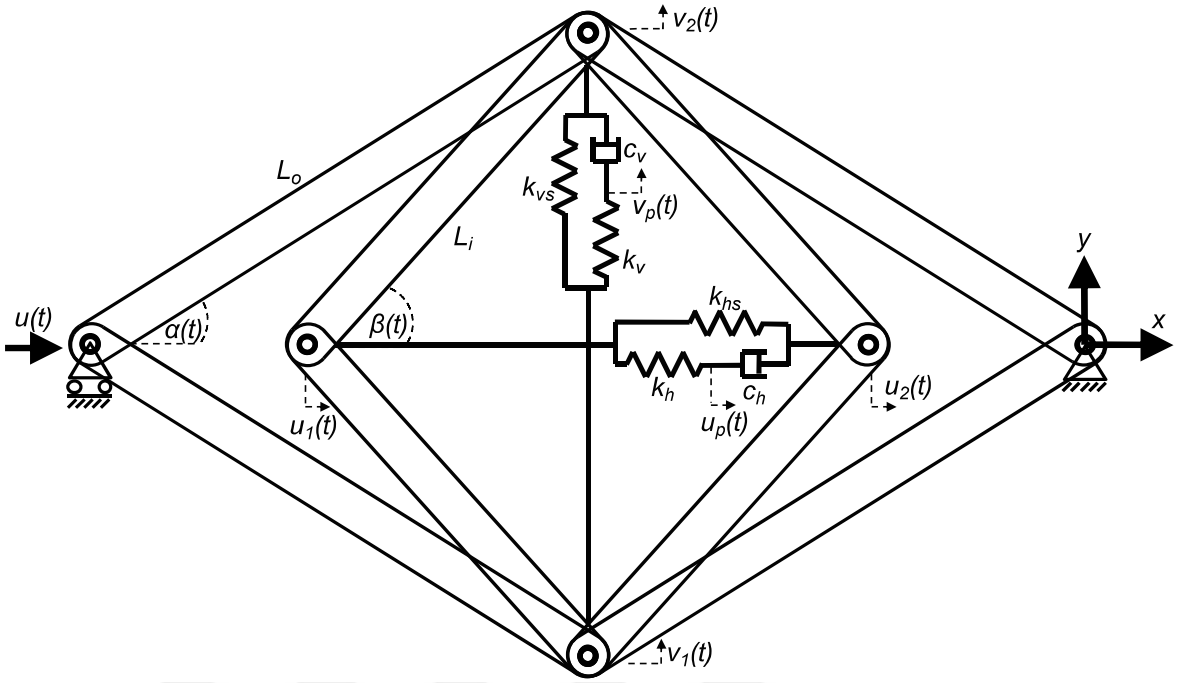


Figure 2.5. The proposed mechanism model that mimics the mechanical behavior of nonlinear viscoelastic materials.

Dynamic analysis of the proposed model is performed analytically. Horizontal displacement (u) of the left side of the nested mechanism is the only generalized coordinate of this single-degree-of-freedom mechanism. The vertical displacements v_1 and v_2, the horizontal displacements u_1 and u_2 and the angles α and β can be obtained in terms of u. Auxiliary points are added between k_h and c_h, and k_v and c_v with displacements u_p and v_p, respectively as shown in Figure 2.5. Hence, there are two more degrees of freedom of this system when the coupling points are considered.

First, the relations between the geometric parameters are derived. The current length of the mechanism is equal to the distance between the left most joint and the origin. The horizontal length of the system is ℓ and its initial value is ℓ_i. The angle of the outer links, α, is related to u and the length of the outer links, L_o, as

$$\ell = \ell_i - u = 2L_o \cos\alpha. \tag{2.4}$$

As the input displacement (u) increases, the length of the mechanism decreases with a rate given by

$$\frac{d\ell}{dt} = -\frac{du}{dt}. \tag{2.5}$$

Solving for α in Equation (2.4), one obtains

$$\alpha = cos^{-1}\left(\frac{\ell}{2L_o}\right). \tag{2.6}$$

β should be larger than α and it can be determined by

$$sin\beta = \frac{L_o}{L_i} sin\alpha. \tag{2.7}$$

Substituting α in Equation (2.6) into Equation (2.7) and using the relation

$$sin(cos^{-1}\varphi) = \sqrt{1-\varphi^2} \tag{2.8}$$

β can be expressed as

$$\beta = sin^{-1}\left(\frac{L_o}{L_i}\sqrt{1-\left(\frac{\ell}{2L_o}\right)^2}\right). \tag{2.9}$$

The positions of the inner link joints, x_1, x_2, their displacements u_1, u_2, and their first time derivatives are calculated as

$$x_1 = -L_o cos(\alpha) - L_i cos(\beta). \tag{2.10}$$

Substituting Equation (2.6) and Equation (2.9) into Equation (2.10) and making use of Equation (2.8), Equation (2.10) becomes

$$x_1 = -\frac{1}{2}\left(\ell + \sqrt{\ell^2 - 4{L_o}^2 + 4{L_i}^2}\right). \tag{2.11}$$

Then, u_1 and $\dot{u}_1$ can be calculated as

$$u_1 = x_1 - x_{1\mathrm{i}} = -\frac{1}{2}\left(\ell + \sqrt{\ell^2 - 4{L_o}^2 + 4{L_i}^2}\right) + \frac{1}{2}\left(\ell_0 + \sqrt{{\ell_0}^2 - 4{L_o}^2 + 4{L_i}^2}\right) \quad (2.12)$$

$$\dot{u}_1 = -\frac{\dot{\ell}}{2} - \frac{1}{2}\frac{\ell\,\dot{\ell}}{\sqrt{\ell^2 - 4{L_o}^2 + 4{L_i}^2}}. \quad (2.13)$$

Similarly, x_2, u_2 and $\dot{u}_2$ are derived as

$$x_2 = -L_o cos(\alpha) + L_i cos(\beta) \quad (2.14)$$

$$u_2 = x_2 - x_{2\mathrm{i}} = -\frac{1}{2}\left(\ell - \sqrt{\ell^2 - 4{L_o}^2 + 4{L_i}^2}\right) + \frac{1}{2}\left(\ell_0 - \sqrt{{\ell_0}^2 - 4{L_o}^2 + 4{L_i}^2}\right) \quad (2.15)$$

$$\dot{u}_2 = -\frac{\dot{\ell}}{2} + \frac{1}{2}\frac{\ell\,\dot{\ell}}{\sqrt{\ell^2 - 4{L_o}^2 + 4{L_i}^2}}. \quad (2.16)$$

The positions of the upper and lower joints, y_1 and y_2, are given as

$$y_2 = -y_1 = L_o sin(\alpha). \quad (2.17)$$

Substituting Equation (2.6) and making use of Equation (2.8), Equation (2.17) becomes

$$y_2 = -y_1 = \frac{1}{2}\sqrt{4{L_o}^2 - \ell^2}. \quad (2.18)$$

Moreover, v_1, v_2, $\dot{v}_1$ and $\dot{v}_2$ are derived as

$$v_2 = -v_1 = \frac{1}{2}\sqrt{4{L_o}^2 - \ell^2} - \frac{1}{2}\sqrt{4{L_o}^2 - {\ell_0}^2} \quad (2.19)$$

$$\dot{v}_2 = -\dot{v}_1 = -\frac{1}{2}\frac{\ell\,\dot{\ell}}{\sqrt{4{L_o}^2 - \ell^2}}. \tag{2.20}$$

The Maxwell arms of the inner mechanisms are composed of serially connected spring and dashpot elements (k_h and c_h; k_v and c_v). The total extension in the horizontal Maxwell arm, u_t, is given by the difference between the horizontal displacements u_1 and u_2, which is also equal to the sum of the extensions of the spring and dashpot (u_s and u_d) as

$$u_t = u_2 - u_1 = u_s + u_d. \tag{2.21}$$

A negative value of u_t indicates contraction of the Maxwell arm. Moreover, time derivative of u_t can be obtained as

$$\dot{u}_t = \dot{u}_2 - \dot{u}_1 = \dot{u}_s + \dot{u}_d. \tag{2.22}$$

The resistive forces of the spring and dashpot, F_s and F_d, due to their extension or contraction are equal to each other, since they are connected in series. For the horizontal Maxwell arm, the forces are as follows

$$F_s = F_d \quad or \quad k_h\, u_s = c_h\, \dot{u}_d. \tag{2.23}$$

Rearranging Equation (2.23) gives

$$\frac{k_h}{c_h} u_s = \dot{u}_d. \tag{2.24}$$

Substituting Equation (2.24) in Equation (2.22) gives

$$\dot{u}_t = \dot{u}_s + \frac{k_h}{c_h} u_s. \tag{2.25}$$

Equation (2.25) can be rewritten as

$$e^{\frac{k_h}{c_h}t}\frac{du_s}{dt}+\frac{k_h}{c_h}u_s e^{\frac{k_h}{c_h}t}=\dot{u}_t e^{\frac{k_h}{c_h}t}. \tag{2.26}$$

Then, it can be solved as

$$\int d\left(u_s e^{\frac{k_h}{c_h}t}\right)=\int \dot{u}_t e^{\frac{k_h}{c_h}t}dt. \tag{2.27}$$

Considering the initial condition as $u_s(0)=0$ and taking the integral using time increments of Δt, change in the length of the spring, u_s, and its rate, $\dot{u}_s$, at time $t=i\Delta t$ is obtained as

$$u_s(\mathrm{i}\Delta\mathrm{t})=\frac{\dot{u}_t(\mathrm{i}\Delta\mathrm{t})c_h}{k_h}-\frac{\dot{u}_t\big((\mathrm{i}-1)\Delta\mathrm{t}\big)c_h}{k_h}e^{-\frac{k_h}{c_h}\Delta t}+u_s\big((\mathrm{i}-1)\Delta\mathrm{t}\big)e^{-\frac{k_h}{c_h}\Delta t} \tag{2.28}$$

$$\dot{u}_s(\mathrm{i}\Delta\mathrm{t})=\dot{u}_t\big((\mathrm{i}-1)\Delta\mathrm{t}\big)e^{-\frac{k_h}{c_h}\Delta t}-\frac{k_h}{c_h}u_s\big((\mathrm{i}-1)\Delta\mathrm{t}\big)e^{-\frac{k_h}{c_h}\Delta t}. \tag{2.29}$$

Equation (2.28) and Equation (2.29) can be explicitly calculated (for *i*=1, 2, …, *n*) by using a predefined time step (Δt). Vertical displacement can be obtained using a similar procedure. Total force on the left side of the mechanism can easily be determined using the trigonometric relations as

$$F_t(t)=\big(k_{hs}u_t(t)+k_h u_s(t)\big)\tan\beta(t)\cot\alpha(t)+\big(k_{vs}v_t(t)+k_v v_s(t)\big)\cot\alpha(t). \tag{2.30}$$

2.2.2. Numerical Model of the Nested Linkage Mechanism

The model described in Section 2.1 is replicated in ADAMS software. This model is created using the same linkage lengths, spring and dashpot element coefficients and investigated under the same loading conditions. Figure 2.6 shows the ADAMS model. There are 8 links attached to each other for forming a two nested mechanism extender structure. Two Standard Linear Solid (SLS) elements are added horizontally and vertically. The

movement of the right-most joint (b) is restrained and load is applied to the left-most joint (a) along the x-direction. Since the model is created in 2D, all the links and joints are constrained to move in x and y directions and can rotate around z axis. The springs and dashpots in the horizontal SLS element can only move in the x direction whereas the vertical SLS element can move in x and y directions. As the input displacement $u(t)$ is given in the x direction, the springs and dashpots can only translate but not rotate. With this approach, SLS elements can only generate force response on their axial directions. Resulting force is calculated at point (a) where the input is applied.

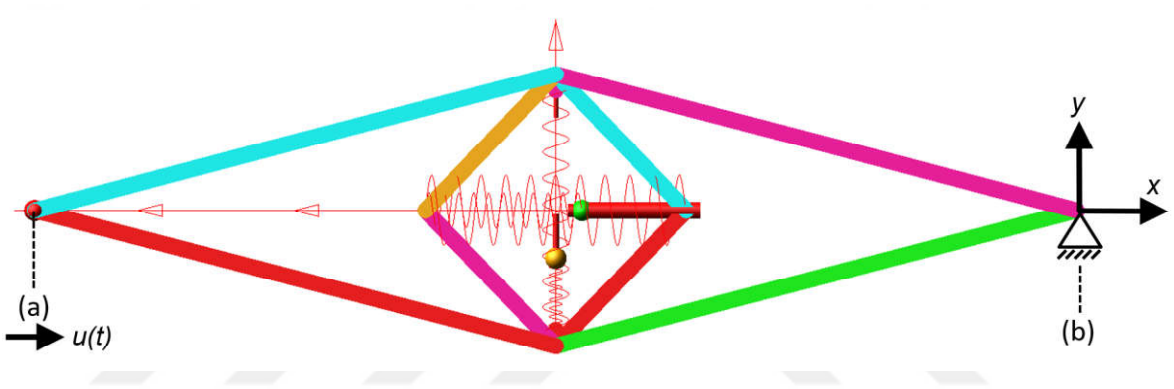


Figure 2.6. The proposed mechanism model created in ADAMS software that mimics the mechanical behavior of nonlinear viscoelastic materials.

2.2.3. Comparison of Analytical and Numerical Models

The calculations shown in the previous chapter were conducted in MATLAB. For verifying the calculations, mechanism model is duplicated in ADAMS software and same test scenarios are applied. According to the results, both MATLAB code and ADAMS model responded exactly the same. For verification, two different values are investigated. Firstly, the inner nested mechanism's horizontal and vertical end points where the horizontal and vertical SLS elements are attached are checked for the displacements u_1 and u_2 and velocities $\dot{u}_1$ and $\dot{u}_2$ under four different test scenarios which are quasi-static, ramp-and-hold, hysteresis and dynamic loading. Secondly, the overall response of the models F_t are compared. Horizontal and vertical displacement and velocity values are critical since the SLS elements are composed of a serially attached spring and dashpot with a parallel attached spring element. The serially attached elements are compressing according to the loading

scenarios' displacement and velocity. However, these displacements and velocities are not linearly related to the input. For instance, under dynamic loading scenario, there will be phase lag in serially attached spring and dashpot compression / extension behavior according to the spring and dashpot parameter values. Figure 2.7 shows the inner mechanism's (a) horizontal displacement, (b) horizontal velocity, (c) vertical displacement and (d) vertical velocity responses under quasi-static response. For the velocity plots in Figure 2.7b and Figure 2.7d, both the ADAMS measured velocity value and ADAMS calculated velocity values can be seen. ADAMS velocity values are calculated using time derivative of displacement.

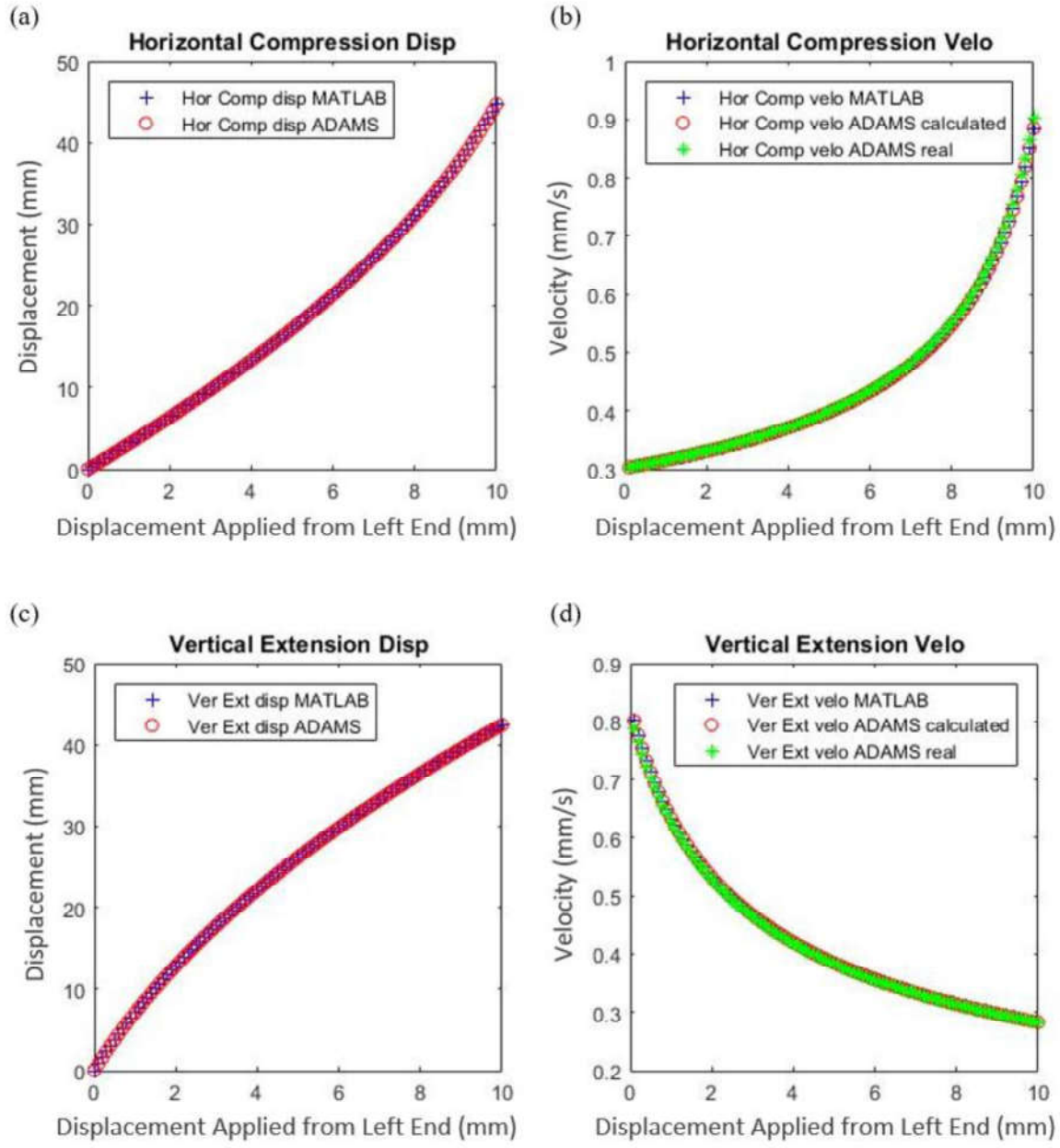


Figure 2.7. Inner mechanism's horizontal (a) displacement, (b) horizontal velocity, (c) vertical displacement and (d) vertical velocity responses under quasi-static loading.

Figure 2.8, Figure 2.9, and Figure 2.10 are also show the similar results for ramp-and-hold loading, hysteresis loading and dynamical loading, respectively. In Figure 2.9b and Figure 2.9d calculated and real velocity values are a little different. This is due to the calculation time step size difference between ADAMS and the numerical calculation formula.

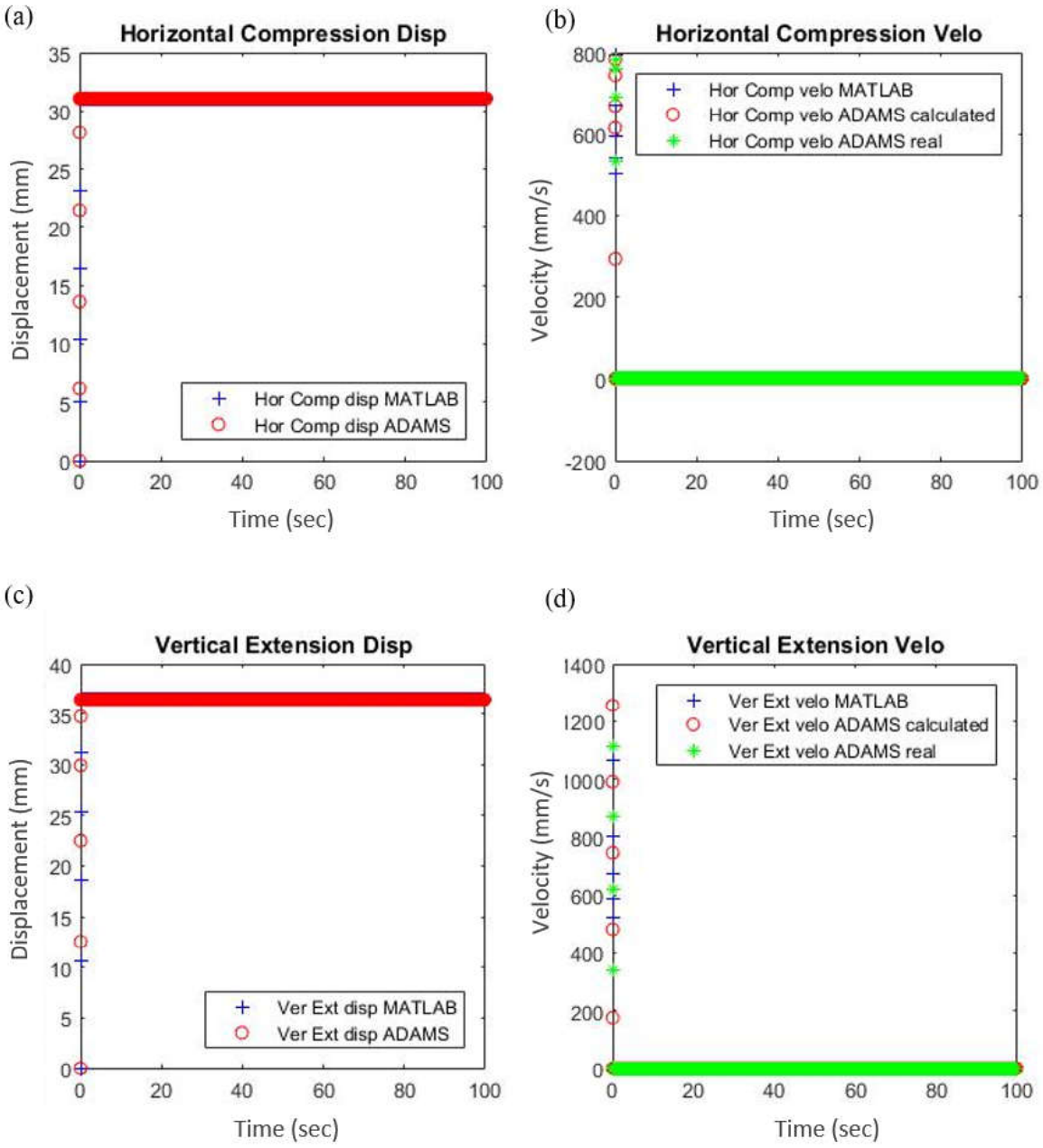


Figure 2.8. Inner mechanism's horizontal (a) displacement, (b) horizontal velocity, (c) vertical displacement and (d) vertical velocity responses under ramp-and-hold loading.

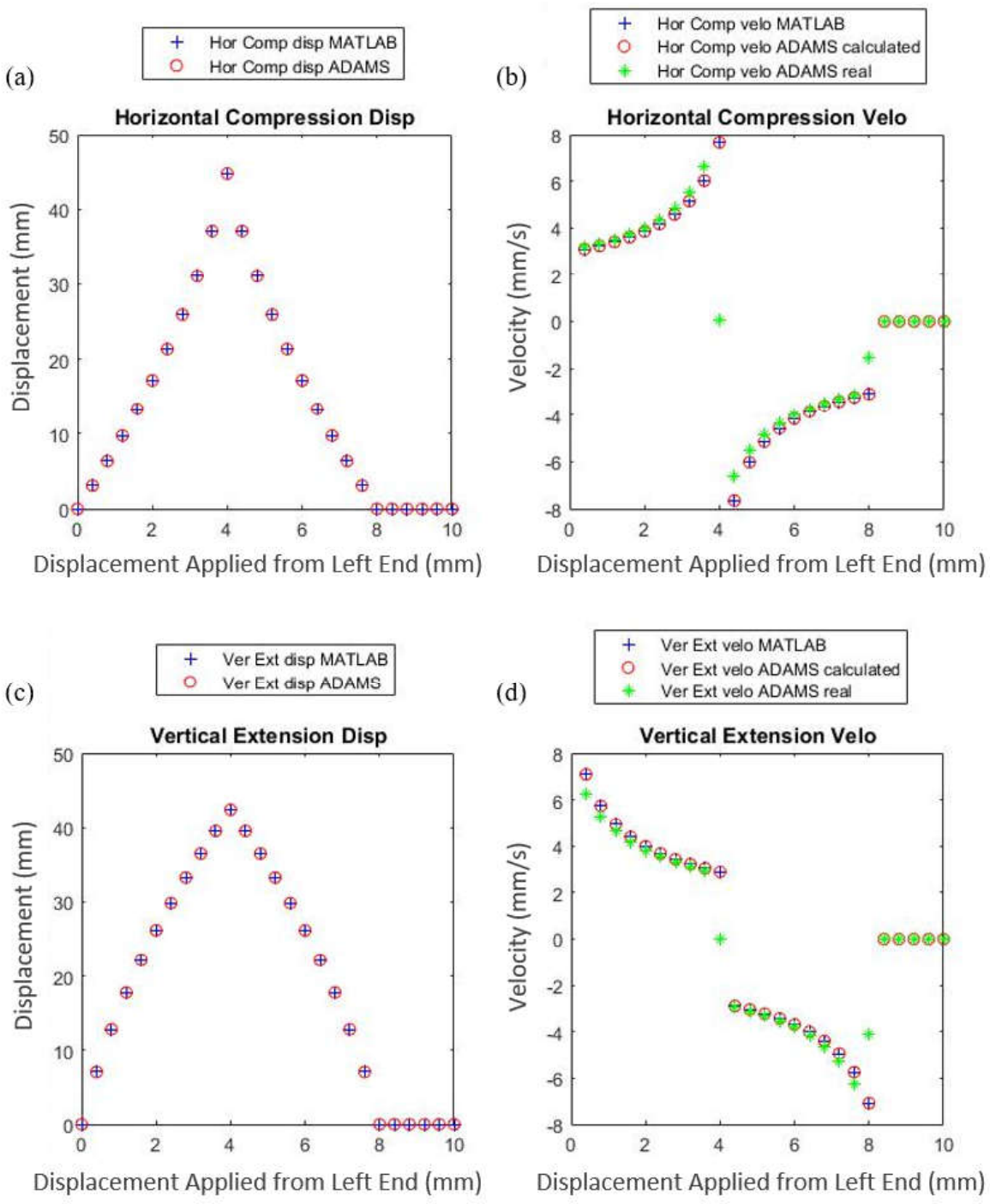


Figure 2.9. Inner mechanism's horizontal (a) displacement, (b) horizontal velocity, (c) vertical displacement and (d) vertical velocity responses under hysteresis loading.

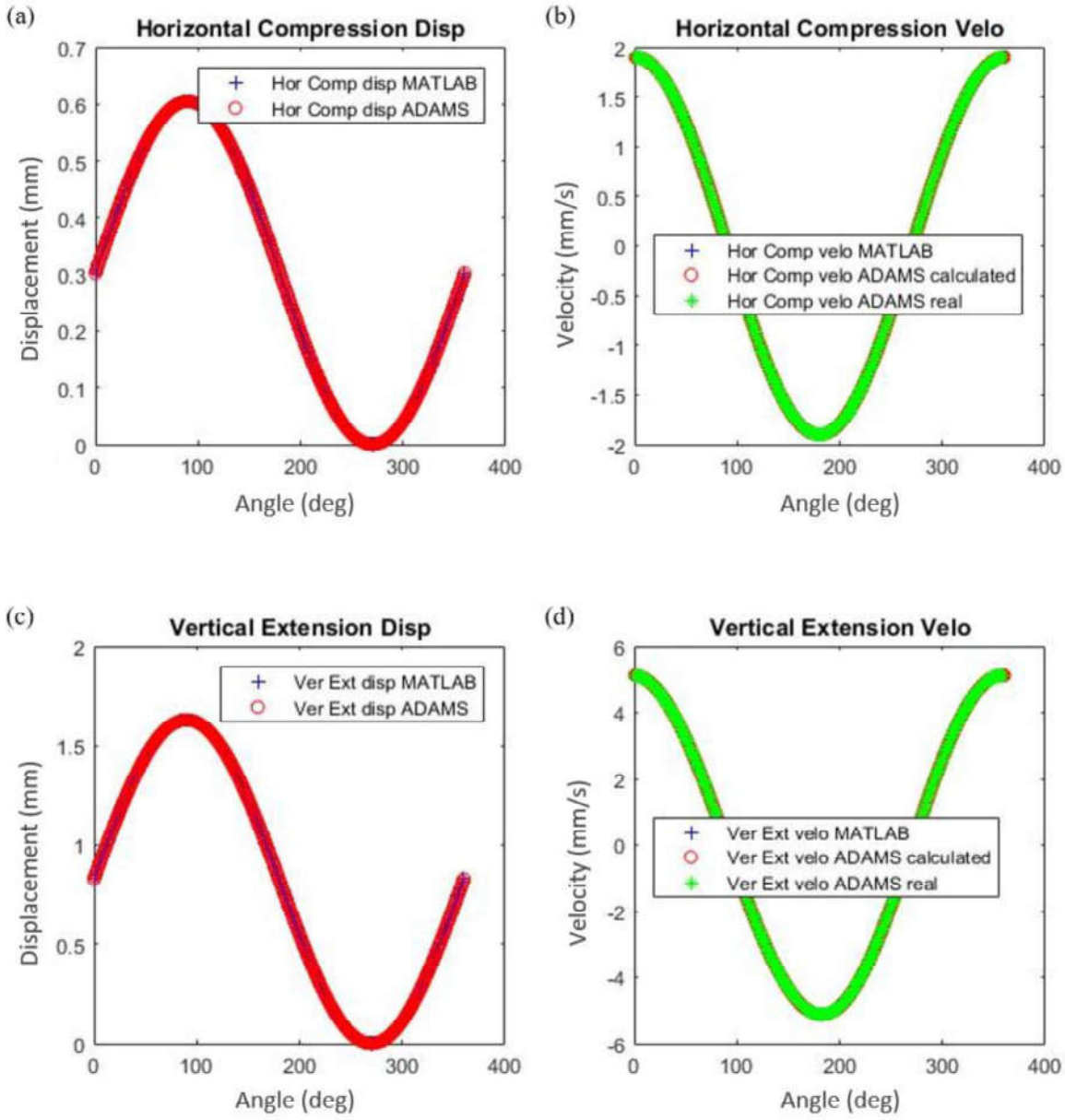


Figure 2.10. Inner mechanism's horizontal (a) displacement, (b) horizontal velocity, (c) vertical displacement and (d) vertical velocity responses under dynamic loading.

The overall force responses F_t of the MATLAB and ADAMS models are compared. For increasing the accuracy, ramp-and-hold and hysteresis loading responses are calculated in two different loading speeds. For the dynamic loading, two different frequencies are used, as well. Figure 2.11 shows the comparison of MATLAB and ADAMS model results under quasi-static loading. Figures 2.11 to 2.17 shows exactly same responses for ramp-and-hold, hysteresis and dynamic loading scenarios and verifies that the MATLAB model behaves exactly the same as the ADAMS model.

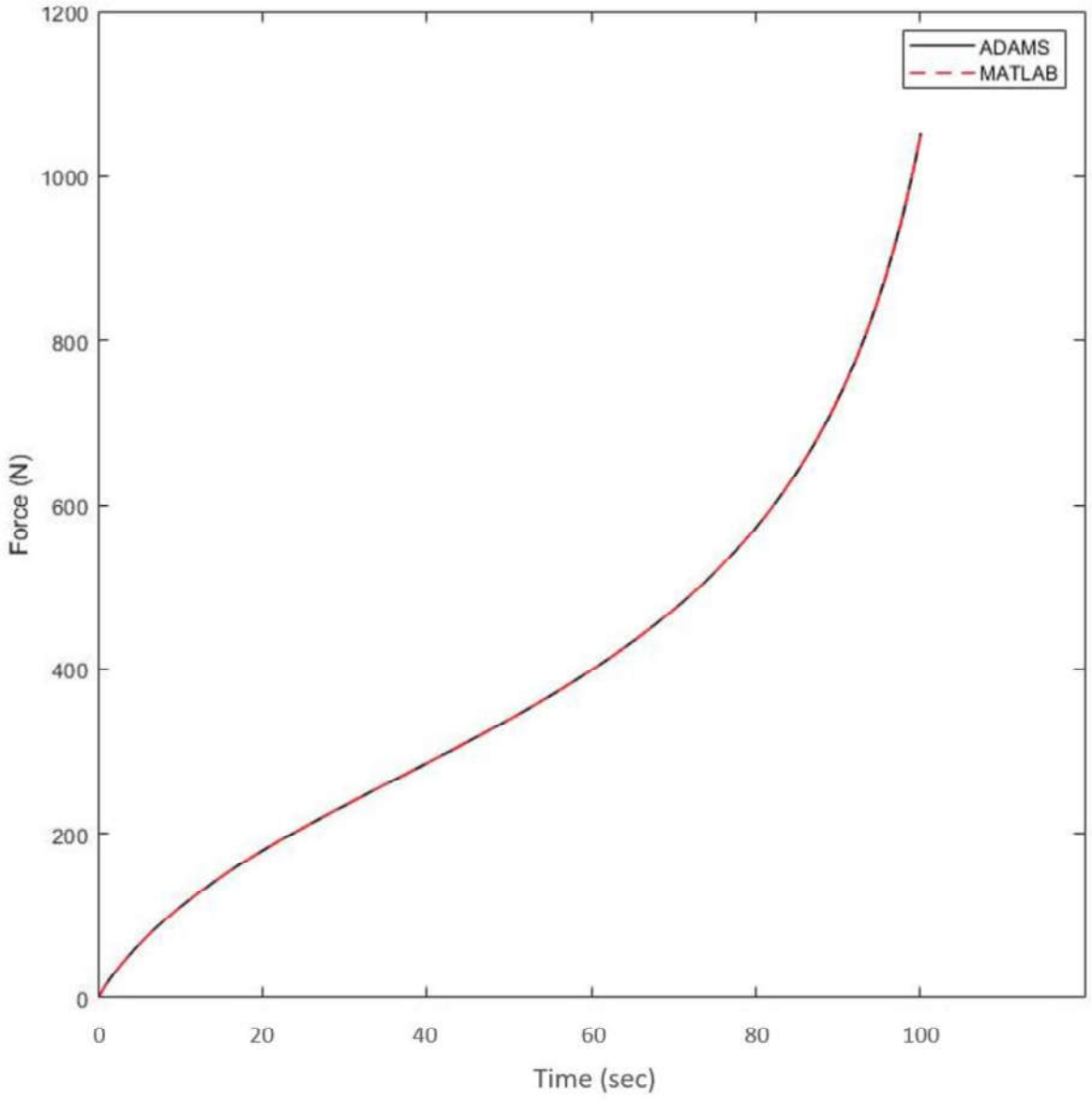


Figure 2.11. Responses of MATLAB and ADAMS model results under quasi-static loading (0.1 mm/sec).

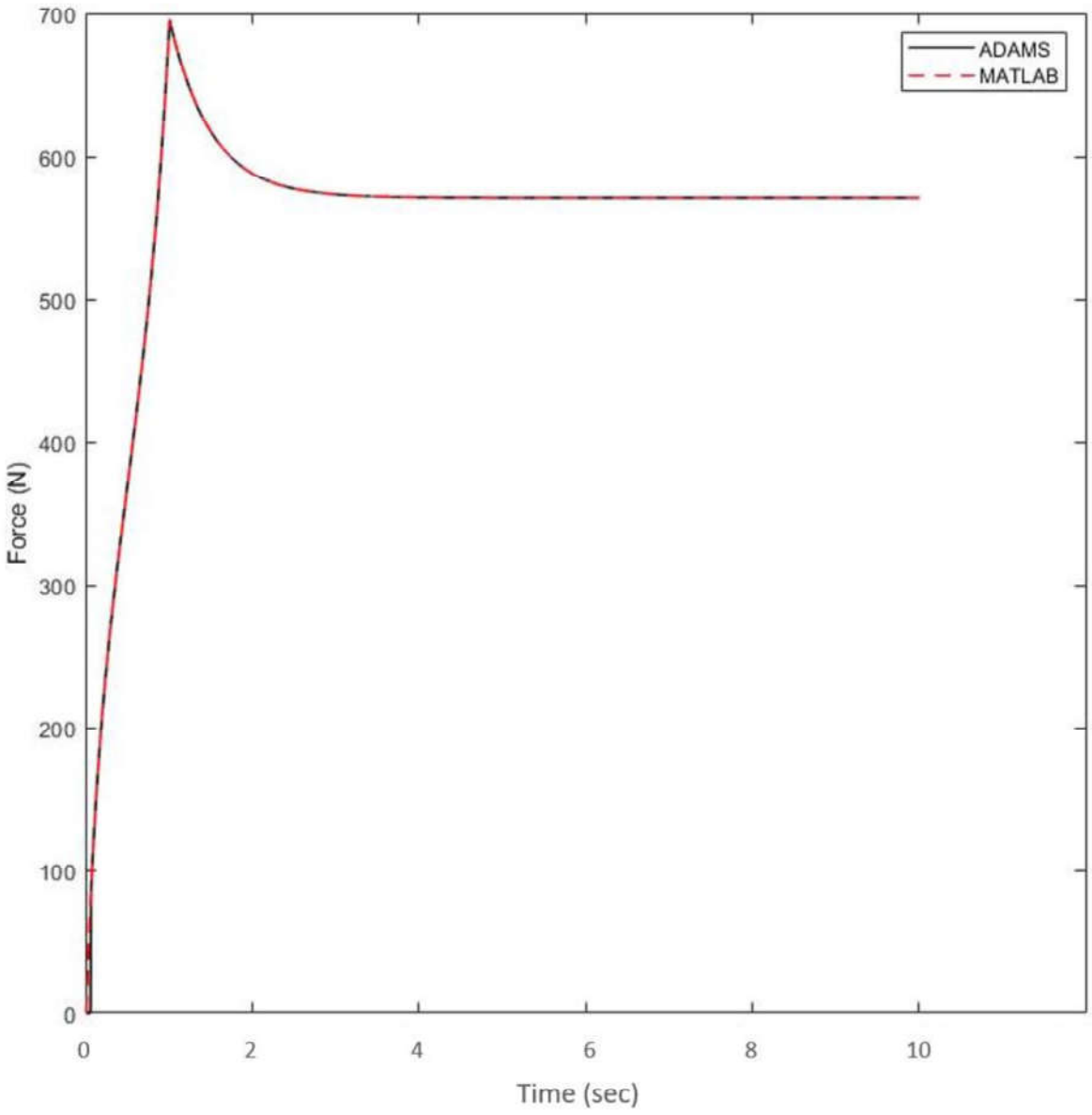


Figure 2.12. Responses of MATLAB and ADAMS model results under slow ramp-and-hold loading (8 mm/sec).

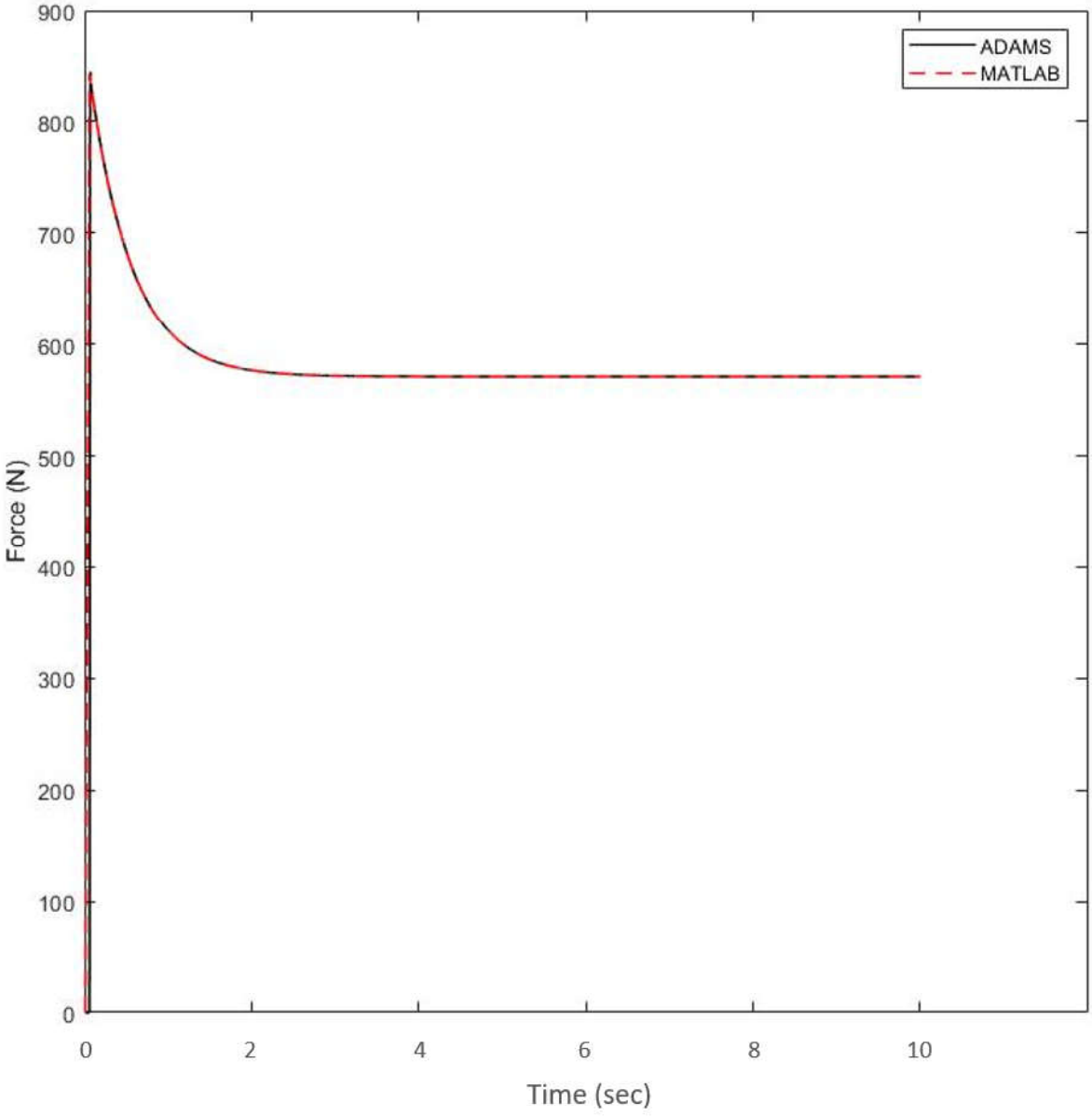


Figure 2.13. Responses of MATLAB and ADAMS model results under fast ramp-and-hold loading (800 mm/sec).

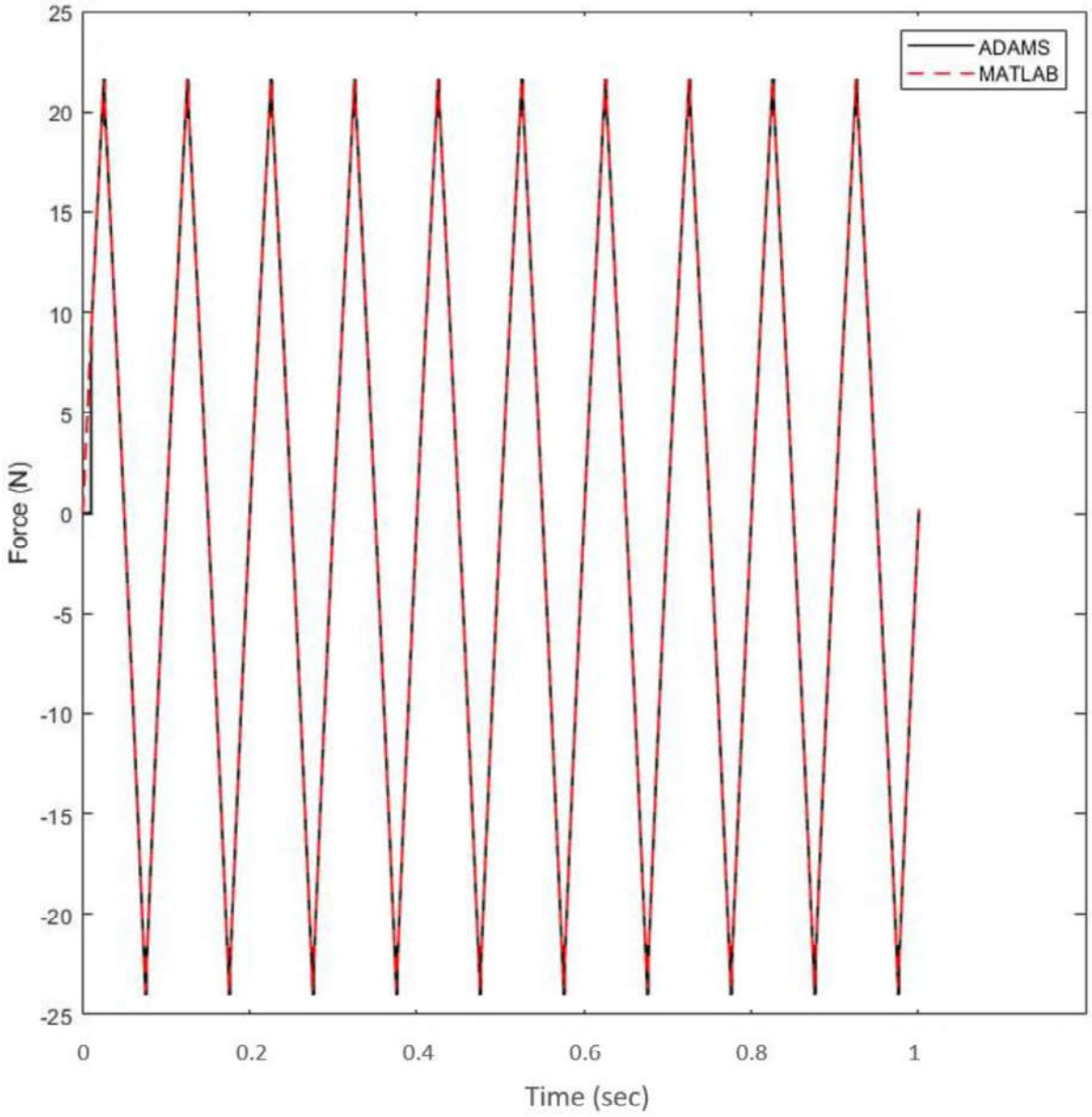


Figure 2.14. Responses of MATLAB and ADAMS model results under slow hysteresis loading (4 mm/sec).

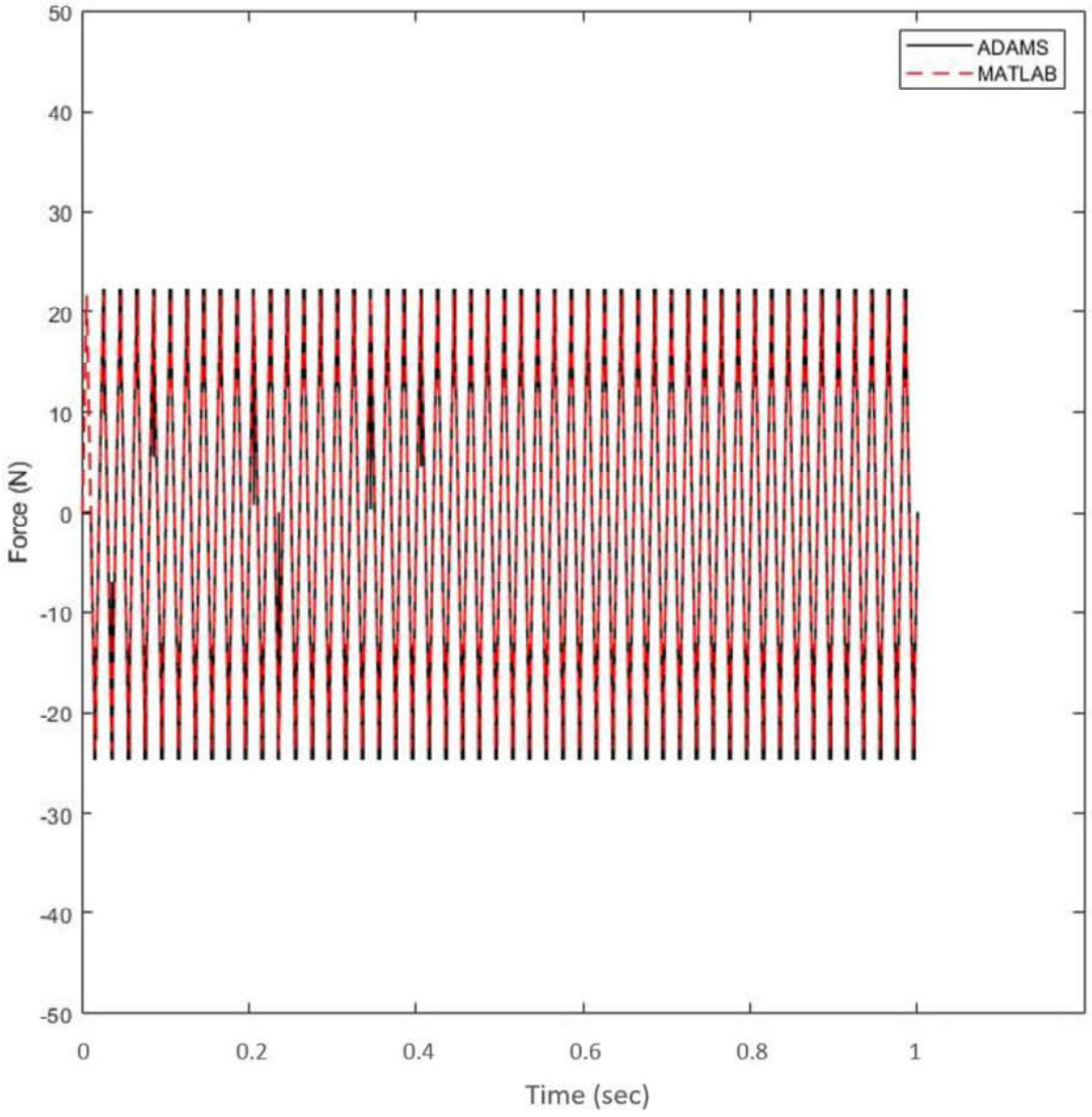


Figure 2.15. Responses of MATLAB and ADAMS model results under fast hysteresis loading (20 mm/sec).

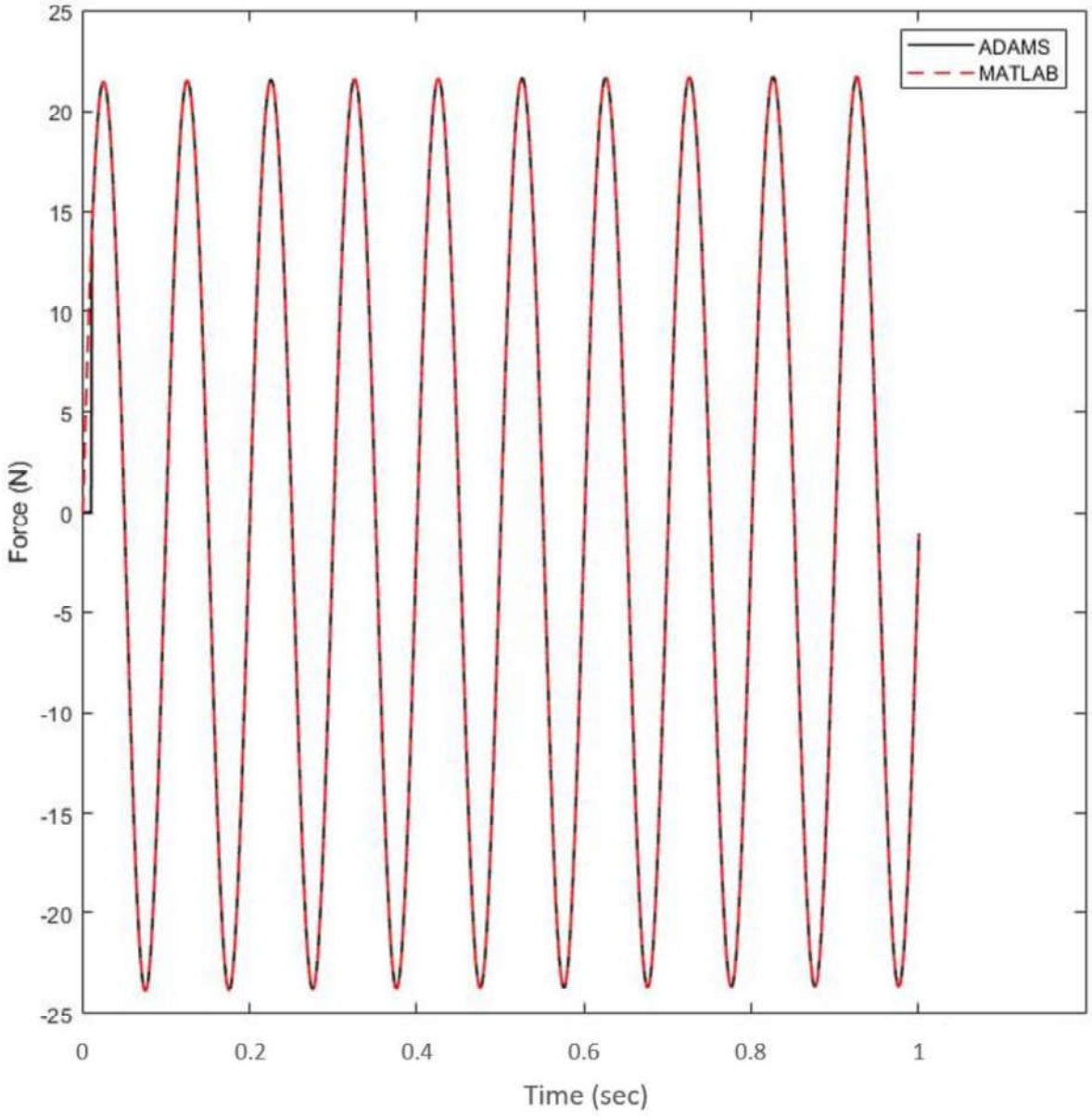


Figure 2.16. Responses of MATLAB and ADAMS model results under slow dynamic loading (10Hz).

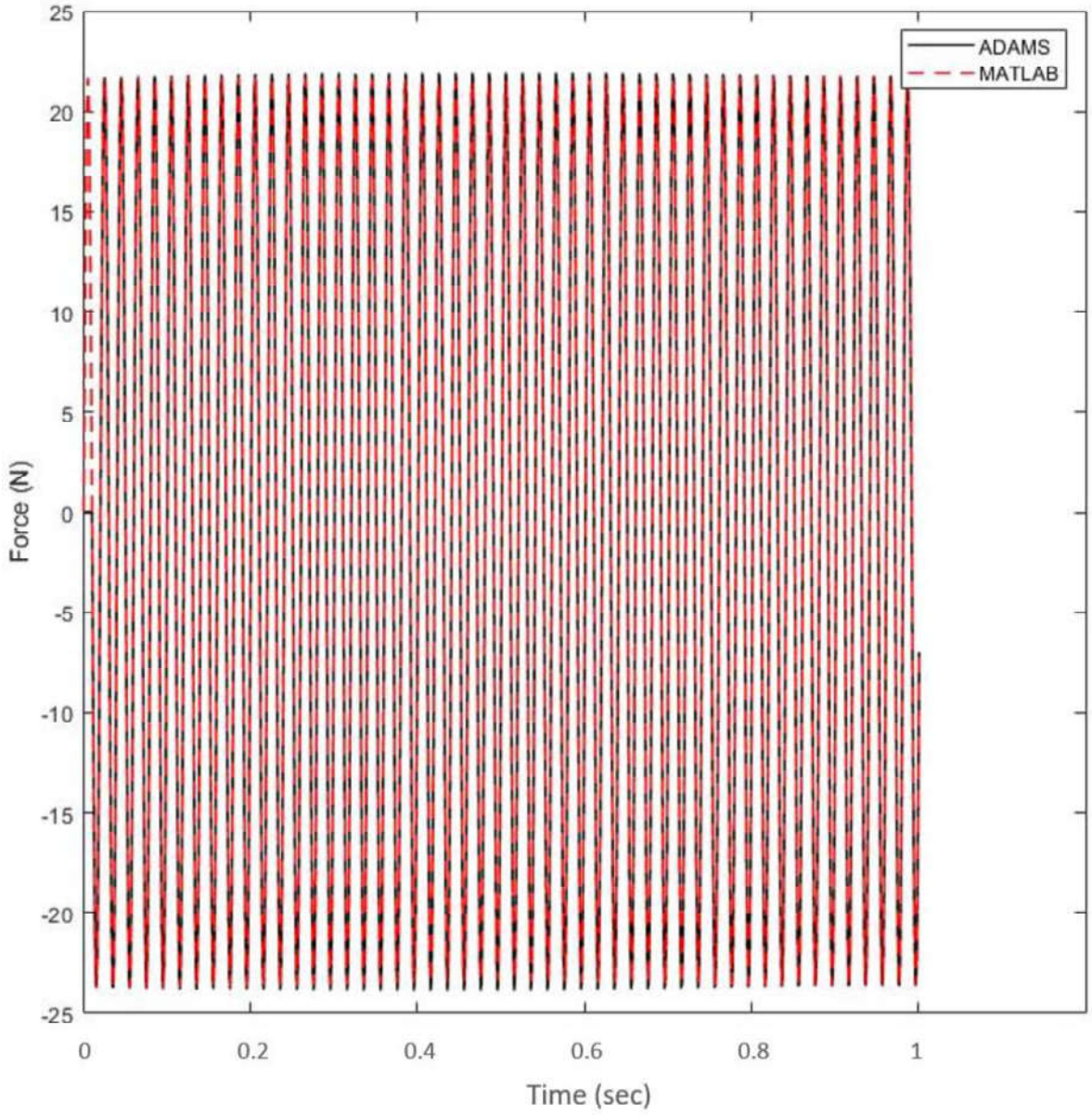


Figure 2.17. Responses of MATLAB and ADAMS model results under fast dynamic loading (50Hz).

Figures 2.7 to 2.17 show that both MATLAB and ADAMS models give the same results for various loading conditions. However, the MATLAB model runs much faster than the ADAMS model. Thus, parametric studies and optimization are conducted using the MATLAB model.

2.3. Parametric Studies

The external loading is applied to the left-most joint as displacement, $u(t)$; the resistive force of the mechanism $F_t(t)$, to this movement is calculated using the analysis explained in the previous section. The mechanical response of the mechanism as force versus displacement, time, or frequency is examined for different parameter values, i.e., stiffness coefficients k_{hs}, k_{vs}, k_h and k_v, damping coefficients c_h and c_v, lengths of inner and outer links L_i and L_o and the initial angle of the outer link α_0. A parametric study is conducted in order to see how the individual parameters affect the mechanical response in four different testing scenarios and how they contribute to the simulation of nonlinear viscoelastic material behaviour. The parameter values of the reference configuration of the system are given in Table 2.3. The mechanical response of the mechanism is examined by varying a single parameter and keeping the others constant.

Table 2.3. The reference configuration for the proposed model.

k_{hs} (N/mm)	k_h (N/mm)	c_h (Ns/mm)	k_{vs} (N/mm)	k_{vs} (N/mm)	c_v (Ns/mm)	L_o (mm)	L_i (mm)	α (deg)
10	10	10	10	10	10	100	35	7

Hyperelastic materials exhibit nonlinear mechanical response under quasi-static loading. In early phases of loading, the material shows softening behaviour with increasing strain due to reorientation and alignment of polymer chains along the loading direction (Bergstrom and Boyce, 1998). This softening behaviour reveals itself mostly in polymers containing reinforcing agent (carbon black) (Bergstrom and Boyce, 2000; Ren et al., 2015). At intermediate stages of loading, stiffening behaviour dominates due to stretching of free polymer chains. The proposed mechanism model can exhibit this characteristic behaviour. Figure 2.18 shows the individual effects of a vertical spring, a horizontal spring as well as their combined effect. In this figure, k_h, k_v, c_h and c_v are not included since the force on them will be zero due to very slow loading rate. As it can be seen in Figure 2.18a and Figure 2.18d, vertical spring (k_{vs}) imparts softening behaviour under quasi-static loading scenario whereas horizontal spring (k_{hs}) imparts hardening behaviour (see Figure 2.18b and Figure 2.18e). A combination of vertical and horizontal springs (see Figure 2.18c and Figure 2.18f)

provides an initial softening response followed by a hardening response as seen in various elastomers.

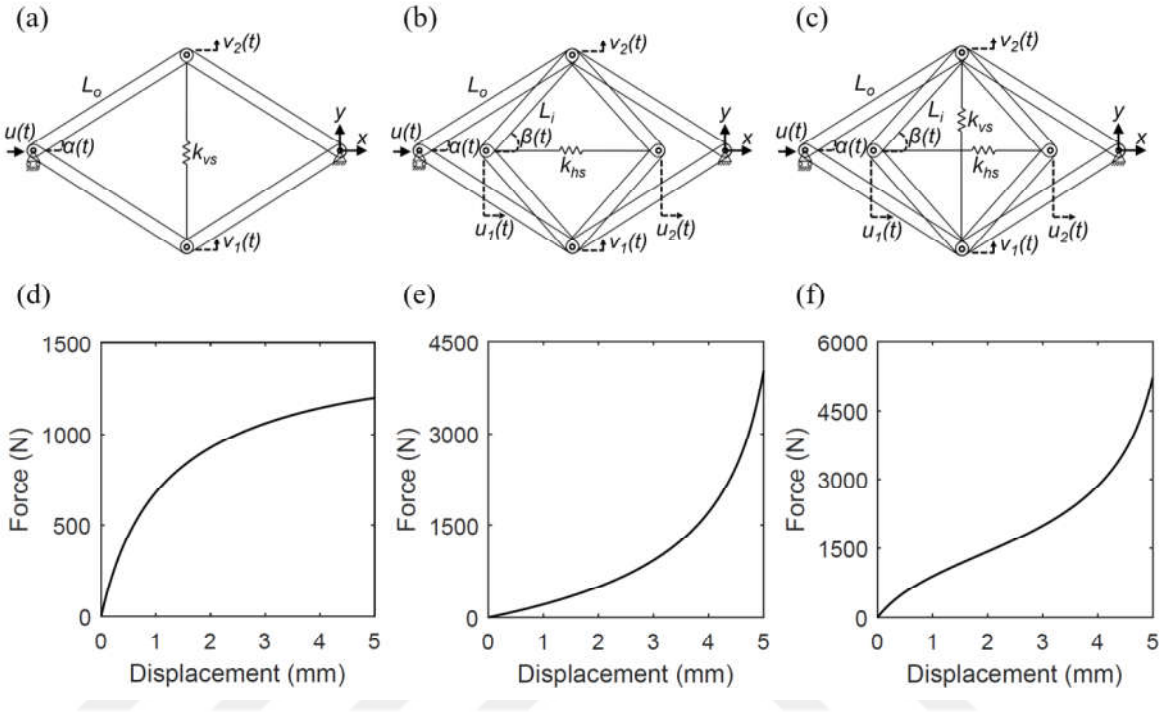


Figure 2.18. (a) Vertical spring and outer four-bar linkage, (b) horizontal spring, inner and outer four-bar linkages, (c) Horizontal and vertical springs, inner and outer four-bar linkages. (d) Effect of vertical spring as softening response, (e) effect of horizontal spring as hardening response, (f) combined effect of horizontal and vertical springs as initial softening and later hardening response. Response is obtained for 10 mm compression with parameter values given in Table 2.3.

During quasi-static loading scenario, the most effective parameters are observed to be k_{vs}, k_{hs}, and α_0. As shown in Figure 2.19a, the stiffness of the vertical spring k_{vs}, controls the initial softening behavior of the system. In early phases of loading, the slope of the force-displacement curve, i.e., the stiffness of the mechanism, decreases with increasing displacement. This behaviour becomes more apparent with higher values of k_{vs}. The horizontal spring, on the other hand, contributes mainly to stiffening response in later stages of loading (see Figure 2.19b). The initial angle of the outer links, α_0, is an effective parameter on the stiffening behavior at the later stages of the loading as seen in Figure 2.19c. As it is seen in Figure 2.19d, L_i mainly affects the later parts of the loading. The

characteristics of the response can be adjusted by changing the values of k_{vs}, k_{hs}, α_0 and L_i. The nested links together with the horizontal spring provide nonlinear stiffening response because of the geometric nonlinearity of the system. The other parameters do not significantly affect the overall response in quasi-static loading.

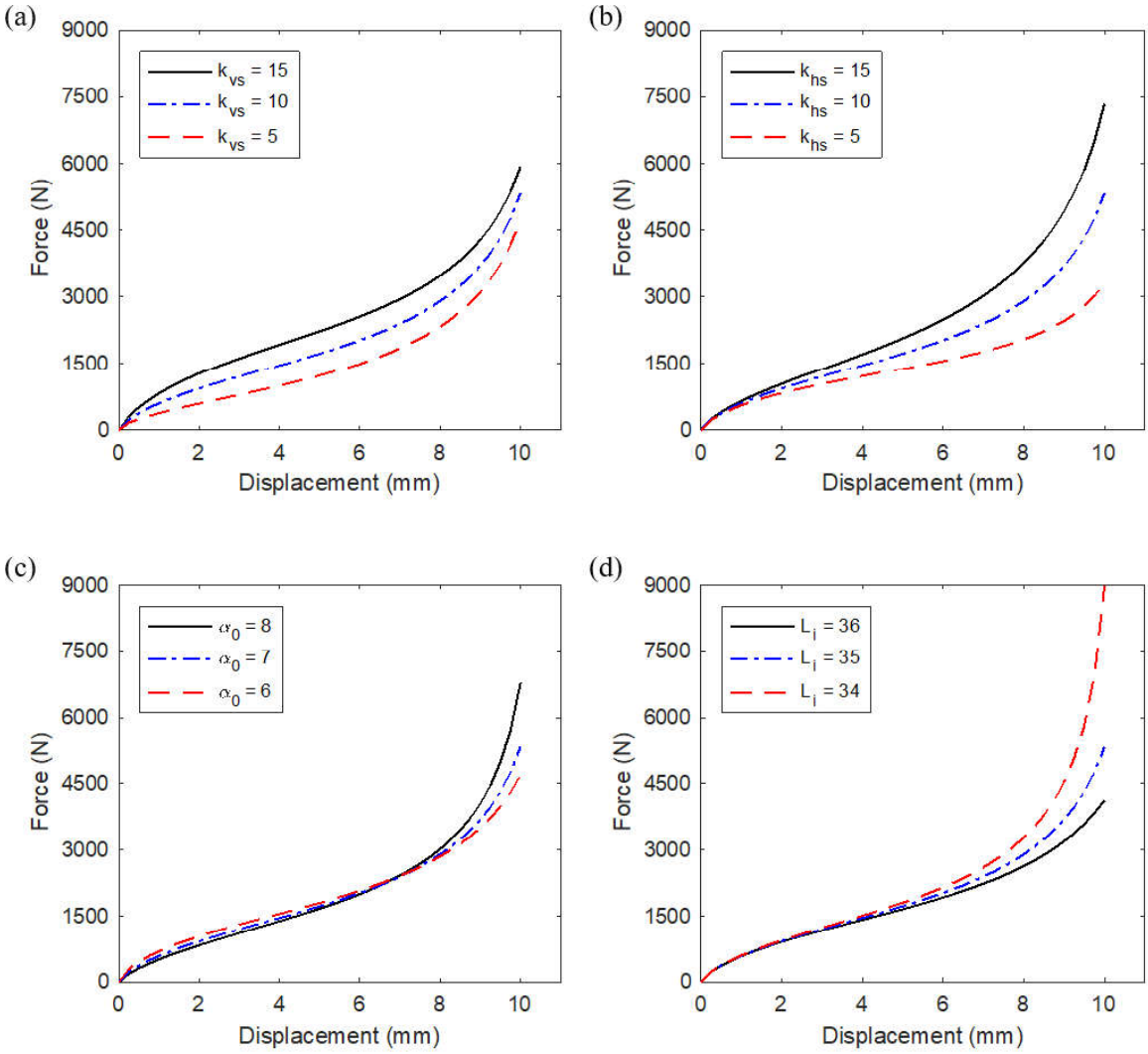


Figure 2.19. The effects of (a) k_{vs}, (b) k_{hs}, (c) α_0, and (d) L_i on the response of the mechanism under quasi-static loading. The blue dashed-dotted line represents the response of the reference configuration.

Viscoelastic materials exhibit stress-relaxation response due to realignment of polymer chains after an applied deformation. This deformation characteristic varies mainly with the material composition, excitation velocity, and amplitude. Under ramp-and-hold loading, relaxation response is generally not uniform with a fast drop at the beginning followed by

gradual relaxation. In order to simulate this characteristic behaviour, the mechanism models in Figure 2.20 are considered. Figure 2.21 shows the relaxation response of different mechanism designs due to 8 mm compression applied in 0.05 seconds followed by one-second relaxation time. By choosing different values for the spring rate, k_h, and the damping coefficient, c_h, in the single SLS models (see Table 2.4), fast and slow relaxation rates are realized while the maximum force and steady state force levels remain nearly the same. The combination of horizontal and vertical SLS elements provides about the same maximum force and the steady state force levels, but a different relaxation response. As seen in Figure 2.21, the double SLS provides a similar relaxation rate as single SLS 2 in the early phases of the relaxation; but changes its characteristics such that the relaxation rate is similar to that of single SLS 1 in the later stages of relaxation. Therefore, by using double SLS, different relaxation characteristics of viscoelastic materials can be simulated that cannot be simulated by a single SLS.

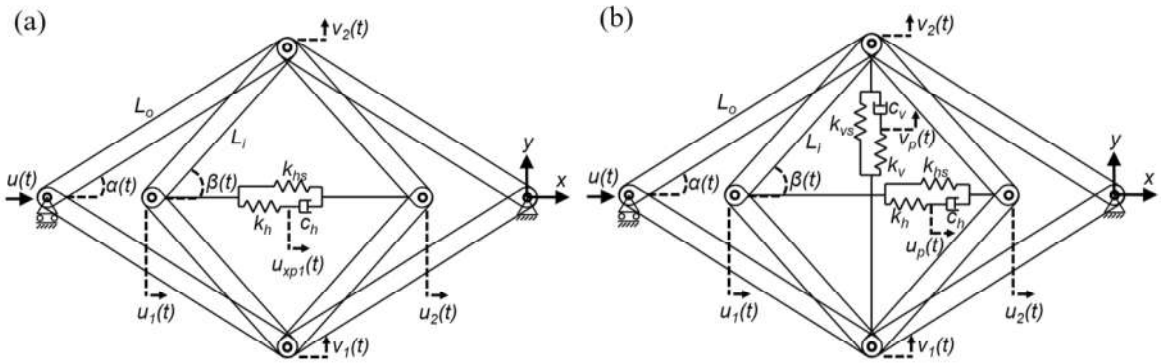


Figure 2.20. (a) Single SLS element in the mechanism, (b) double SLS elements in the mechanism.

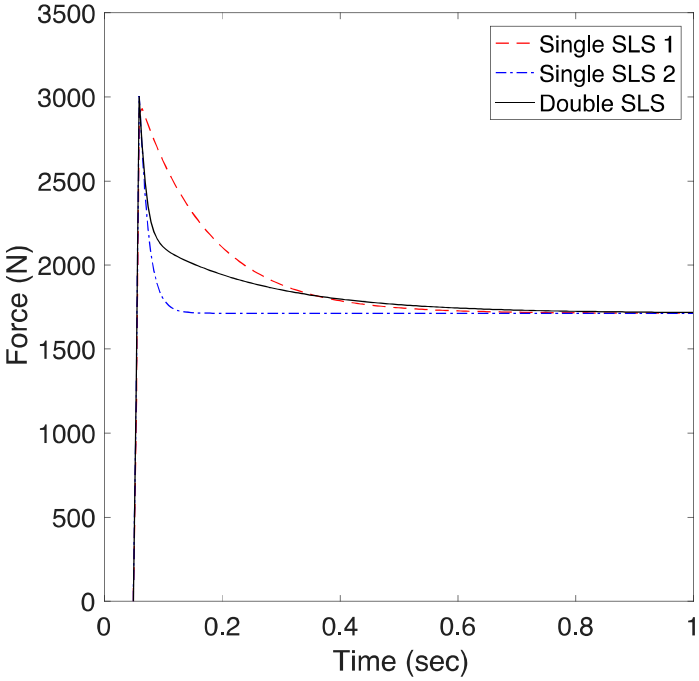


Figure 2.21. The effect of different SLS configurations on relaxation response after 8 mm compression applied in 0.05sec. The parameter values are given in Table 2.4.

Table 2.4. Parameters used in Figure 2.21.

	k_{hs} (N/mm)	k_h (N/mm)	c_h (Ns/mm)	k_{vs} (N/mm)	k_{vs} (N/mm)	c_v (Ns/mm)	L_o (mm)	L_i (mm)	α (deg)
Single SLS 1	10	10	3.4	-	-	-	100	35	7
Single SLS 2	10	12	0.5	-	-	-	100	35	7
Double SLS	6	10	0.15	6	7	3	100	35	7

Relaxation curve of viscoelastic materials is generally a complex curve that cannot be expressed with a single-term (Ciambella et al., 2010; Oman and Nagode, 2014). This is why analytical studies (Vandenbroucke et al., 2010; Wang and Han, 2013) generally use exponential formulations with minimum two terms to model relaxation response. The mechanism model proposed in this study includes two SLS elements positioned horizontally and vertically, which provide different relaxation rates due to different set of parameters (k_{hs}, k_h, c_h vs k_{vs}, k_v, c_v), and parameters for geometric nonlinearity of the mechanism (L_o, L_i, α_o). As seen in Table 2.3, there are nine parameters that can be changed to tune the response of the mechanism model. However, L_o is not changed as the main curve characteristics are affected by the ratio of L_o to L_i. In order to see the effects of the remaining

eight parameters on the relaxation response, 8 mm displacement is applied to the left joint in 0.05 seconds, then the mechanism is kept at that state for 10 seconds and the resistive force generated by the mechanism is calculated for different values of these parameters. As seen in Figure 2.22a and Figure 2.22b, k_{hs} and k_{vs} influence the steady state response of the system, while the amount of relaxation (the difference between the peak force and the steady-state force levels) and the relaxation rate remain the same. k_h and k_v mainly influence the start point of the relaxation curve (see Figure 2.22c and Figure 2.22d), whereas, c_h and c_v influence the relaxation rate (see Figure 2.22e and 2.22f). L_i and α_0 affect the steady state response without altering the relaxation rate as seen in Figure 2.22g and Figure 2.22h.

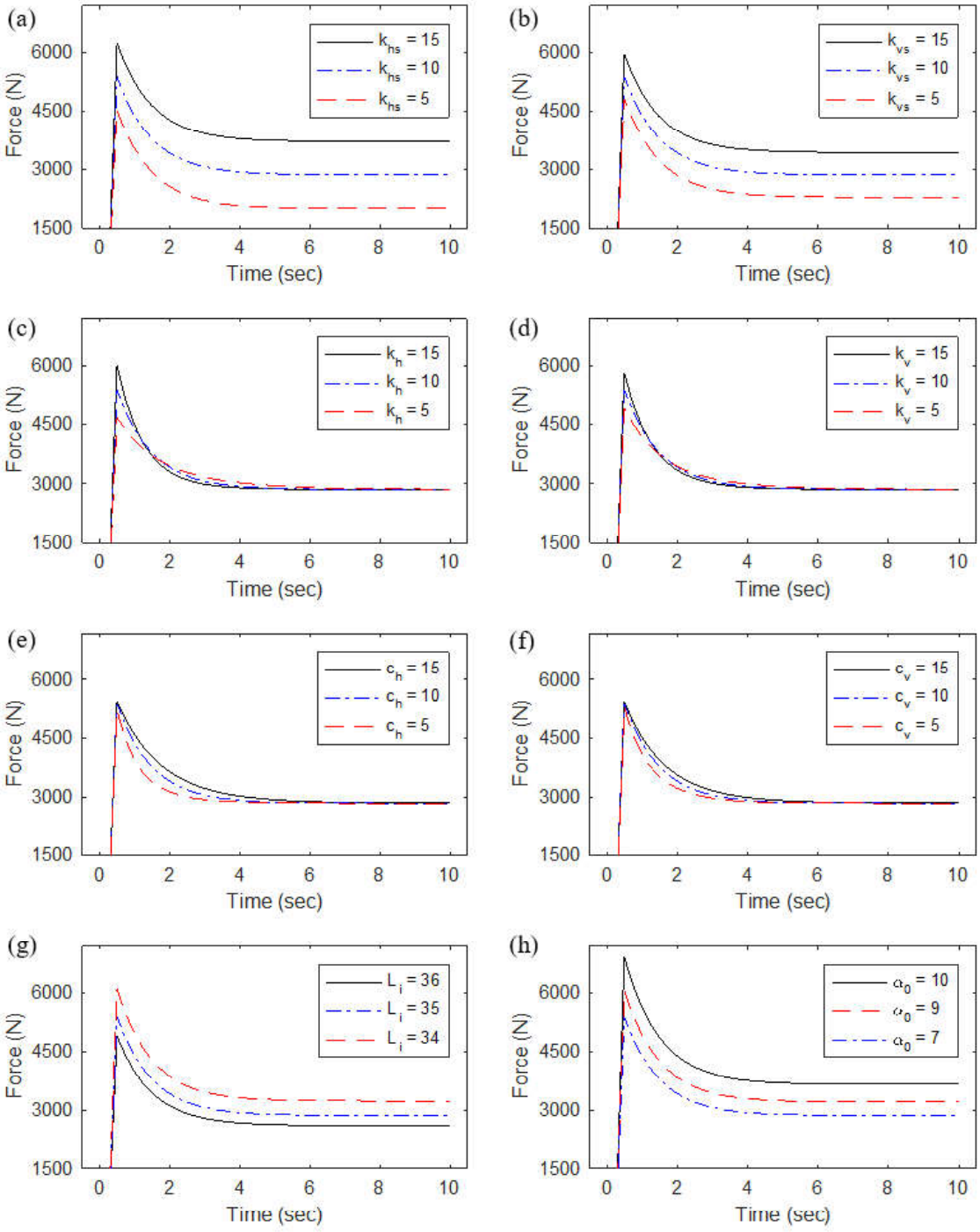


Figure 2.22. The effects of (a) k_{hs}, (b) k_{vs}, (c) k_h, (d) k_v, (e) c_h, (f) c_v, (g) L_i, and (h) α_0 on the relaxation response of the mechanism under ramp-and-hold loading. The blue dashed-dotted line represents the response of the reference configuration.

Viscoelastic materials show different stress-strain responses during loading and unloading phases. The difference in force-displacement curves in loading and unloading phases gives rise to energy loss in each load cycle, which is called “hysteresis.” In order to observe the effects of the system parameters on the hysteresis response, the mechanism is compressively loaded and unloaded to 10 mm in 10 seconds. As seen in Figure 2.23a and Figure 2.23b, k_{hs} affects the stiffening part of the hysteresis curve, whereas k_{vs} affects the initial softening part and shifts the hysteresis curve. Similarly, k_h mainly affects the stiffening part of curve, while k_v affects mainly the softening part (see Figure 2.23c and Figure 2.23d). However, as the loading and unloading rates are low, the effect of k_{hs} and k_{vs} are more pronounced then k_h and k_v. On the other hand, k_h and k_v are more effective than k_{hs} and k_{vs} in changing the amount of hysteresis. As seen in Figure 2.23e and Figure 2.23f, c_h mainly affects the end of the loading cycle (stiffening part of the curve), whereas c_v affects mainly the end of the unloading cycle. Besides, both of these variables are effective in changing the amount of hysteresis. Decrease in L_i leads to a significant increase in the resistive force in the stiffening part without changing the low-displacement characteristics (see Figure 2.23g). Notice that, for the smaller value of L_i (34 mm) the inner mechanism tends to close at large displacements which results in a highly nonlinear force-displacement response. Similar to L_i, α_0 also affects the stiffening part of the curve, but its effect is less pronounced (compare Figure 2.23g and Figure 2.23h). Furthermore, α_0 changes the initial softening part of the loading curve whereas L_i has no effect on this part.

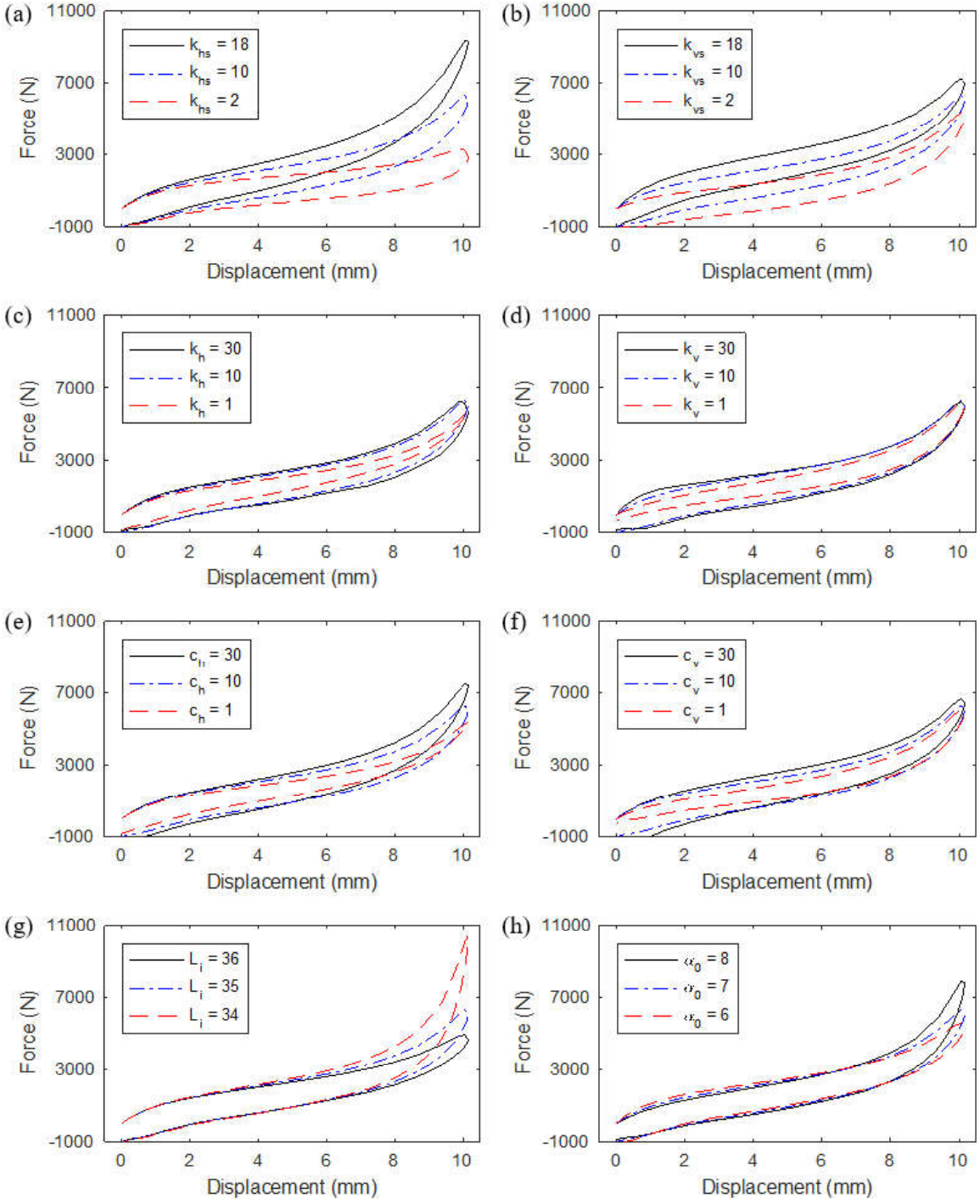


Figure 2.23. The effects of (a) k_{hs}, (b) k_{vs}, (c) k_h, (d) k_v, (e) c_h, (f) c_v, (g) L_i, and (h) α_0 on the hysteresis behavior of the mechanism. The blue dashed-dotted line represents the response of the reference configuration.

In order to observe dynamic stiffness response of materials, samples are repeatedly compressed and/or extended to the same strain with continually increasing frequencies. Nonlinear viscoelastic materials show higher stiffness at higher excitation frequencies. Dashpot elements in the proposed mechanism model impart this property to the system. If the frequency is increased while keeping the amplitude the same, the velocity increases; accordingly, the resistance force generated by the dashpots increases and thus the overall stiffness increases. Consequently, the proposed mechanism shows increasing stiffness response with increasing frequency. In order to see the effects of the parameters on the dynamic stiffness behaviour of the mechanism, it is repeatedly compressed by 1 mm, while increasing the frequency from 0 Hz to 100 Hz and the resistive force applied by the mechanism is used for calculating the dynamic stiffness values. Figure 2.24 shows the effects of the system parameters on the dynamic response. For the results in Figure 2.24, k_h is taken as 100 N/mm, k_v is taken as 3 N/mm and c_v is taken as 0.3 Ns/mm for better comparison. Other values are from Table 2.3. When k_{hs} and k_{vs} are increased, the overall response is shifted upwards without changing the stiffening characteristics (see Figure 2.24a and Figure 2.24b). As seen in the Figure 2.24c and Figure 2.24d, k_h and k_v change the slope of the curve without changing the starting point. k_v is more dominant due to the dimensions of the system and the small amplitude excitation. c_h is effective on the slope of the response mainly in the intermediate and high frequencies without changing the initial point (see Figure 2.24e. c_v is more effective at lower frequencies. As seen in Figure 2.24f, larger values of c_v, lead to increased stiffness of the mechanism at smaller frequencies as opposed to c_h. L_i shifts the dynamic stiffness response of the system at intermediate and high frequencies (see Figure 2.24g). As it is seen in Figure 2.24h, α_0 shifts the response without significantly altering stiffening characteristics.

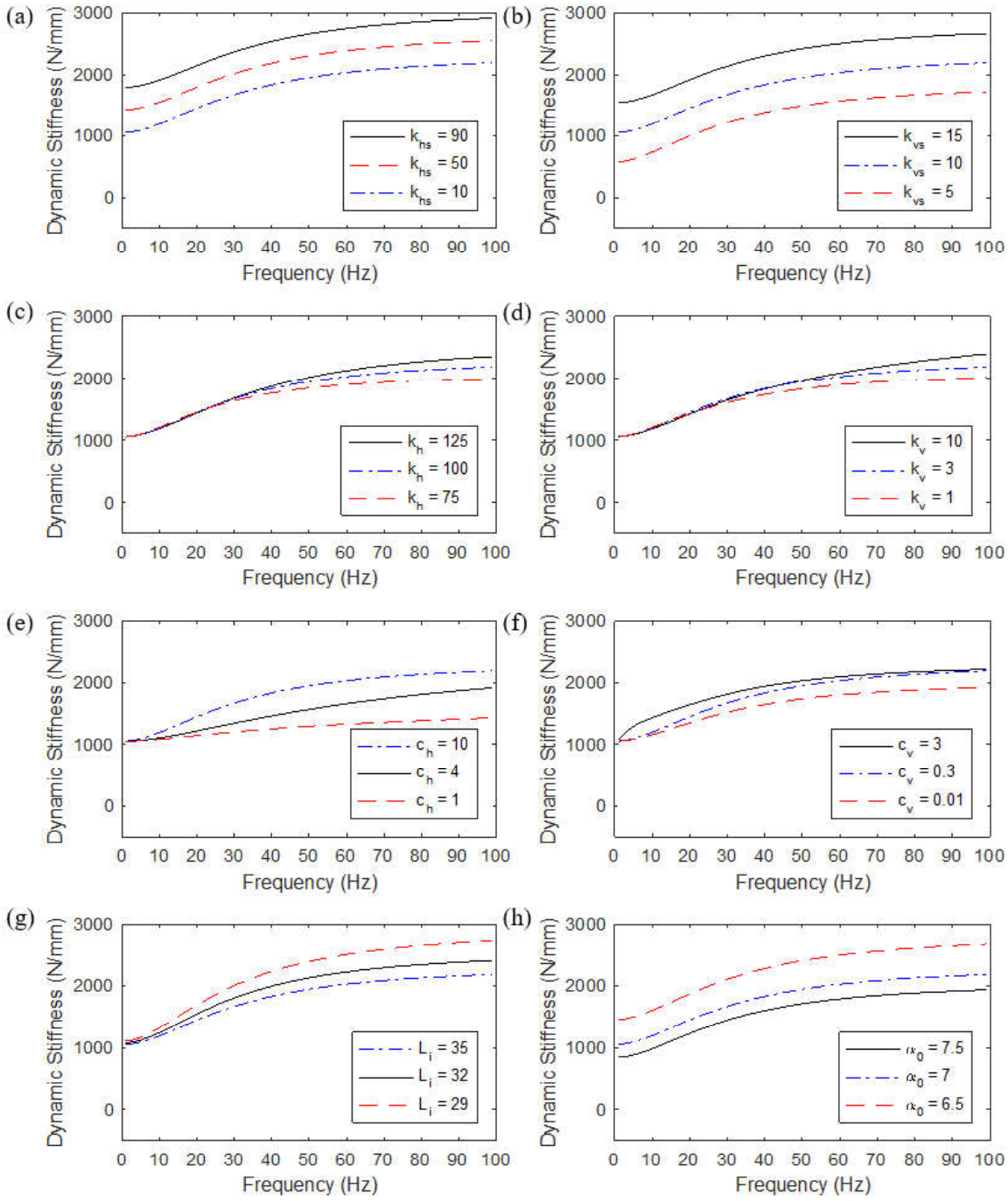


Figure 2.24. The effects of (a) k_{hs}, (b) k_{vs}, (c) k_h, (d) k_v, (e) c_h, (f) c_v, (g) L_i, and (h) α_0 on the dynamic stiffness response of the mechanism under dynamic loading. k_h is taken as 100 N/mm, k_v is taken as 3 N/mm and c_v is taken as 0.3 Ns/mm for better comparison. Other values are from Table 2.3. The blue dashed-dotted line represents the response of the reference configuration.

3. COMPARISON OF TEST DATA AND MODEL RESPONSE

3.1. Double Combinations of Literature Test Data

In order to see how well the mechanism simulates nonlinear viscoelastic material behaviour, the response exhibited by the mechanism model is compared with the material response observed in experiments. As mentioned before, nonlinear viscoelastic material response in four test scenarios is simulated, which are quasi-static loading, ramp-and-hold loading, hysteresis loading, and dynamic loading. Unfortunately, no study in the literature simultaneously presents test data obtained under all these four different loading conditions for a nonlinear viscoelastic material. Comparisons are made with the studies that include two different loading conditions simultaneously.

In order to make comparisons, first, image-processing software (GetData) is used to generate data points from the curves given in previous studies. Then, the parameter values of the mechanism model are optimized so that its response fits the test data. For this purpose, objective functions are defined representing the difference between the measured material response and the calculated model response. Each data point of the model response is subtracted from the target data. These individual differences are used for calculating the total error by summing their squares. The sum of total errors of the two individual test scenarios are minimized for reducing the difference between the model response and the test results. The optimization problem formulation is given as

$$min\ f = \sum_{i=1}^{n} (T_{1i} - R_{1i})^2 + \sum_{i=1}^{n} (T_{2i} - R_{2i})^2 \tag{3.1}$$

where R_{1i} and R_{2i} are the data points on the first and second response curves obtained from two different test scenarios and T_{1i} and T_{2i} are the data points of the corresponding target curves, respectively. Moreover, there are n data points on each curve. To solve the optimization problem, lower and upper limits of the parameters are defined. Random values are chosen between these limits to define the initial configuration of the mechanism as

starting point of the optimization. Two curve fits among four different alternatives (quasi-static, ramp-and-hold, hysteresis, dynamic stiffness) will be satisfied with the same parameter values. Nonlinear-least square curve fit solver is used in MATLAB for the optimization process. Trust-region-reflective algorithm is used to minimize the objective function. In order to eliminate worse local minima, the optimization process in repeated 750 times starting from randomly chosen initial points. The strain values for the proposed mechanism in below figures are calculated as the ratio of applied displacement to initial horizontal length of the mechanism.

Bergstrom and Boyce (Bergstrom and Boyce, 2000) provided quasi-static and hysteresis loading test results for elastomers (chloroprene and natural rubber with carbon black). The strain rate was 0.01/s for compressive hysteresis loading. The material response is simulated by the mechanism model with the optimized parameter values of k_{hs} = 0.00779 N/mm, k_h = 0.0087 N/mm, c_h = 0.0008 Ns/mm, k_{vs} = 0.0048 N/mm, k_v = 13.1 N/mm, c_v = 0 Ns/mm, L_o = 100 mm, L_i = 35.1 mm, and α_o = 7.211 degrees for both loading cases. As seen in Figure 3.1, quasi-static response is closely approximated, while a small deviation appears in the hysteresis response at the end of the loading phase.

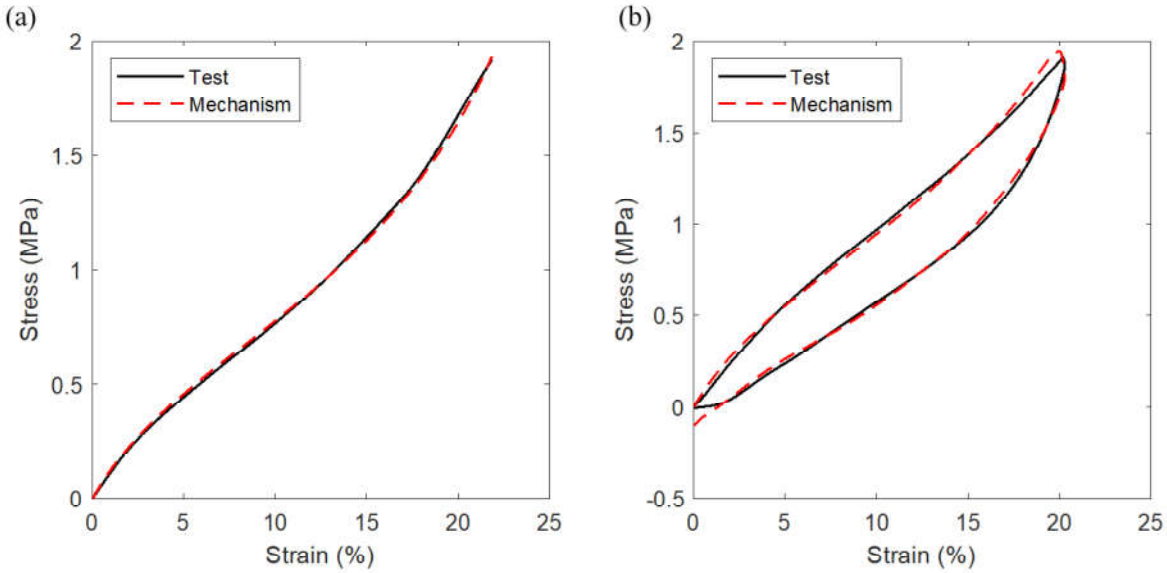


Figure 3.1. Comparison of the mechanism response and the material response reported by Bergstrom and Boyce (Bergstrom and Boyce, 2000) for (a) quasi-static loading and (b) hysteresis loading.

Ciambella et al. (Ciambella et al., 2010) provided ramp-and-hold and hysteresis loading test results for a cylindrical carbon-black-filled rubber. The strain rate was 1.09/s for compressive hysteresis loading and the duration of the compression was 0.7 sec for ramp-and-hold loading. The material response is simulated by the mechanism model with parameter values of k_{hs} = 0.01347 N/mm, k_h = 0.025 N/mm, c_h = 0.1199 Ns/mm, k_{vs} = 0.002688 N/mm, k_v = 0.002268 N/mm, c_v = 0.00054 Ns/mm, L_o = 100 mm, L_i = 34.73 mm, and α_o = 6.285 degrees. As seen in Figure 3.2, both ramp-and-hold loading and hysteresis loading scenarios are well simulated with the proposed model.

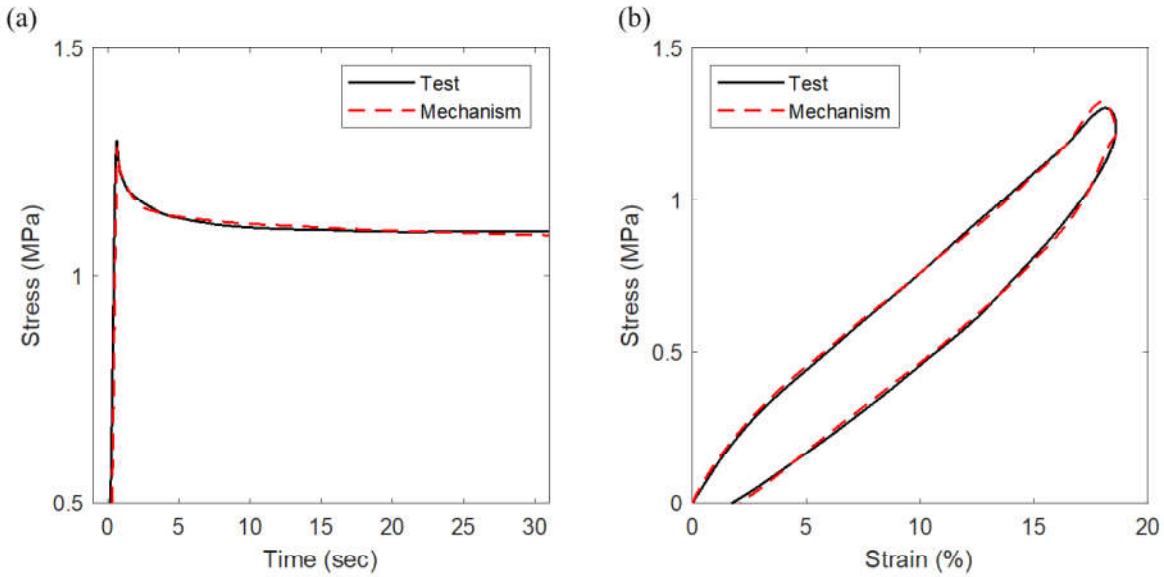


Figure 3.2. Comparison of the mechanism response and the material response reported by Ciambella et.al. (Ciambella et al., 2010) for (a) ramp-and-hold loading and (b) hysteresis loading.

Oman and Nagode provided quasi-static and ramp-and-hold loading test results for filled rubber (Oman and Nagode, 2014). The main purpose of that study was to understand the material responses under different loading scenarios of creep and stress-relaxation tests. The material response is simulated by the present mechanism model with parameter values of k_{hs} = 0.00248 N/mm, k_h = 0.04518 N/mm, c_h = 0.02036 Ns/mm, k_{vs} = 45.33 N/mm, k_v = 5.686 N/mm, c_v = 58.01 Ns/mm, L_o = 100 mm, L_i = 99.54 mm, and α_o = 84.43 degrees under tensile quasi-static loading and instantaneous tensile ramp-and-hold loading. As seen in Figure 3.3, the mechanism mimics the material response obtained in quasi-static and ramp-and-hold tests quite well.

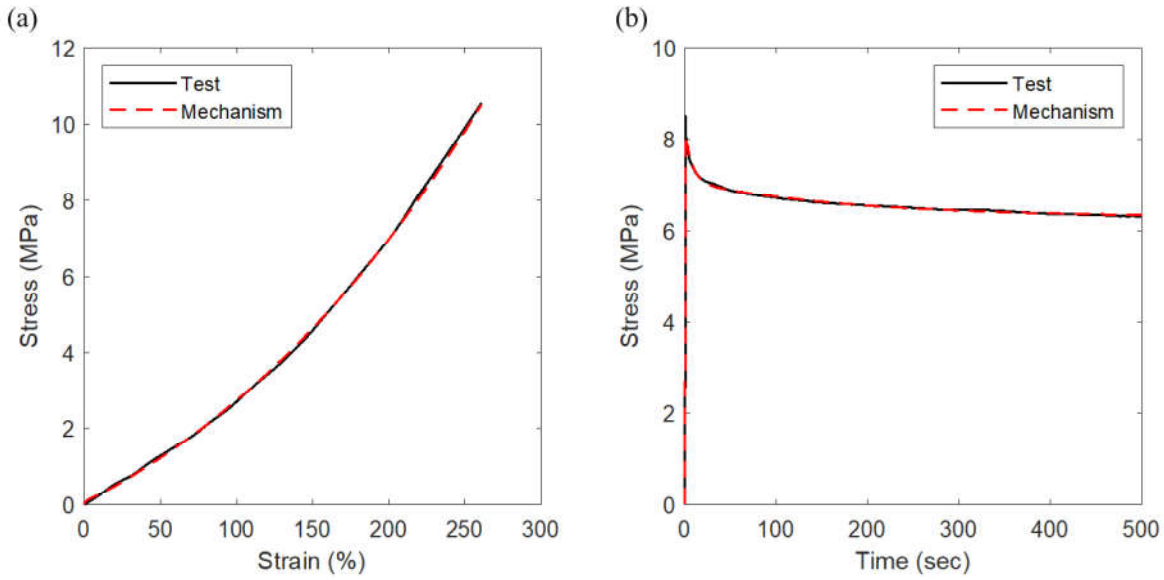


Figure 3.3. Comparison of the mechanism response and the material response reported by Oman and Nagode (Oman and Nagode, 2014) for (a) quasi-static loading and (b) ramp-and-hold loading.

Tarrago and Leif (Garcia Tarrago et al., 2007) conducted a study on carbon-black filled rubber bushings to reveal the effects of amplitude and frequency on axial dynamic stiffness. The frequency of the compressive hysteresis load was 0.1 Hz and the range of frequency for dynamic loading was 0-100 Hz. The first loop of the hysteresis curves is used for comparison. The material response is simulated by the mechanism model with parameter values of k_{hs} = 0.08245 N/mm, k_h = 21.42 N/mm, c_h = 26.2 Ns/mm, k_{vs} = 13.22 N/mm, k_v = 2.993 N/mm, c_v = 0.2359 Ns/mm, L_o = 100 mm, L_i = 34.93 mm and α_o = 7.263 degrees. As seen in Figure 3.4, the response of the mechanism model and the material response in hysteresis and dynamic stiffness tests compare very well.

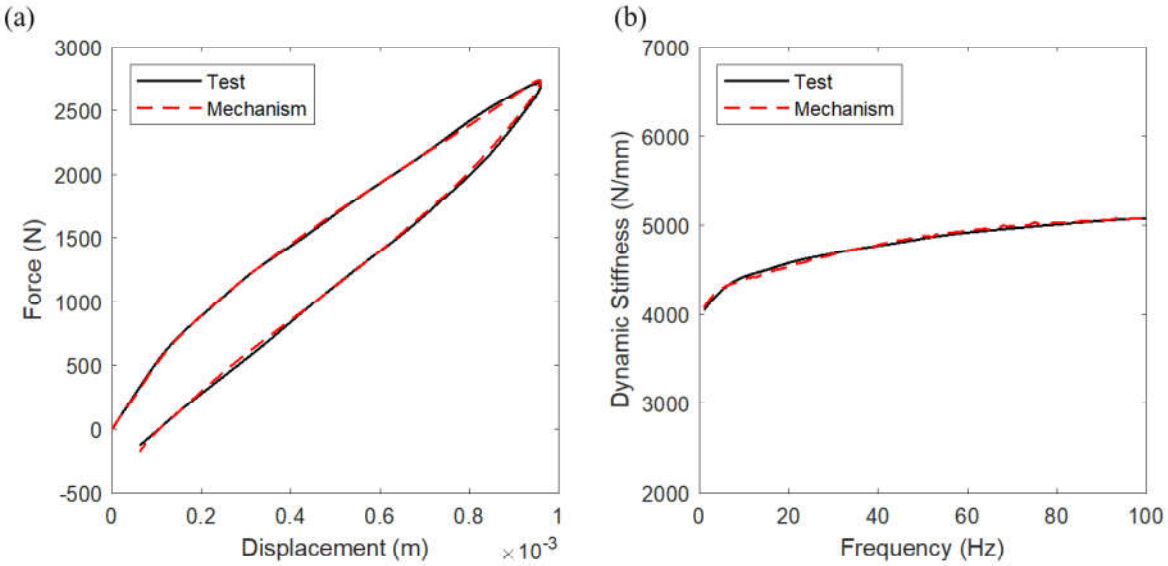


Figure 3.4. Comparison of the mechanism response and the material response reported by Tarrago and Leif (Garcia Tarrago et al., 2007) for (a) hysteresis loading and (b) dynamic loading.

3.2. Material Samples and Experiments

The main aim of this study is to closely mimic the responses of a sample in quasi-static, ramp-and-hold, hysteresis, and dynamic loading tests by using the same set of parameters. To minimize the error between the numerical and experimental results, an optimization study is conducted with the objective function given as

$$min\ f = \sum_{i=1}^{n}(T_{1i} - R_{1i})^2 + \sum_{i=1}^{n}(T_{2i} - R_{2i})^2 + \sum_{i=1}^{n}(T_{3i} - R_{3i})^2 + \sum_{i=1}^{n}(T_{4i} - R_{4i})^2 \quad (3.2)$$

where R_{1i}, R_{2i}, R_{3i} and R_{4i} are the data points of four different test scenarios of the model and T_{1i}, T_{2i}, T_{3i} and T_{4i} are the data points of the corresponding target curves, respectively. The n data points on each curve are used for calculation. Random initial parameters are used in the optimization process, and lower and upper bounds are defined for each parameter. All four test scenarios are weighted equally in the optimization process. For the optimization process, MATLAB nonlinear-least square curve fit solver is used. For minimizing the error function, Trust-region-reflective algorithm is utilized. To avoid local minima, 1000

optimization runs are conducted with randomly selected initial points. Then, the best outcome is determined.

3.2.1. Material Samples

For the purpose of obtaining four different test responses (quasi-static, ramp-and-hold, hysteresis and dynamic loading), three different carbon black vulcanized rubber samples are used, which can be seen in Figure 3.5. The samples are selected according to their stiffness and damping values for extending the material variety.

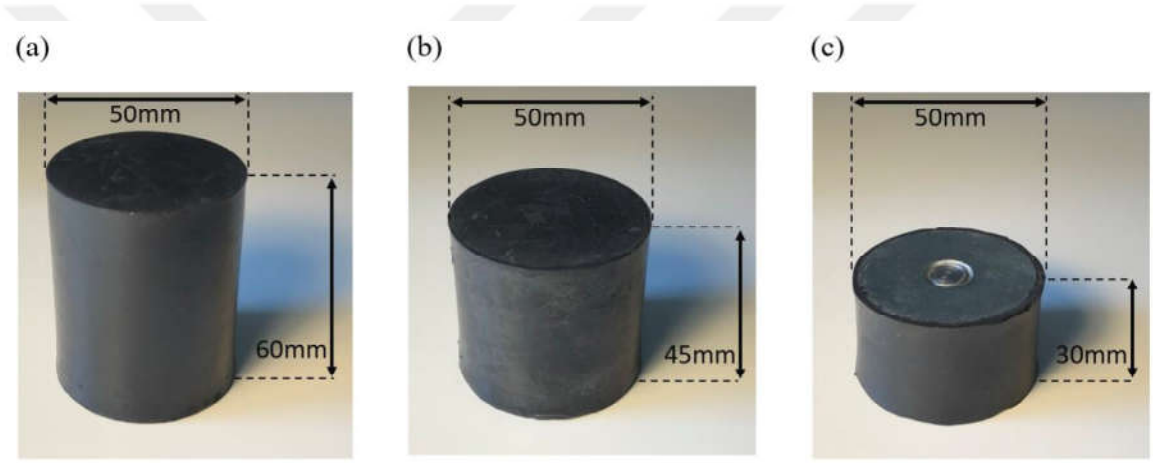


Figure 3.5. Samples used in four different test scenarios: (a) Long sample (L_0 = 60mm, 36 Shore A hardness), (b) Medium sample (L_0 = 45mm, 38 Shore A hardness), (c) Short sample (L_0 = 30mm, 40 Shore A hardness).

Notice that all samples are 50mm in diameter, but their heights are different (30mm, 45mm and 60mm). There is a steel connection plate with a nut welded to its center at the bottom part of the medium and long samples. The same type of steel plate exists for the bottom part of the short sample. But there is also a top steel plate for the short sample. The steel plates and the welded nuts can be seen in the x-ray images in Figure 3.6. Notice that the thicknesses of the steel plates are quite small compared to the overall size of the samples.

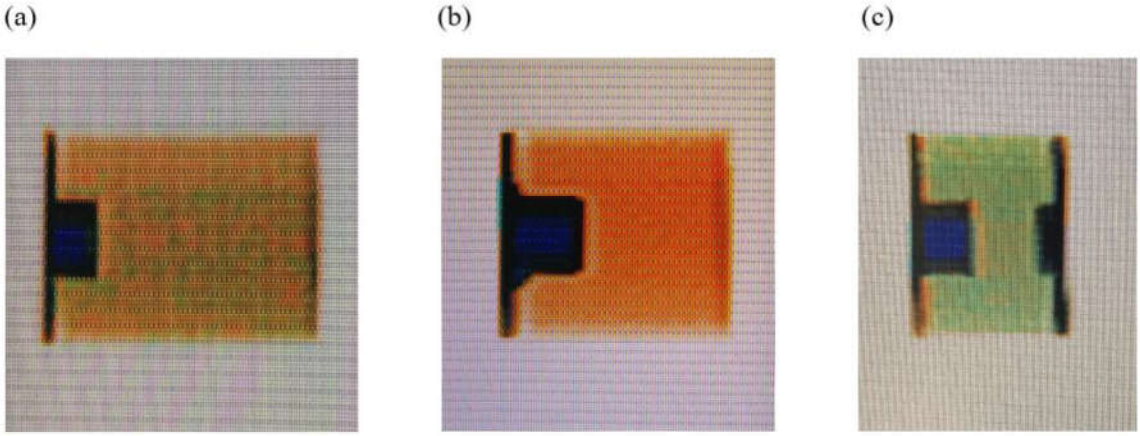


Figure 3.6. X-ray image of the (a) long sample (L_0 = 60mm, 36 Shore A hardness), (b) medium sample (L_0 = 45mm, 38 Shore A hardness) and (c) short sample (L_0 = 30mm, 40 Shore A hardness).

3.2.2. Experiments

All four test scenarios (quasi-static, ramp-and-hold, hysteresis and dynamic loading) are applied to the three material samples mentioned in the previous section. The quasi-static loading, ramp-and-hold loading, and hysteresis experiments are conducted in the Zwick / Roell Z010 testing machine (Figure 3.7a) in compression mode (Figure 3.7b) and the data is collected with the computer attached to the device (Figure 3.7c). The displacements and displacement rates are presented in Table 3.1. Notice that the long sample is compressed up to 20mm, the medium sample is compressed up to 9mm and the short sample is compressed up to 6mm for all the test scenarios, however, the displacement rates for different test scenarios are obviously different. As the x-ray image (Figure 3.6) shows, the short sample has less room for compression until the nuts that are welded to the top and bottom plates may start damaging the rubber part in between. Hence, a smaller displacement (6mm) is utilized.

Table 3.1. Displacements and displacement rates applied for quasi-static, ramp-and-hold and hysteresis tests.

		Long Sample (L_o = 60mm, 36 Shore A)	Medium Sample (L_o = 45mm, 38 Shore A)	Short Sample (L_o = 30mm, 40 Shore A)
Quasi-static	Disp	20mm	9mm	6mm
	Disp rate	2mm/min	2mm/min	2mm/min
Ramp-and-Hold	Disp	20mm	9mm	6mm
	Disp rate	1000mm/min for 1.2sec 0mm/min for 60sec	1000mm/min for 0.54sec 0mm/min for 60sec	1000mm/min for 0.36sec 0mm/min for 60sec
Hysteresis	Disp	20mm	9mm	6mm
	Disp rate	200mm/min	200mm/min	200mm/min

The testing machine is operated for the three different test scenarios (quasi-static, ramp-and-hold and hysteresis) one-by-one without changing the set-up or removing the sample between clamps and exactly the same initial conditions are obtained before each test. In other words, once the displacement is initialized, the same initial force value is reached. Hence, no permanent deformation is observed. Moreover, during the compression test with largest displacement value, the sample is visually checked, and no cracks are seen. Figure 3.8 shows the long sample in initial condition without any compression (zero displacement) and after 20mm compression during quasi-static loading.



Figure 3.7. Test setup components (a) Zwick / Roell Z010, (b) compression tools and sample and (c) computer.

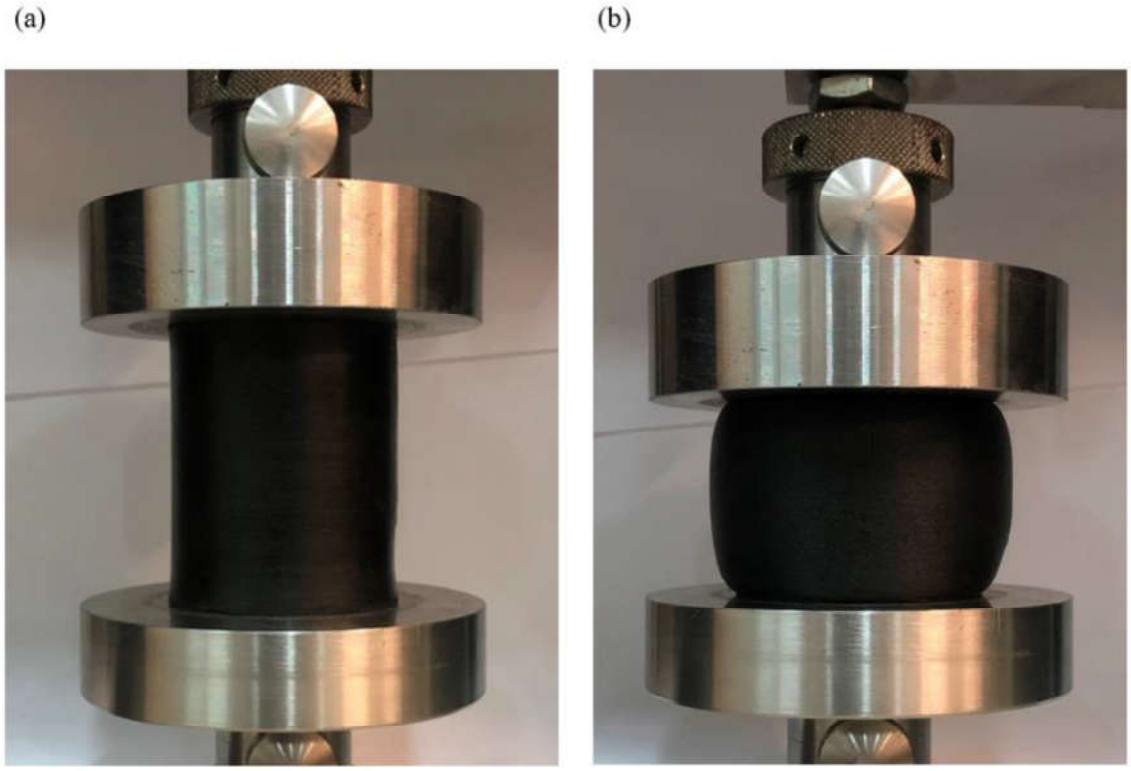


Figure 3.8. Long sample (a) initial condition without any compression and (b) after 20mm compression during quasi-static loading test.

Dynamic stiffness measurements are conducted with Ling Dynamic Systems electromagnetic shaker (LDS V450) shown in Figure 3.9. For this purpose, rubber samples are placed on top of the shaker. Moreover, a proof mass is placed on top of the rubber sample and an accelerometer is attached to the upper surface of the proof mass to measure the output vibration. In addition, there is another accelerometer is used on the bottom plate below the rubber sample to measure the input vibration. These two accelerometers are connected to a two-channel Polytec data acquisition device. By using the input and output acceleration values, the transmissibility can be obtained. The long sample is 153.5g, medium sample is 133g and short sample is 139.7g whereas the proof mass is 4000g. Electromagnetic shaker is used for excitation up to 180Hz for the long sample, up to 300Hz for the medium sample and up to 360Hz for the short sample.



Figure 3.9. Dynamic stiffness test set-up with electromagnetic shaker, the proof mass and the accelerometers.

According to the method mentioned by Koblar (Koblar and Boltezar, 2016), measured transmissibility data in real and imaginary format can be used to calculate dynamic stiffness, k_{dyn}. Figure 3.10 shows the real and imaginary parts of the transmissibility for the three samples.

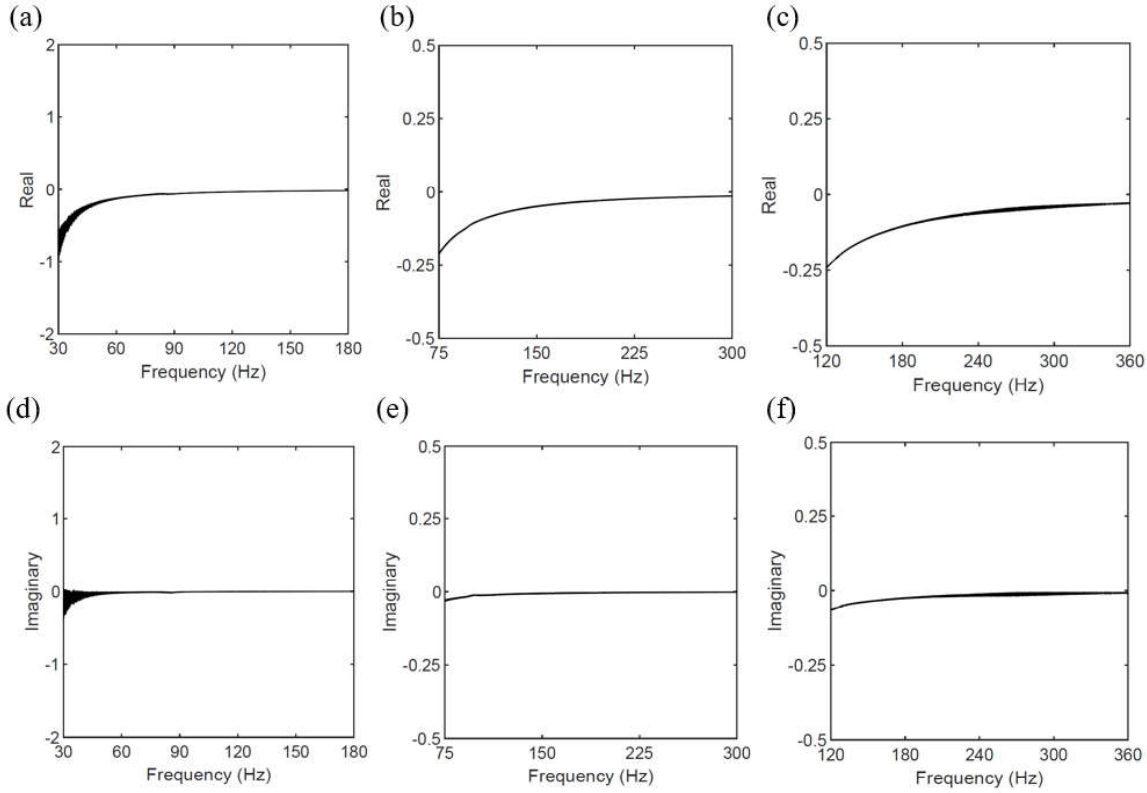


Figure 3.10. Real and imaginary parts of transmissibility for the (a) long sample real part, (b) medium sample real part, (c) short sample real part, (d) long sample imaginary part, (e) medium sample imaginary part, (f) short sample imaginary part.

Once the transmissibility data is obtained, the dynamic stiffness is calculated as

$$k_{dyn} = m_p(2\pi f)^2 \frac{Im(T)^2 + (Re(T) - 1)Re(T)}{Im(T)^2 + (Re(T) - 1)^2} \tag{3.3}$$

where m_p is the proof mass in kg, f is the frequency in Hz and $Re(T)$ and $Im(T)$ are the real and imaginary parts of the transmissibility, respectively. Due to the calculation methodology, data at low frequencies can be erroneous. Thus, low frequency data (<30Hz, <75Hz, and <120Hz for the long, medium and short samples, respectively) are not used. So, the frequency ranges for the transmissibility plots are 30-180Hz, 75-300Hz and 120-360Hz for the long, medium and short samples, respectively. Around 90Hz, there is a resonance of the shaker on its fixture, so the transmissibility plot shows some irregularity. To obtain a useful transmissibility curve for the optimization process, second order polynomial curve

fitting is used. The original data and the trend line for the long, medium and short samples are shown in Figure 3.11a, Figure 3.11b and Figure 3.11c, respectively.

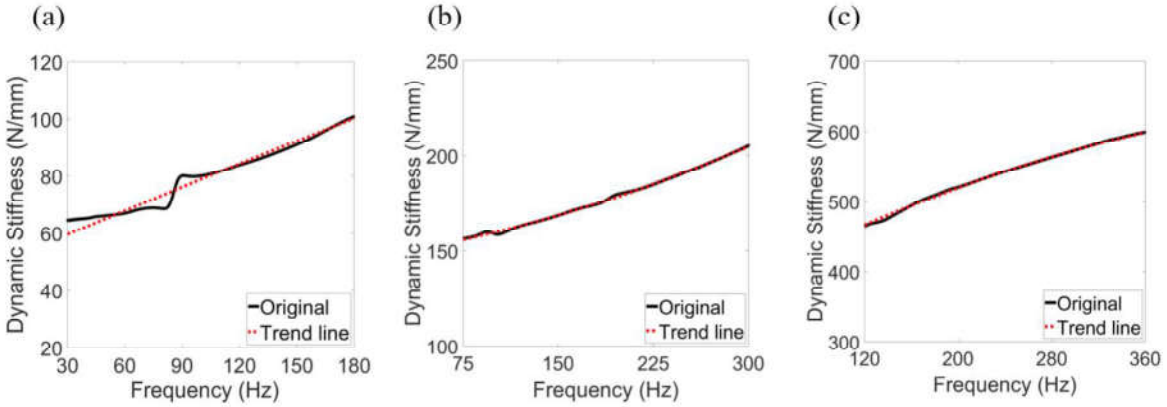


Figure 3.11. Dynamic stiffness original test data with trend line used in optimization process for the (a) long sample, (b) medium sample and (c) short sample.

3.3. Model Calibration Using Four Different Test Results

For the comparison of the test data and the model response, the parameters used for model tuning are, horizontal SLS element parallel spring k_{hs}, serially connected spring k_h, serially connected dashpot c_h, vertical SLS element parallel spring k_{vs}, serially connected spring k_v, serially connected dashpot c_v, inner arm length L_i, and initial angle of the outer mechanism α_o. Sample outer arm length L_o is equated to the sample length ($L_o = 60\text{mm}$ for the long sample, $L_o = 45\text{mm}$ for the medium sample and $L_o = 30\text{mm}$ for the short sample), hence it is not a free parameter. In summary, there are 8 tuning parameters in the model.

The long, medium and short samples are subjected to quasi-static loading, ramp-and-hold loading, hysteresis and dynamic stiffness tests. The displacements and displacement rates in quasi-static, ramp-and-hold and hysteresis tests can be seen in Table 3.1. All test scenarios are replicated in the nested linkage mechanism model and comparison of test and model responses are presented in Figures 3.12 to 3.14. It can be seen that the model fit is quite successful in all cases with some small mismatches. If the optimization process were conducted by considering only two test cases (e.g., quasi-static loading and hysteresis) as in

Figures 3.1 to 3.4, a better fit could be obtained for the selected two cases. As the aim in this study is to have a good fit to all four loading scenarios, some compromise is acceptable.

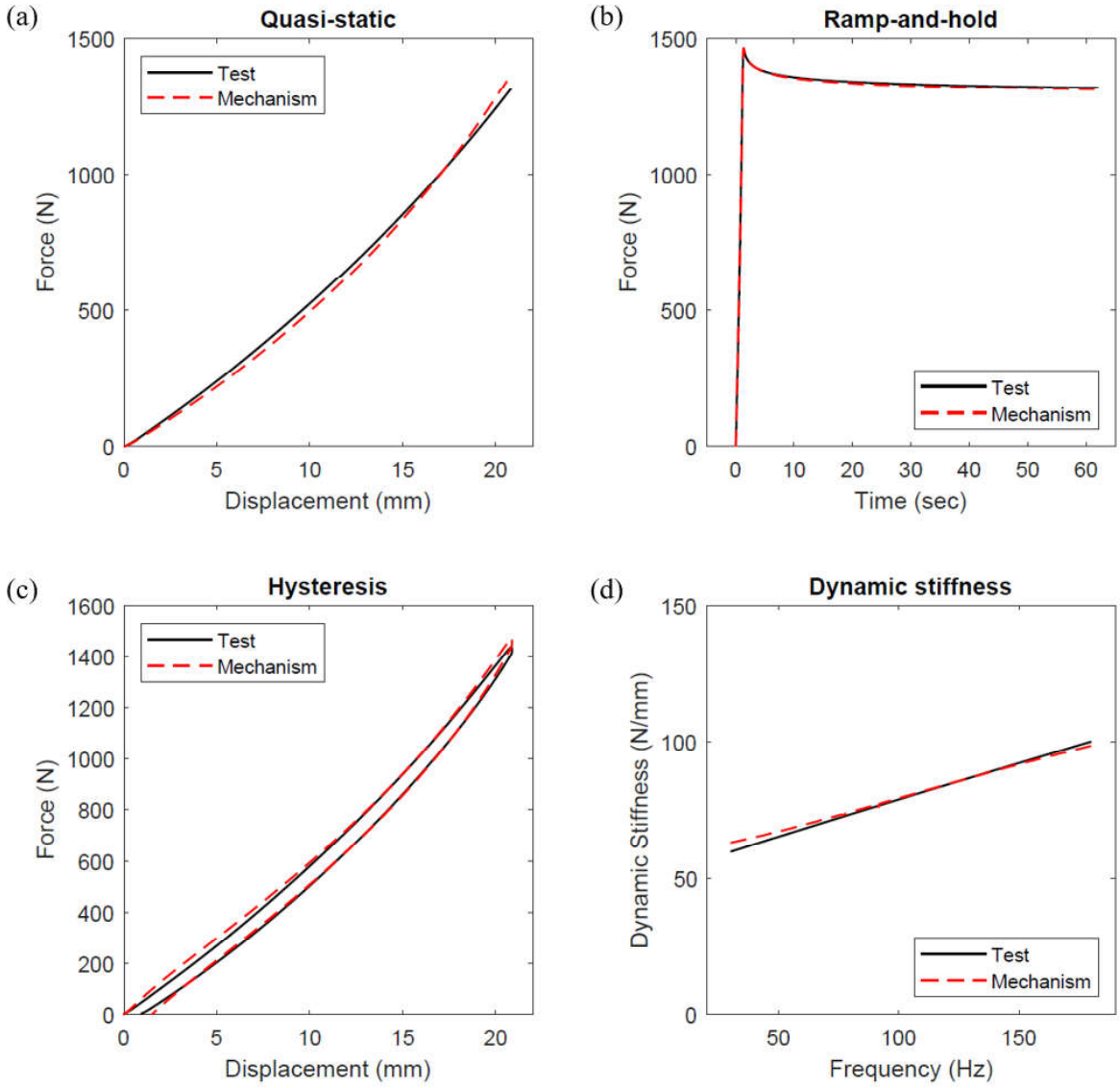


Figure 3.12. Long sample (L_0 = 60mm, 36 Shore A hardness) experimental and mechanism model response comparison. (a) quasi-static loading, (b) ramp-and-hold loading, (c) hysteresis and (d) dynamic stiffness.

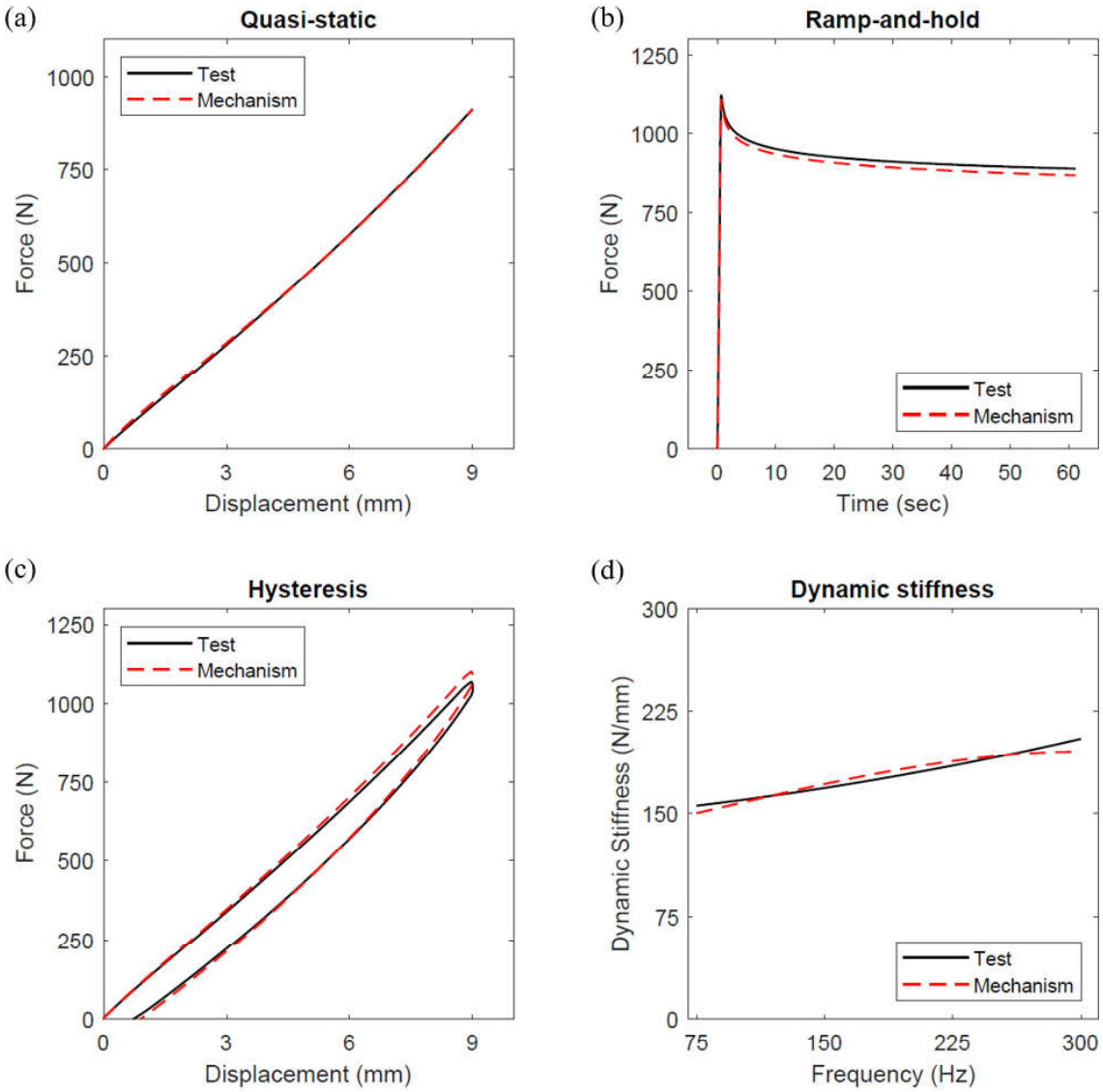


Figure 3.13. Medium sample (L_0 = 45mm, 38 Shore A hardness) experimental and mechanism model response comparison. (a) quasi-static loading, (b) ramp-and-hold loading, (c) hysteresis and (d) dynamic stiffness.

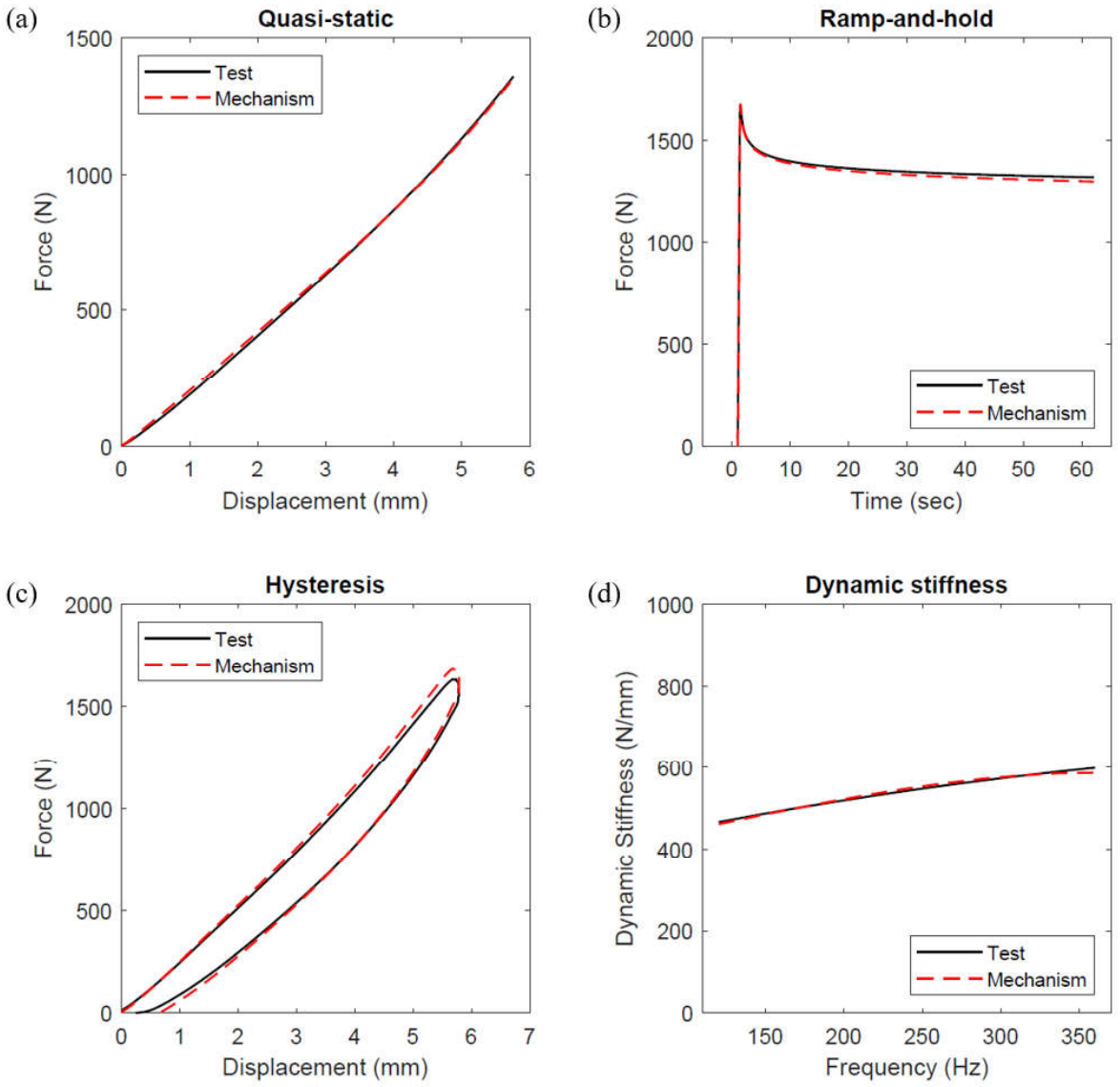


Figure 3.14. Short sample (L_0 = 30mm, 40 Shore A hardness) experimental and mechanism model response comparison. (a) quasi-static loading, (b) ramp-and-hold loading, (c) hysteresis and (d) dynamic stiffness.

Table 3.2 shows the optimally tuned parameter values for the long, medium and short samples. Long sample (L_0 = 60mm, 36 Shore A hardness) has the lowest stiffness and damping values whereas the short sample (L_0 = 30mm, 40 Shore A hardness) has the highest stiffness and damping values.

Table 3.2. Optimally tuned parameter values for the long, medium and short samples.

	Long Sample (L_0 = 60mm 36 Shore A)	Medium Sample (L_0 = 45mm 38 Shore A)	Short Sample (L_0 = 30mm 40 Shore A)
k_{hs} (N/mm)	42.08	75.9	118.6
k_h (N/mm)	0.00045	18.5	38.9
c_h (Ns/mm)	27.1	306	414.5
k_{vs} (N/mm)	0	1.04	14.71
k_v (N/mm)	1.58	30.7	324
c_v (Ns/mm)	0.0959	0.0035	0.0168
L_i (mm)	50.9	41.3	25.9
α_0 (degrees)	10.1	20.4	25.5

3.4. Comparison of Nested Linkage Mechanism model with the Well-Known Spring-Dashpot Based Models

The proposed nested linkage mechanism model and the well-known spring-dashpot based models are compared for investigating their experimental response replication capability. For this purpose, medium sample test results are used (see Figure 3.13). The well-known spring-dashpot based models are tuned to the test results in Figure 3.13. The optimized stiffness and damping values of each model calibrated according to the medium sample test data is given in Table 3.3.

Table 3.3. Optimally tuned parameter values of the Maxwell, Kelvin-Voigt and Standard Linear Solid models considering the medium sample test results in Figure 3.13.

	Maxwell	Kelvin-Voigt	Standard Linear Solid
k_s (N/mm)	-	-	99.43
k (N/mm)	355.6	99.94	97.35
c (Ns/mm)	1699.9	7.34×10^{-5}	13.43

Figure 3.15 shows the medium sample experimental responses together with the mechanism, Maxwell, Kelvin-Voigt and Standard Linear Solid model responses. It is seen that the proposed mechanism model matches very well with all four test results. However, the well-known spring-dashpot models show some discrepancies in various test results.

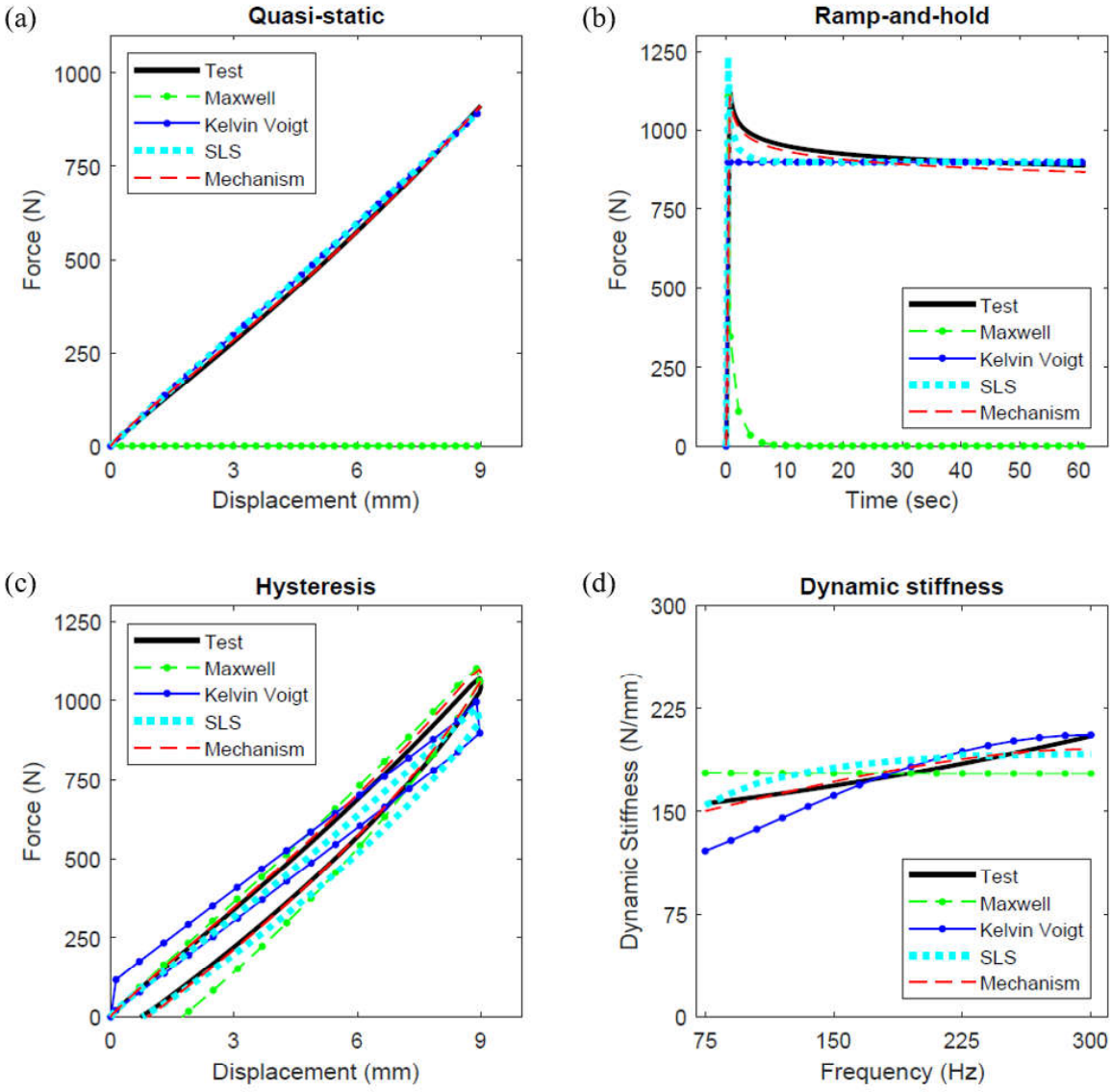


Figure 3.15. Medium sample experimental response comparison with the mechanism, Maxwell, Kelvin-Voigt and Standard Linear Solid model responses. (a) quasi-static loading, (b) ramp-and-hold loading, (c) hysteresis and (d) dynamic stiffness.

The quasi-static test result can be seen in Figure 3.15a. Notice that the sample shows some initial softening and slight hardening response and the proposed nested linkage mechanism can capture this nonlinear response. Kelvin-Voigt and Standard Linear Solid models can only show linear response (straight lines in Figure 3.15a). However, the Maxwell model fails to mimic the quasi-static test response. As a spring is serially attached to a dashpot in the Maxwell model, the dashpot absorbs all the displacement input and do not generate any resistive force due to near-zero loading speed.

The ramp-and-hold test result is shown in Figure 3.15b. The proposed mechanism model captures both the peak value and the relaxation response quite well. The Standard Linear Solid model shows some relaxation response, but the peak value and the relaxation rate are not matched well with the test result. Kelvin-Voigt model can match the steady state value, but it cannot show any relaxation behavior as there is no serially attached spring-dashpot in the model. The Maxwell model can show relaxation behavior due to the serially attached spring-dashpot, but the steady state value is zero rather than a non-zero value as in the test result. The dashpot element absorbs all the displacement input as time passes, so no reaction force remains in the steady state condition.

The hysteresis test result is depicted in Figure 3.15c. The proposed mechanism model closely matches the test result. The Standard Linear Solid model matches the initial part of the curve but fails to match the final part (peak value). The Maxwell model matches the final part of the curve but fails to match the initial part. The Kelvin-Voigt model cannot display a curved hysteresis response due to parallel attachment of the spring and dashpot in the model.

Dynamic stiffness test result can be seen in Figure 3.15d. Again, the best match can be obtained with the proposed nested linkage mechanism model. The Kelvin-Voigt and Standard Linear Solid models can show increasing dynamic stiffness behavior as frequency increases, however, the Maxwell model shows almost constant stiffness in the frequency range of interest.

When all the curves in Figure 3.15 are compared, the best matches are obtained with the proposed nested linkage mechanism model. When the responses of the well-known spring-dashpot based models are compared among themselves, the Standard Linear Solid

(SLS) model gives the best responses. As the nested linkage mechanism model contains two SLS elements, it can have dual relaxation rate. Hence, relaxation behavior is fitted more closely. Although linear springs and dashpots are used in the nested linkage mechanism model, as a result of the geometric nonlinearity of the mechanism, the linear elements displace nonlinearly and the material nonlinearity is simulated in the quasi-static, ramp-and-hold, hysteresis, and dynamic stiffness cases.

3.5. Material Response Prediction by Using the Model Calibrated with Two Test Results

Figures 3.12 to 3.14 show that the nested linkage mechanism can accurately capture the response in the four different tests once optimal parameter tuning (model calibration) is achieved using the data in all four tests. One of the aims in this study is to select two tests for model calibration and predict the response in the other two tests. If this can be achieved, the model can be tuned with less test responses but still can predict the other test responses to save time and effort. As there are four different tests, there are six different double combinations ($C(4,2) = 4!/(2! \times 2!) = 6$) for the calibration tests.

A DOE study is conducted, and it is seen that dynamic stiffness test result is the hardest to predict by using the other test results whereas quasi-static test result is easiest to predict as there is no damping effect due to very slow loading rate. Hence, dynamic stiffness test scenario is selected as one of the calibration tests. The second calibration test can be ramp-and-hold or hysteresis test scenario. Consequently, for long, medium and short samples, both ramp-and-hold & dynamic stiffness and hysteresis & dynamic stiffness test scenarios are investigated in detail. Table 3.4 shows the optimally tuned parameter values in these cases.

Table 3.4. Optimally tuned parameter values obtained by only using ramp-and-hold & dynamic stiffness or hysteresis & dynamic stiffness test results of the long, medium and short samples.

	Long Sample		Medium Sample		Short Sample	
	(L_0 = 60mm, 36 Shore A)		(L_0 = 45mm, 38 Shore A)		(L_0 = 30mm, 40 Shore A)	
	Ramp-and-hold & Dynamic stiffness	Hysteresis & Dynamic Stiffness	Ramp-and-hold & Dynamic stiffness	Hysteresis & Dynamic Stiffness	Ramp-and-hold & Dynamic stiffness	Hysteresis & Dynamic Stiffness
k_{hs} (N/mm)	39.95	39.8	123.1	112.9	101.3	74.94
k_h (N/mm)	2.48	3.64	0.16	0.197	9.68	9.68
c_h (Ns/mm)	1.031	1.68	455	987.9	21.6	98.8
k_{vs} (N/mm)	0.00243	0	2.02×10^{-5}	0.284	34.2	37.7
k_v (N/mm)	3.03	2.12	3.63	4.02	312	324
c_v (Ns/mm)	1.097	0.796	4.8×10^{-4}	2.58×10^{-4}	0.0259	0.0261
L_i (mm)	52.1	52.1	44.8	44.3	24.7	23.7
α_0 (degrees)	16.3	15.3	19.2	18.8	27.8	27.7

In Figure 3.16, Figure 3.17 and Figure 3.18, the nested linkage mechanism model is calibrated using ramp-and-hold and dynamic stiffness test results of the long, medium and short samples, respectively. It can be seen that ramp-and-hold and dynamic stiffness test scenarios for each sample have very good fits since the model is tuned for these two test scenarios. The other two test responses, i.e., quasi-static and hysteresis loading are predicted by using the tuned parameter values. Although there is some mismatch in the predictions, general trends are captured well.

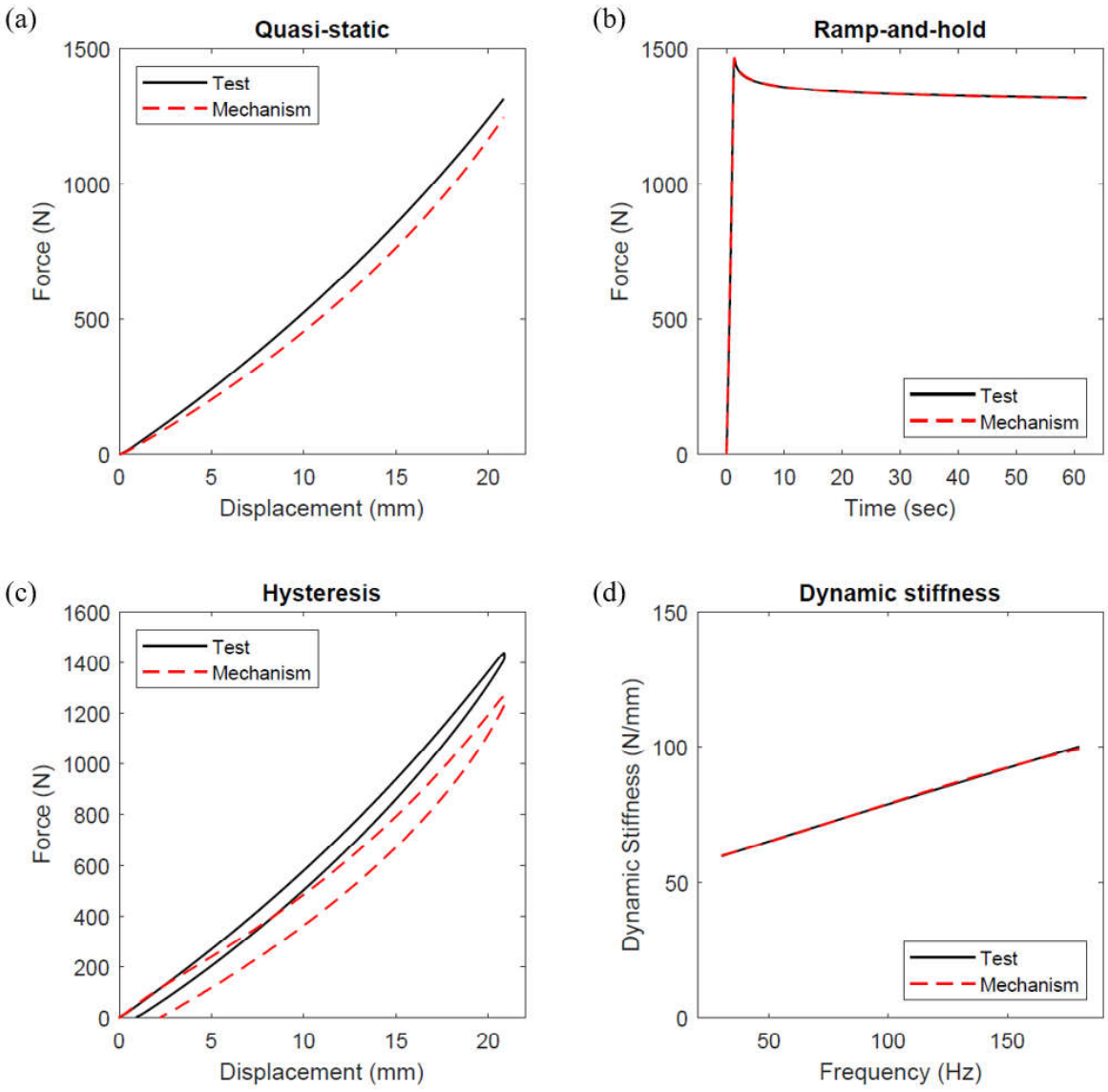


Figure 3.16. Long sample experimental and mechanism model response comparison. (a) quasi-static loading, (b) ramp-and-hold loading, (c) hysteresis and (d) dynamic stiffness. Model is tuned using ramp-and-hold and dynamic stiffness responses only.

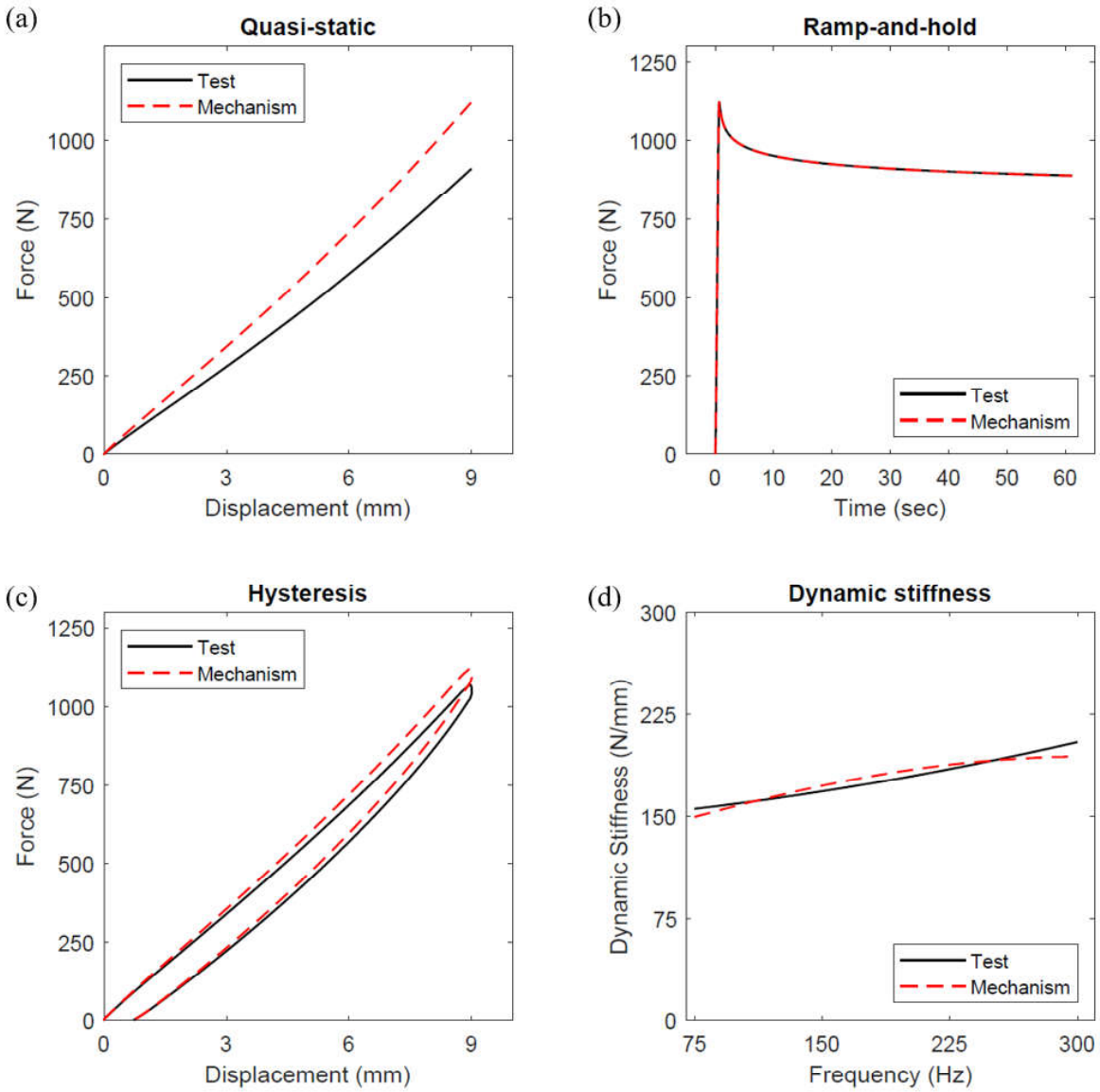


Figure 3.17. Medium sample experimental and mechanism model response comparison. (a) quasi-static loading, (b) ramp-and-hold loading, (c) hysteresis and (d) dynamic stiffness. Model is tuned using ramp-and-hold and dynamic stiffness responses only.

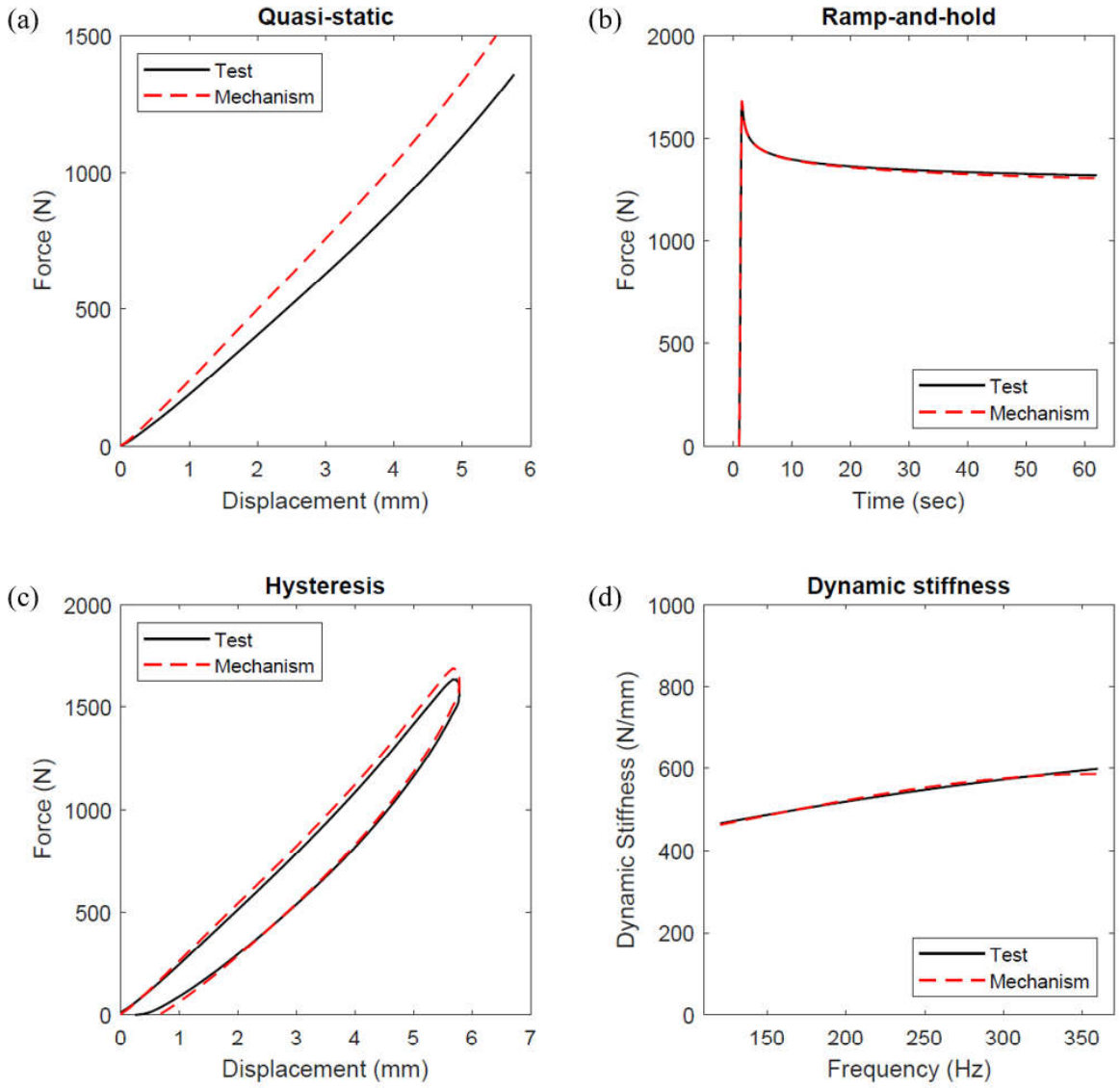


Figure 3.18. Short sample experimental and mechanism model response comparison. (a) quasi-static loading, (b) ramp-and-hold loading, (c) hysteresis and (d) dynamic stiffness. Model is tuned using ramp-and-hold and dynamic stiffness responses only.

In Figure 3.19, Figure 3.20 and Figure 3.21, the nested linkage mechanism model is calibrated using hysteresis and dynamic stiffness test results of the long, medium and short samples, respectively. As expected, hysteresis and dynamic stiffness test scenarios have very good fits since the model is tuned for these two test scenarios. The other two test responses, i.e., quasi-static and ramp-and-hold loading, are tried to be predicted by using the tuned parameter values. Although there are some small mismatches, the trends of quasi-static responses are predicted well for all the samples. Moreover, response regarding the ramp-and-hold scenario is predicted quite accurately for the medium and short samples. On the

other hand, response prediction for the long sample has significant downshift. Ramp-and-hold scenario is very sensitive to the damping coefficients in the model. In the hysteresis graph (Figure 3.19c) the loading and unloading curves are very close to each other. Hence, the long sample has low damping. Capturing the response in the presence of low damping is hard. Consequently, ramp-and-hold loading scenario prediction is not very successful for the long sample.

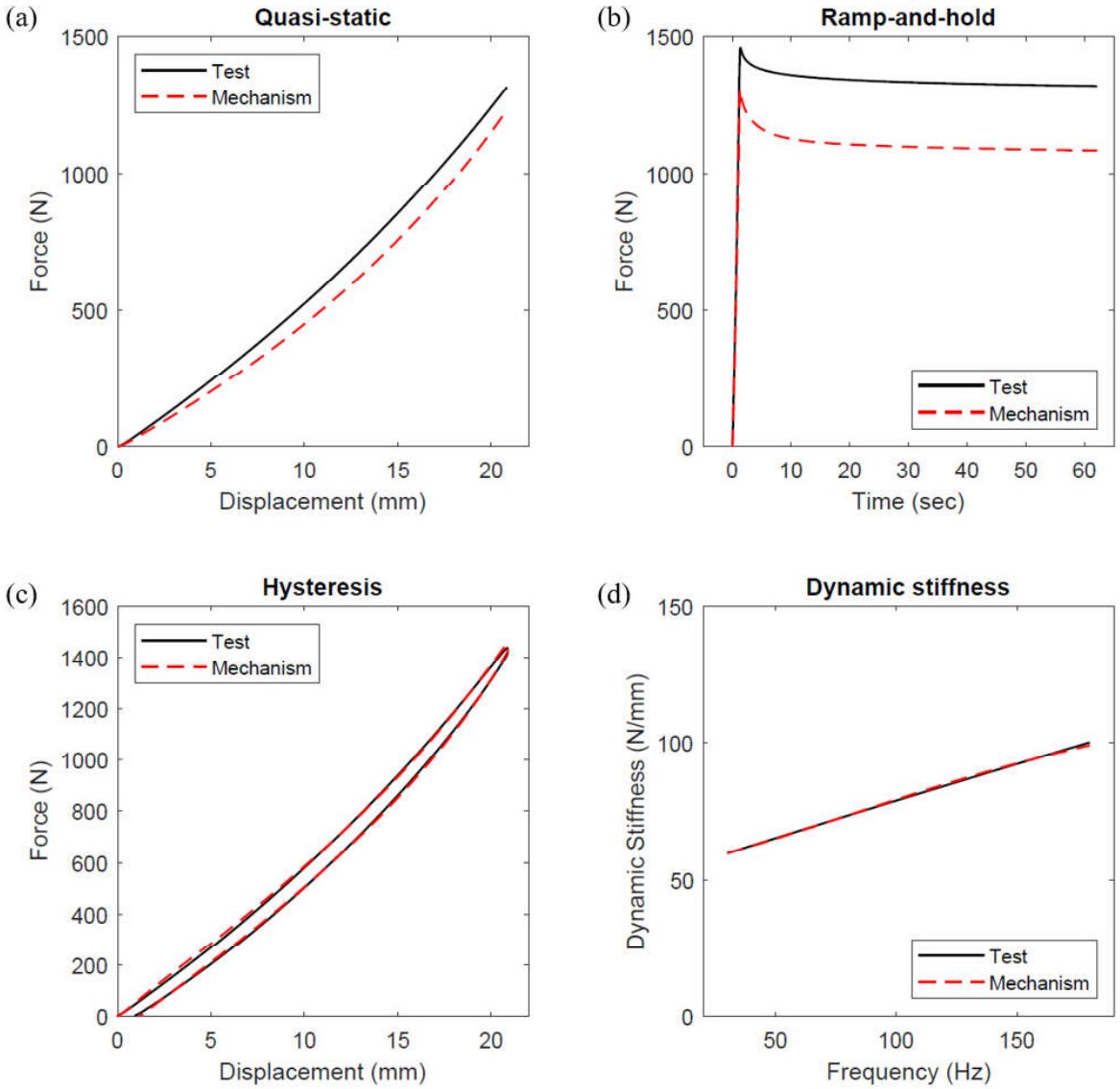


Figure 3.19. Long sample experimental and mechanism model response comparison. (a) quasi-static loading, (b) ramp-and-hold loading, (c) hysteresis and (d) dynamic stiffness. Model is tuned using hysteresis and dynamic stiffness responses only.

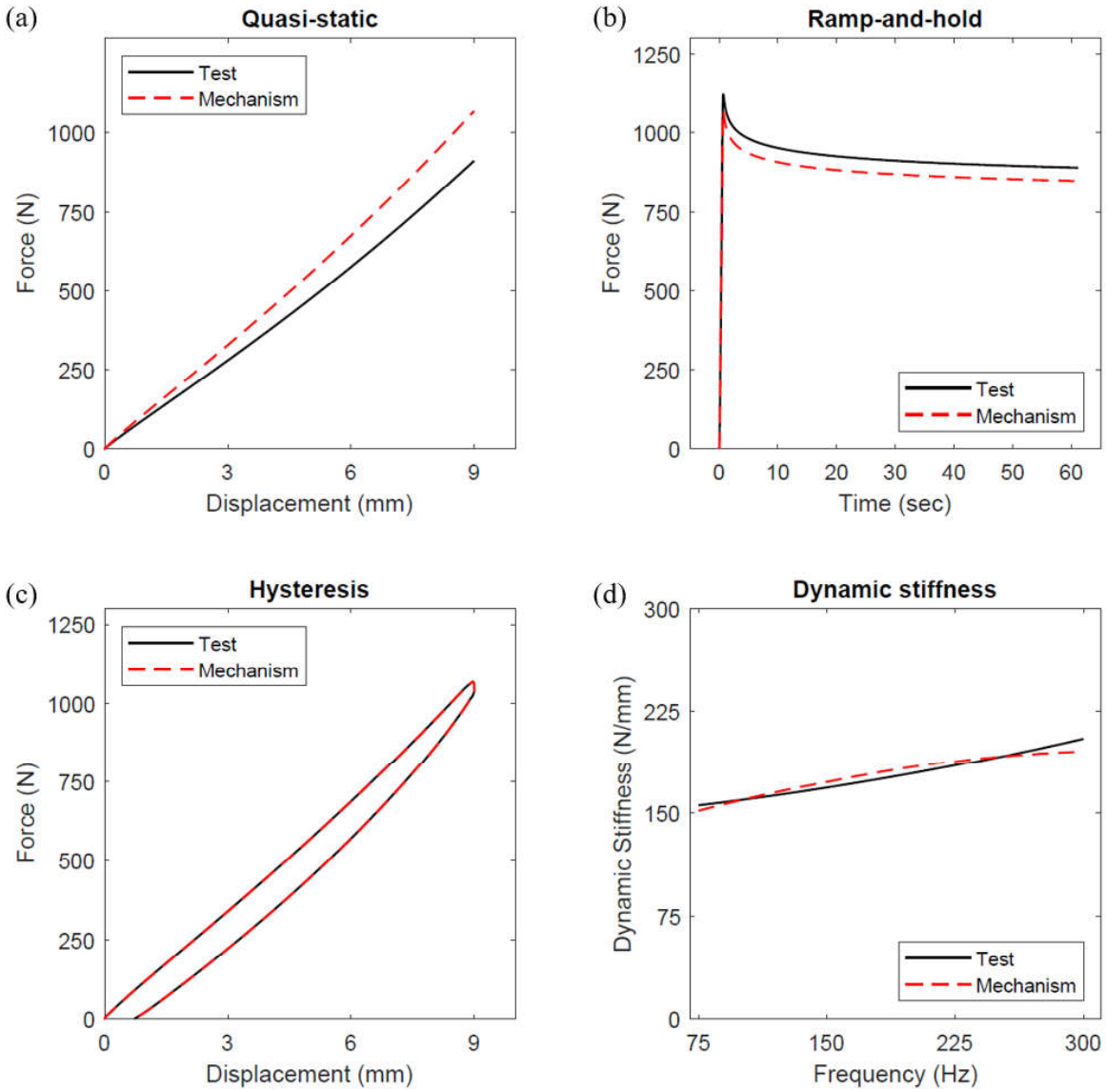


Figure 3.20. Medium sample experimental and mechanism model response comparison. (a) quasi-static loading, (b) ramp-and-hold loading, (c) hysteresis and (d) dynamic stiffness. Model is tuned using hysteresis and dynamic stiffness responses only.

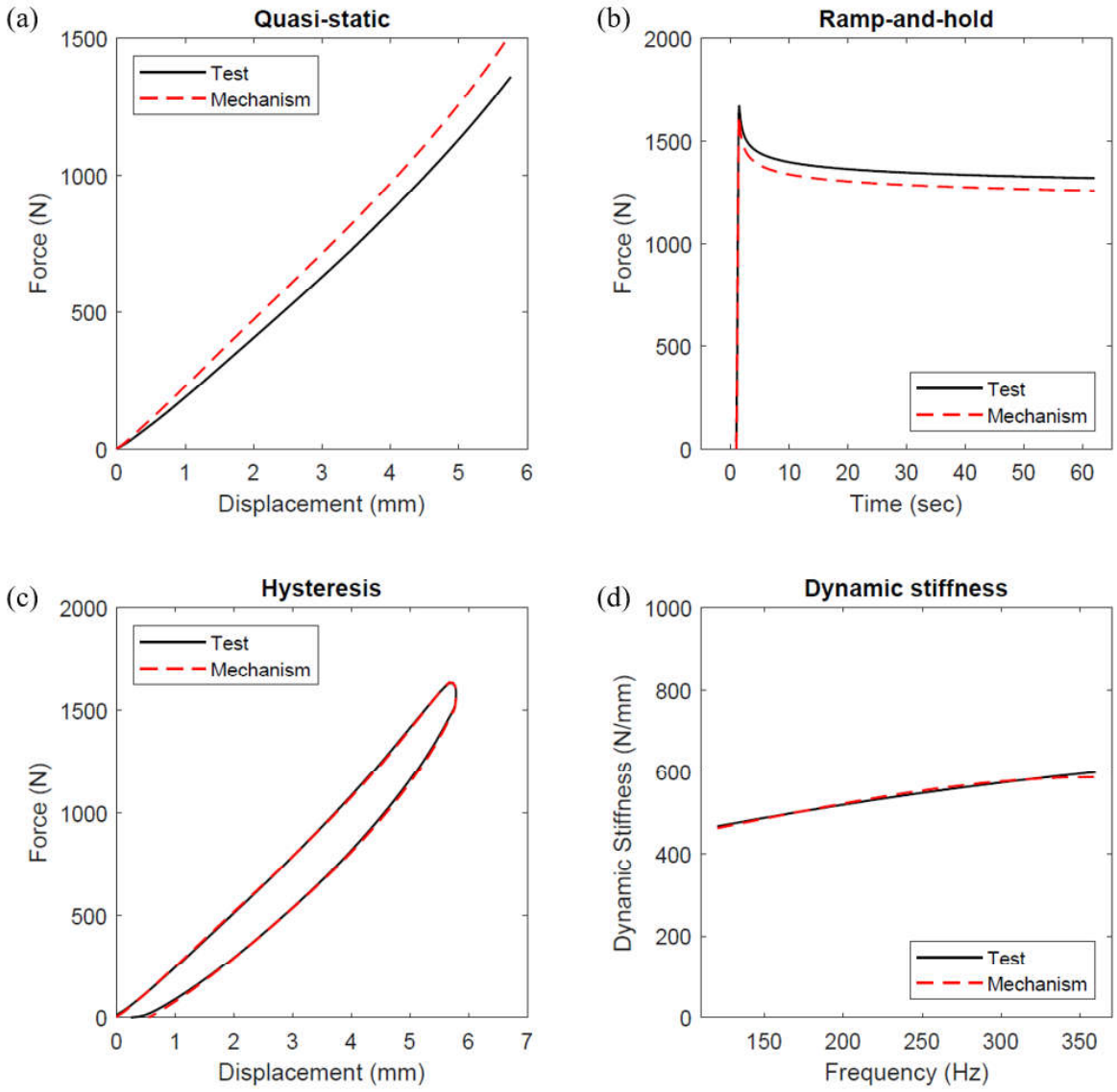


Figure 3.21. Short sample experimental and mechanism model response comparison. (a) quasi-static loading, (b) ramp-and-hold loading, (c) hysteresis and (d) dynamic stiffness. Model is tuned using hysteresis and dynamic stiffness responses only.

When Figures 3.17 to 3.21 are compared, one can see that the best fits are in Figure 3.21. Ramp-and-hold scenario is very sensitive to the damping coefficients in the model. In the hysteresis graph of the long sample Figure 3.19c the loading and unloading curves are very close to each other. Hence, the long sample has low damping. Capturing the response in the presence of low damping is hard. However, the hysteresis graph of the short sample Figure 3.21c shows that there is higher amount of damping. Consequently, ramp-and-hold loading scenario prediction is better for the short sample (please compare Figure 3.19b and Figure 3.21b).

3.6. Material Response Prediction for Different Size Samples

In order to further assess the prediction capability of the nested linkage mechanism model, parameters are obtained for a sample and the responses of a sample from the same material with a different size is estimated for the four test scenarios. The medium sample is selected as the primary sample since its shore hardness value and height is right between all three samples. Another medium sample is used for this study, which is obtained from the same manufactured batch of the original medium sample and experimentally validated as having the same material responses in all four tests. Figure 3.22 show the test set-up using two identical samples in parallel. Photo is taken after 9mm compression for ramp-and-hold loading scenario applied.

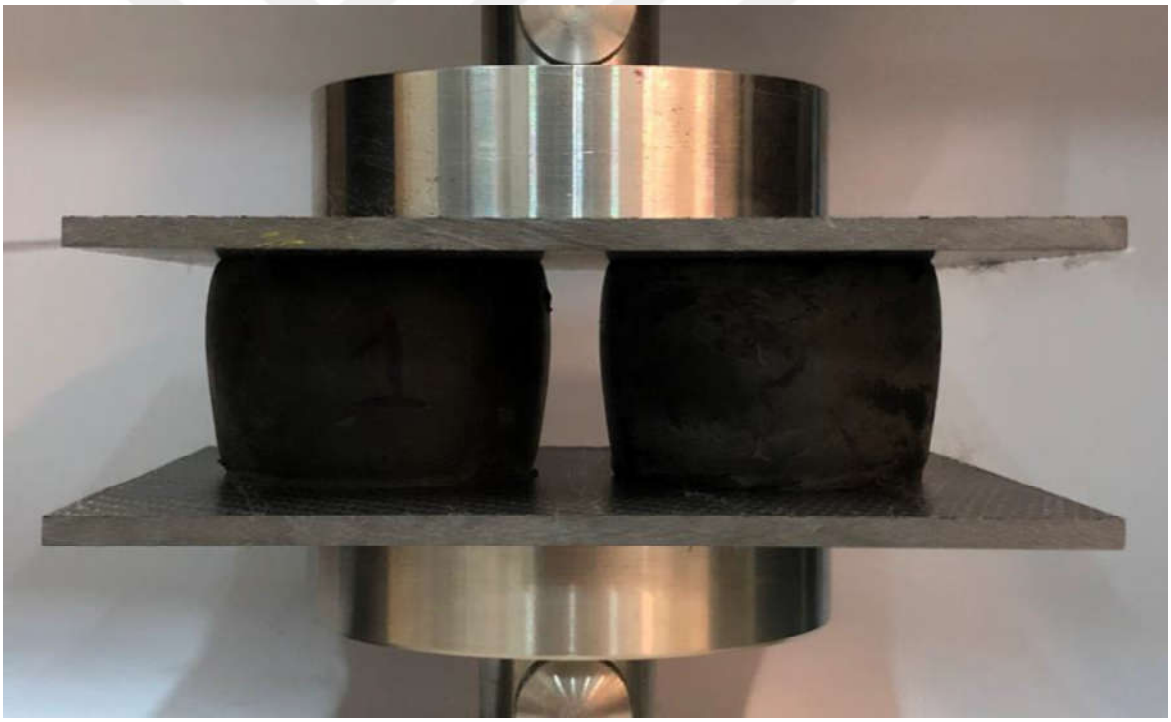


Figure 3.22. Double medium sample experimental test setup. Samples are under 9mm compression state.

Model calibration was achieved for the medium sample, as shown in Figure 3.13. To obtain the response of a sample from the same material and height but with double cross-sectional area, the two medium samples are positioned side-by-side in parallel configuration so that they act as a material with double cross-sectional area. Then, the four test scenarios are applied for this material with double cross-sectional area.

The test results of the double cross-sectional area sample can be predicted by using the parameters of a single medium sample. Among the 8 parameters regarding the medium sample in Table 3.2, L_i and α_o values are not changed since height of the material is not changed, however, all the other parameters are doubled as the cross-sectional area is doubled. Figure 3.23 shows the experimental response of the double cross-sectional area sample, the mechanism model fit using the test results of the double cross-sectional area sample, and the prediction using the parameters regarding a single medium sample. It can be seen that the prediction is quite successful in all four tests.

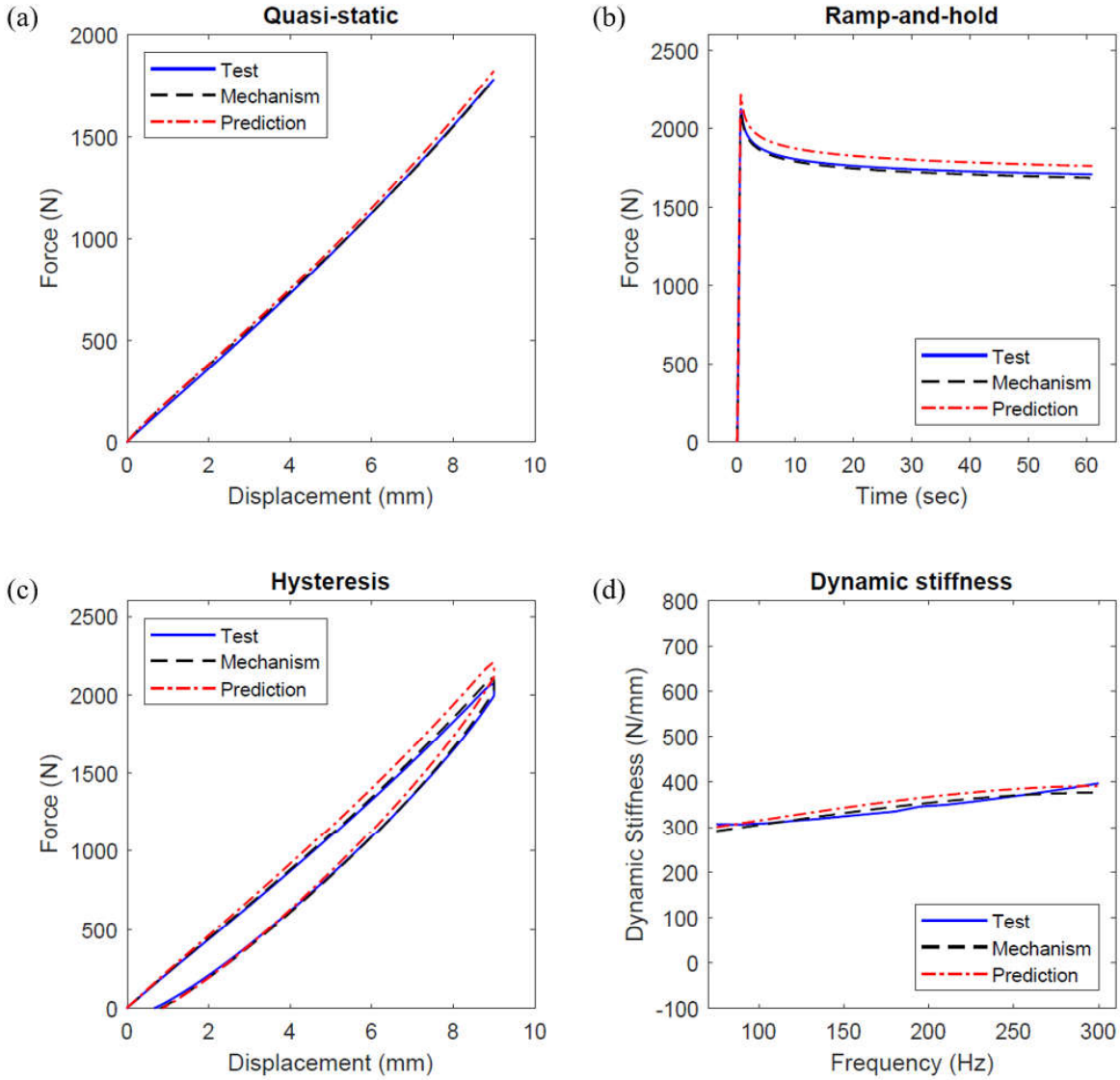


Figure 3.23. Double medium sample experimental response, its mechanism model fit and predicted model response comparison. (a) quasi-static loading, (b) ramp-and-hold loading, (c) hysteresis and (d) dynamic stiffness.

3.7. Calibration of a Reduced Model with Five Parameters Using Four Different Test Results

One of the aims in this study is to evaluate the response of the nested linkage mechanism with reduced number of parameters. Up to now, 8 parameters (L_i, α_o, 3 parameters for the horizontal SLS element, i.e., k_{hs}, k_h, c_h and 3 parameters for the vertical SLS element, i.e., k_{vs}, k_v, c_v) are used in the optimization process. As seen in Figure 3.12, Figure 3.13 and Figure 3.14, fits to all four tests are quite satisfactory. Notice that in Figure 3.12a, Figure 3.13a and Figure 3.14a the samples show slight hardening response. Therefore, both softening and hardening character is not needed for these three samples. It is shown in Section 2.3. that the vertical SLS element directly affects the initial softening behavior of the quasi-static-loading response. Other than quasi-static loading scenario, the other three test scenarios are also affected by the vertical SLS element, but for the aim of reducing the number of parameters, vertical SLS element is deleted as seen in Figure 3.24. Consequently, the number of parameters in the model is reduced from 8 to 5. Then, all four test results are fitted by only using the parameters related to the horizontal SLS element (k_{hs}, k_h, c_h) and the linkage mechanism (L_i, α_0).

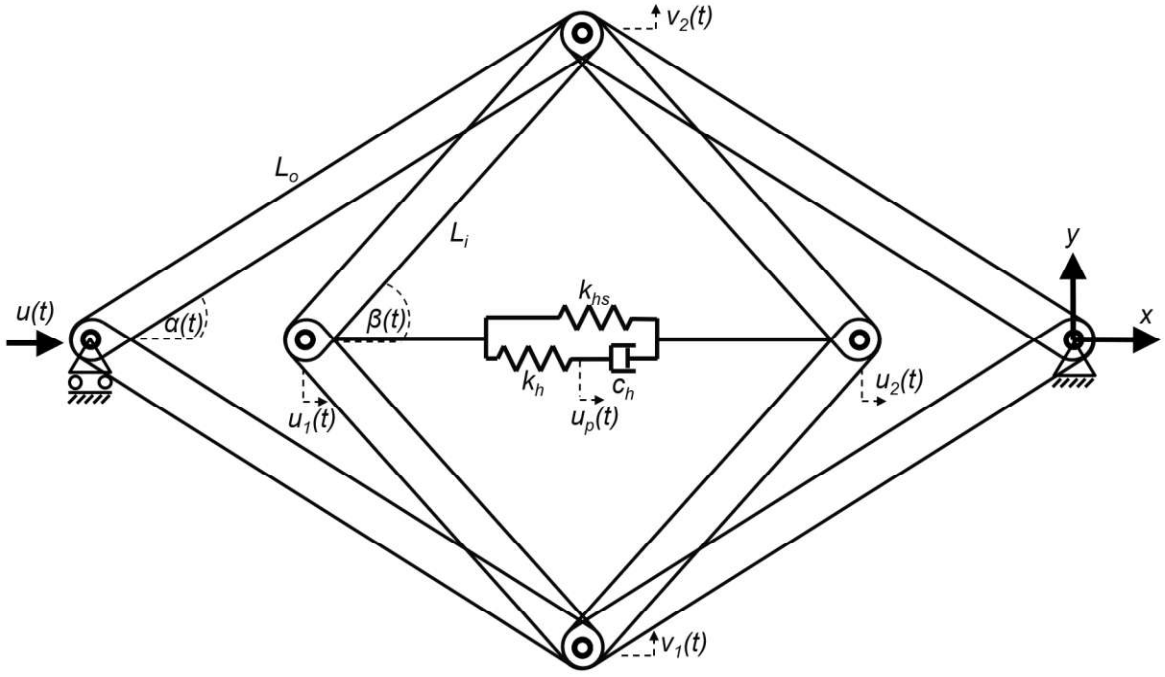


Figure 3.24. Nested linkage mechanism without vertical SLS element.

Figure 3.25, Figure 3.26 and Figure 3.27 show the response of the reduced model with 5 tuning parameters in comparison with the test results of the long, medium and short samples, respectively. Although there are some errors, all four test results are quite accurately replicated considering all the samples. Even though Figure 3.12, Figure 3.13 and Figure 3.14 give more accurate fits with 8 tuning parameters, Figure 3.25, Figure 3.26 and Figure 3.27 give acceptable fits with only 5 tuning parameters.

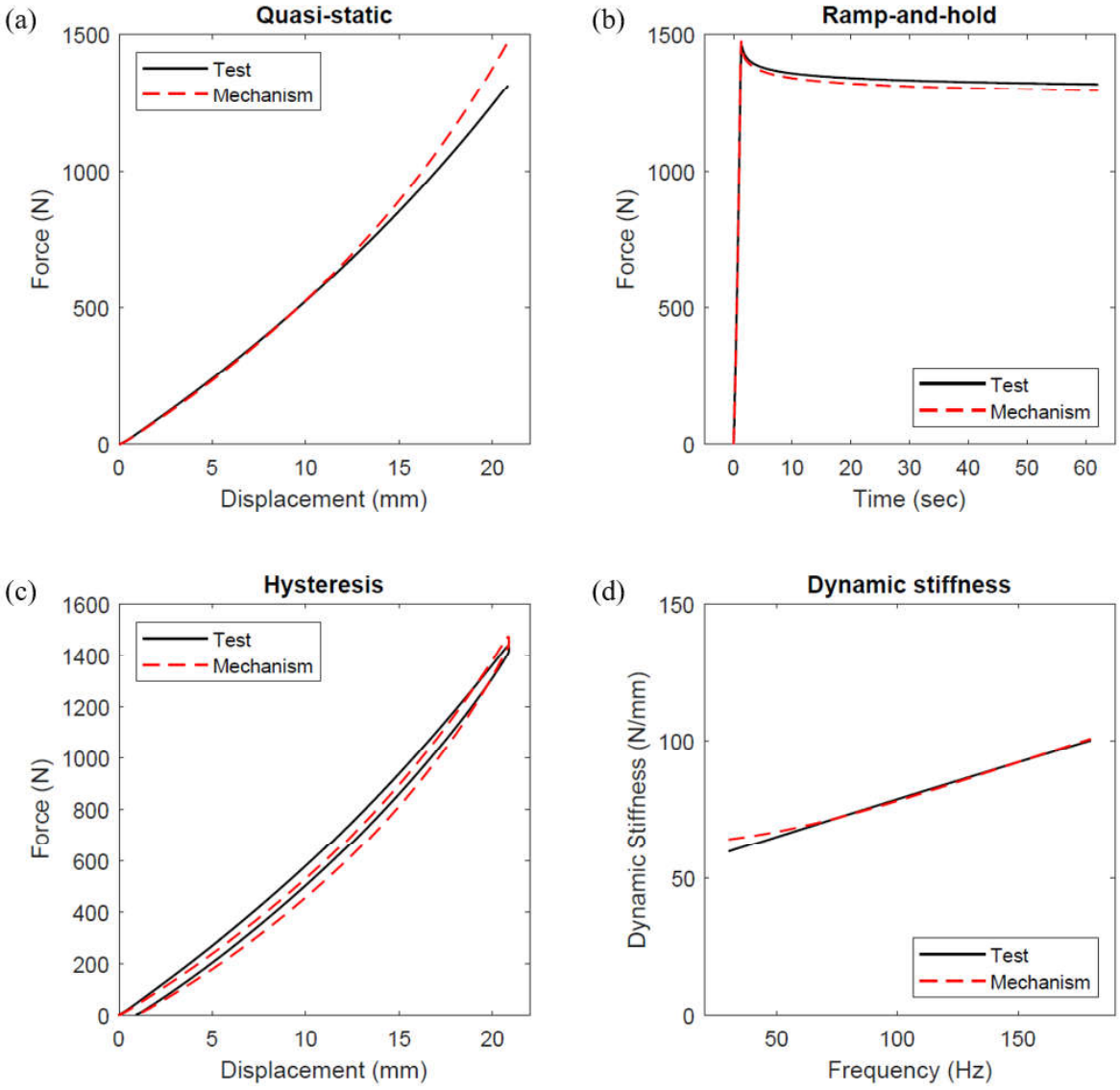


Figure 3.25. Long sample experimental and reduced mechanism model (w/o vertical SLS element) response comparison. (a) quasi-static loading, (b) ramp-and-hold loading, (c) hysteresis and (d) dynamic stiffness.

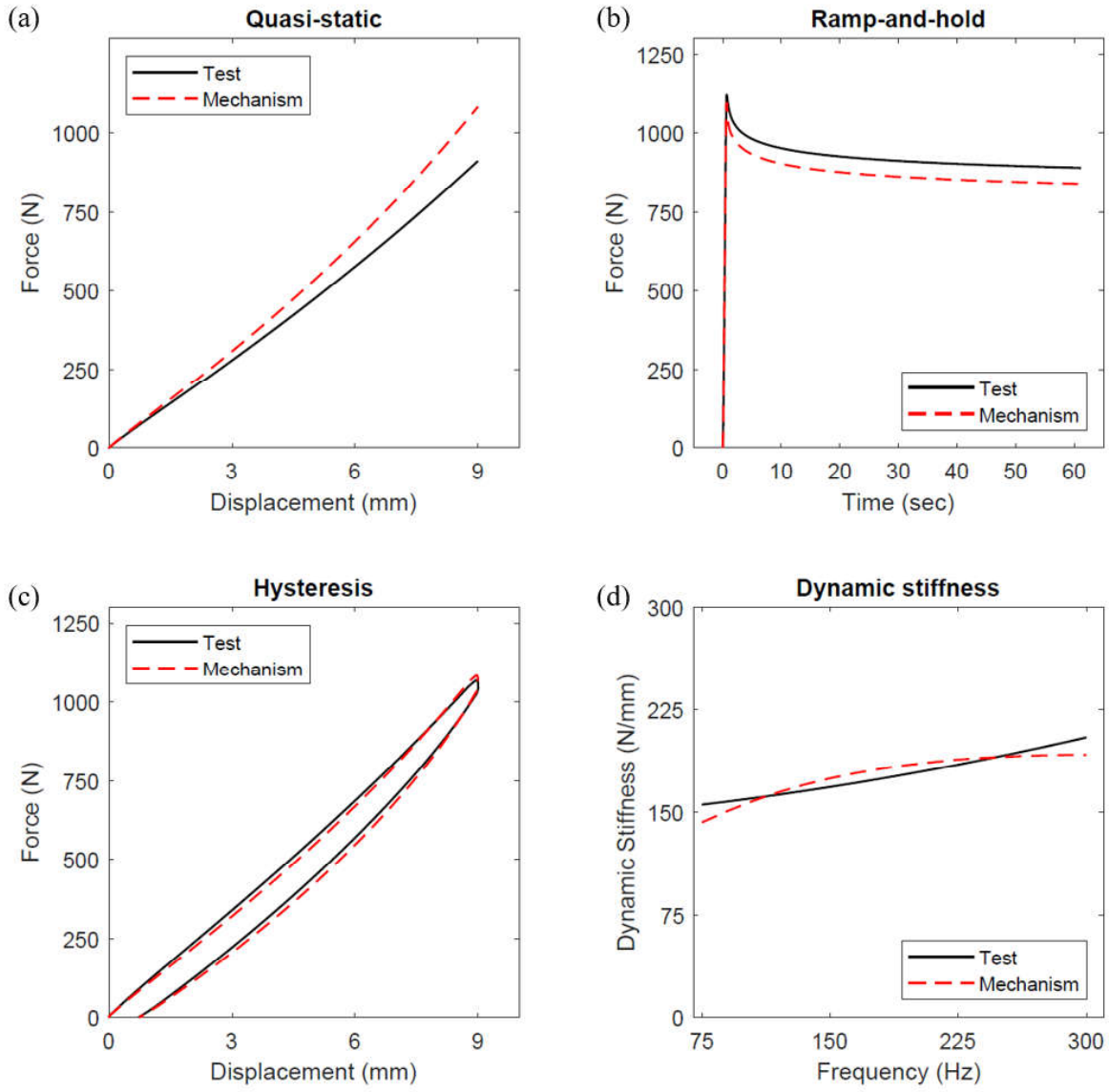


Figure 3.26. Medium sample experimental and reduced mechanism model (w/o vertical SLS element) response comparison. (a) quasi-static loading, (b) ramp-and-hold loading, (c) hysteresis and (d) dynamic stiffness.

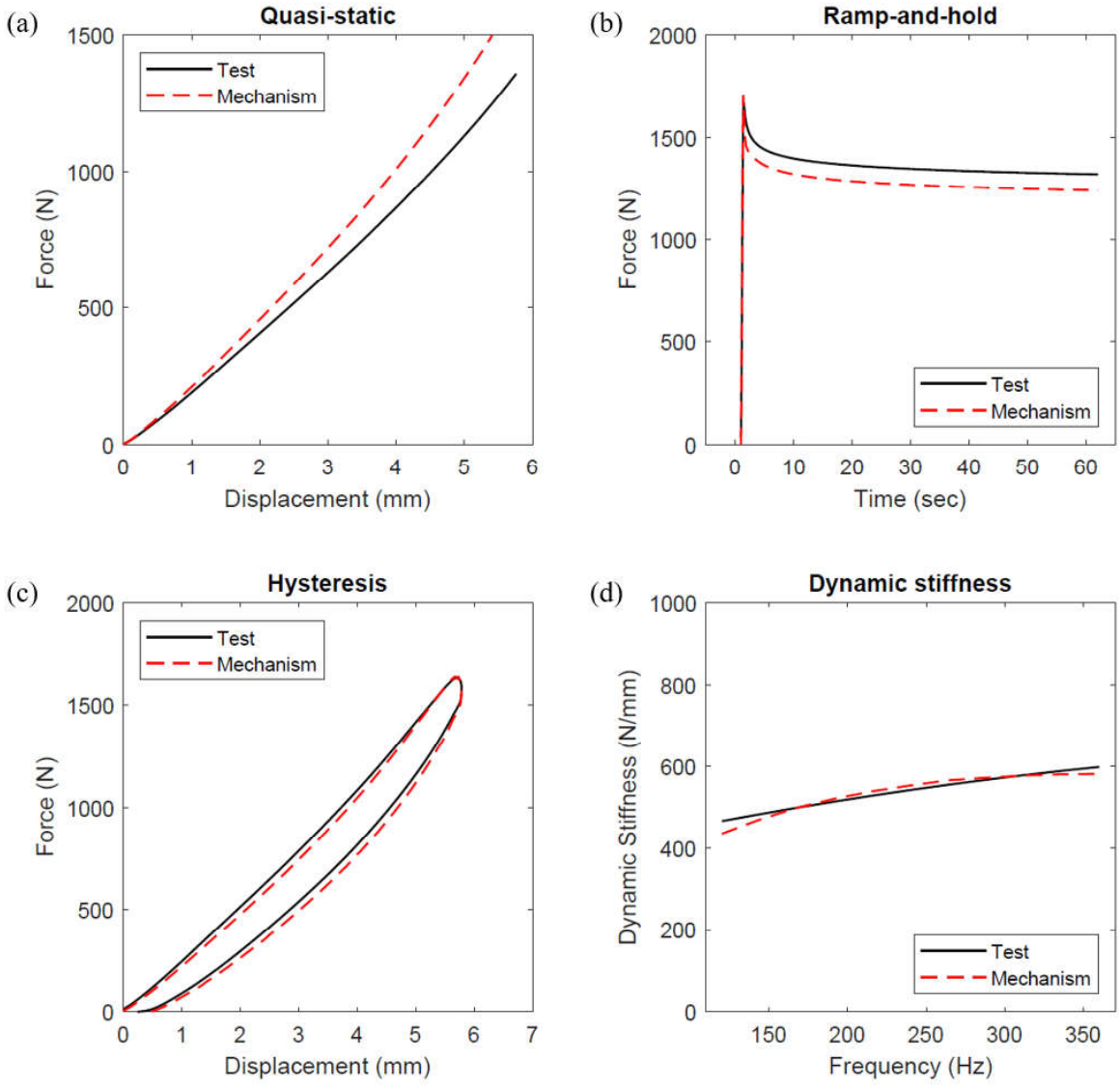


Figure 3.27. Short sample experimental and reduced mechanism model (w/o vertical SLS element) response comparison. (a) quasi-static loading, (b) ramp-and-hold loading, (c) hysteresis and (d) dynamic stiffness.

Table 3.5 shows the optimally tuned parameter values of the reduced model for the long, medium and short samples. As there is no vertical SLS element in the reduced model, the stiffness and damping characteristics of the samples are tried to be captured by only the horizontal SLS elements. Consequently, the parameter values in Table 3.5 are quite different from the ones in Table 3.2, which are provided for the full model with 8 parameters.

Table 3.5. Optimally tuned parameter values of the reduced model (w/o vertical SLS element) for the long, medium and short samples.

	Long Sample (L_0 = 60mm 36 Shore A)	Medium Sample (L_0 = 45mm 38 Shore A)	Short Sample (L_0 = 30mm 40 Shore A)
k_{hs} (N/mm)	42.9	71.8	166.9
k_h (N/mm)	88.9	62.2	256.1
c_h (Ns/mm)	0.016	0.086	0.267
L_i (mm)	49.9	37.6	25.5
α_0 (degrees)	8	19.3	23.6

4. CONCLUSIONS

A mechanism model is proposed to simulate the response of nonlinear viscoelastic materials under quasi-static, ramp-and-hold, hysteresis, and dynamic loading conditions. The geometric nonlinearity of the mechanism arising from the two nested four-bar linkages is used to mimic material nonlinearity. Various parametric studies are conducted to show the versatility of the proposed mechanism model in capturing the response under the aforementioned four different loading conditions. Comparisons with the experimental results obtained in previous studies show that the proposed mechanism model successfully represents nonlinear responses of nonlinear viscoelastic materials.

An experimental investigation is conducted on three different rubber samples under these four different test scenarios. The model successfully mimicked all four test scenarios for the three samples with different stiffness and damping characteristics. It is shown that once the experimental data are provided for a sample for these four different tests, the model can be optimized to capture the material behaviour in these different tests with the same set of parameters. This is an important outcome, even though the model is only composed of linear springs, linear dashpots and linkages, and yet it can provide accurate nonlinear viscoelastic material response for these four different tests. In order to evaluate the prediction capability of the nested linkage mechanism model, parameters of the model are calibrated by using only two test scenarios and the responses in the other two test scenarios are validated. It is seen that dynamic stiffness and hysteresis loading tests or dynamics stiffness and ramp-and-hold loading tests can be used in model calibration. It is shown that response prediction is more successful for materials with higher damping. Moreover, material prediction capability of the nested mechanism model is assessed by obtaining the model parameters for the medium sample and predicting the response of a sample from the same material and height but with double cross-sectional area. The successful prediction shows that once the values of the model parameters are obtained for a sample, its response can be predicted if its size changes. Finally, considering the hardening behaviour of the samples, the number of parameters in the nested linkage mechanism model is reduced from 8 to 5 and it is shown that the reduced model also gives quite satisfactory results.

The mechanism model introduced in this study contains basic structural elements, i.e., links, linear springs, and dashpots. Hence, it can be physically realized. It can be used in various applications as a mechanical system behaving like a rubber. While exhibiting the mechanical response of rubber, the system would not have the undesired properties of rubber like thermal degradation or aging. Considering that individual parts are easily replaceable, the mechanism can be tuned to obtain the desired response.

REFERENCES

Abe, M., J. Yoshida and Y. Fujino, 2004, "Multiaxial Behaviors of Laminated Rubber Bearings and Their Modeling. II: Modelling", *Journal of Structural Engineering*, Vol.130, pp.1133-1144.

Acar, G. and C. Yilmaz, 2013, "Experimental and Numerical Evidence for the Existence of Wide and Deep Phononic Gaps Induced by Inertial Amplification in Two-Dimensional Solid Structures", *Journal of Sound and Vibration*, Vol. 332, pp. 6389-6404.

Agoras, M., O. Lopez-Pamies and P. P. Castaneda, 2009, "A General Hyperelastic Model for Incompressible Fiber-Reinforced Elastomers", *Journal of Mechanics and Physics of Solids*, Vol. 57, pp. 268-286.

Bergstrom, J. S. and M. C. Boyce, 1998, "Constitutive Modeling of the Large Strain Time-Dependent Behavior of Elastomers", *Journal of the Mechanics and Physics of Solids*, Vol. 46, pp. 931-954.

Bergstrom, J. S. and M. C. Boyce, 2000, "Large Strain Time-Dependent Behavior of Filled Elastomers", *Mechanics of Materials*, Vol. 32, pp. 627-644.

Bhuiyan, A. R., Y. Okui, H. Mitamura and T. Imai, 2009, "A Rheology Model of High Damping Rubber Bearings for Seismic Analysis: Identification of Nonlinear Viscosity", *International Journal of Solids and Structures*, Vol. 46, pp. 1778-1792.

Buhan, M. D., A. Gloria, P. L. Tallec and M. Vidrascu, 2015, "Reconstruction of a Constitutive Law for Rubber from in Silico Experiments Using Ogden's Laws", *International Journal of Solids and Structures*, Vol. 62, pp. 158-173.

Carleo, F., J. J. C Busfield, R. Whear and E. Barbieri, 2017, "A New Constitutive Model for Carbon-Black Reinforced Rubber in Medium Dynamic Strains and Medium Strain Rates", *10th European Conference on Constitutive Models for Rubber, ECCMR X*, Munich, Germany 28-31, August, pp. 115-119.

Ciambella, J., A. Paolone and S. Vidoli, 2010, "A Comparison of Nonlinear Integral-Based Viscoelastic Models Through Compression Tests on Filled Rubber", *Mechanics of Materials*, Vol 42, pp. 932-944.

Drozdov, A. D., 1997, "A Constitutive Model for Nonlinear Viscoelastic Media", *International Journal of Solids and Structures*, Vol. 34, pp. 2685-2707.

Feng, B. and R. Z. Gan, 2002, "A Lumped-Parameter Mechanical Model of Human Ear for Sound Transmission", *Proceedings of the Second Joint EMBS/BMES Conference*, Houston, TX, USA 23-26 October, pp. 267-268.

Garcia Tarrago, M. J., J. Vinolas and L. Kari, 2007, "Axial Stiffness of Carbon Black Filled Rubber Bushings Frequency and Amplitude Dependence", *Kautschuk und Gummi, Kunststoffe*, Vol. 60, pp. 43-48.

Hegde, S. and G. K. Ananthasuresh, 2012, "A Spring-Mass-Lever Model, Stiffness and Inertia Maps for Single-Input, Single-Output Compliant Mechanisms", *Mechanisms and Machine Theory*, Vol. 58, pp. 101-119.

Holecek, M. and F. Moravec, 2006, "Hyperelastic Model of a Material Which Microstructure is Formed by Balls and Springs", *International Journal of Solids and Structures*, Vol. 43, pp. 7393-7406.

Iniguez-Macedo, S., R. Lostado-Lorza, R. Escribano-Garcia and M. A. Martinez-Calvo, 2019, "Finite Element Model Updating Combined with Multi-Response Optimization for Hyper-Elastic Materials Characterization" *Materials*, (Basel) 12(7):1019.

Kamaruddin, S., A. B. Chai, C. L. Lim and J. H. Ho, 2017, "Characterization of Static and Dynamic Response of Natural Rubber Bio-Composites", *Journal of Physics: Conference Series*, 908(1).

Khairi, N., 1993, *Rubber as an Engineering Material: Guideline for Users*, Hanser Publishers Inc.

Khajehsaeid, H., J. Arghavani and R. Naghdabadi, 2013, "A Hyperelastic Constitutive Model for Rubber-Like Materials", *European Journal of Mechanics A/Solids*, Vol. 38, pp. 144-151.

Kim, K., J. Lee, J. Ju and D. M. Kim, 2014, "Compliant Cellular Materials with Compliant Porous Structures: A Mechanism Based Materials Design", *International Journal of Solids and Structures*, Vol. 51, pp. 3889-3903.

Lawrence, E. N., 1974, *Mechanical Properties of Polymers and Composites, Volume 2*, Marcel Dekker.

Lewandowski, R. and B. Chorazyczewski, 2010, "Identification of the Parameters of the Kelvin-Voigt and the Maxwell Fractional Models, Used to Modeling of Viscoelastic Dampers", *Computers and Structures*, Vol. 88, pp. 1-17.

Liao, Z., M. Hossain, X. Yao, 2020, "Ecoflex Polymer of Different Shore Hardnesses: Experimental Investigations and Constitutive Modelling", *Mechanics of Materials*, Vol. 144(9), p. 103366.

Mansouri, M. R. and H. Darijani, 2014, "Constitutive Modeling of Isotropic Hyperelastic Materials in an Exponential Framework Using a Self-Contained Approach", *International Journal of Solids and Structures*, Vol. 51, pp. 4316-4326.

McCrum, N. G., C. P. Buckley, C. B. Bucknall, 1988, *Principles of Polymer Engineering*, Oxford University Press.

Muliana, A., K. R. Rajagopal, D. Tscharnuter and G. Pinter, 2016, "A Nonlinear Viscoelastic Constitutive Model for Polymeric Solids Based on Multiple Natural Configuration Theory", *International Journal of Solids and Structures*, Vol. 100-101, pp. 95-110.

Martinez, J. M., A. Boukamel, S. Meo and S. Lejeunes, 2011, "Statistical Approach for a Hyper-Visco-Plastic Model for Filled Rubber: Experimental Characterization and Numerical Modeling", *European Journal of Mechanics – A / Solids*, Vol. 30, pp. 1028-1039.

Natsupakpong, S. and M. C. Cavusoglu, 2010, "Determination of Elasticity Parameters in Lumped Element (Mass-Spring) Models of Deformable Objects", *Graphical Models*, Vol. 72, pp. 61-73.

Noborio, H. and T. Oohara, 2009, "On the Repeatability of Octree-Based Rheology Mass-Spring-Damper Model", *International Workshop on Haptic Audio Visual Environments and Games*, Lecco, Italy 7-8 November, pp. 93-98.

Oman, S. and M. Nagode, 2014, "Observation of the Relation Between Uniaxial Creep and Stress Relaxation of Filled Rubber", *Materials and Design*, Vol. 60, pp. 451-457.

Osterlof, R., H. Wentzel, L. Kari, N. Diercks and D. Wollscheid, 2014, "Constitutive Modeling of the Amplitude and Frequency Dependency of Filled Elastomers Utilizing a Modified Boundary Surface Model", *International Journal of Solids and Structures*, Vol. 51, pp. 3431-3438.

Ozcan, M. U., C. Yılmaz, F. O. Sonmez, 2020, "Visco-Hyperelastic Material Modeling Using Nested Linkage Mechanisms", *International Journal of Solids and Structures*, Vol. 193-194, pp. 393-404.

Pellicer, M. and J. S. Morales, 2004, "Analysis of a Viscoelastic Spring-Mass Model", *Journal of Mathematical Analysis and Applications*, Vol. 294, pp. 687-698.

Ren, Y., S. Zhao, Q. Yao, Q. Li, X. Zhang and L. Zhang, 2015, "Effects of Plasticizers on the Strain-Induced Crystallization and Mechanical Properties of Natural Rubber and Synthetic Polyisoprene", *Royal Society of Chemistry*, Vol. 5, pp. 11317-11324.

Renaud, F., J. L. Dion, G. Chevallier, I. Tawfiq and R. Lemaire, 2011, "A New Identification Method of Viscoelastic Behavior: Application to the Generalized Maxwell Model", *Mechanical Systems and Signal Processing*, Vol. 25, pp. 991-1010.

Rendek, M. and A. Lion, 2010, "Amplitude Dependence of Filler-Reinforced Rubber: Experiments, Constitutive Modeling and FEM-Implementation", *International Journal of Solids and Structures*, Vol. 47, pp. 2918-2936.

Rey, T., G. Chagnon, D. Favier and J. B. L. Cam, 2014, "Hyperelasticity with Rate-Independent Microsphere Hysteresis Model for Rubberlike Materials", *Computational Materials Science*, Vol. 90, pp. 89-98.

San-Vicente, G., I. Aguinaga and J. T. Celigueta, 2012, "Cubical Mass Spring Model Design Based on a Tensile Deformation Test and Nonlinear Material Model", *IEEE Transactions on Visualization and Computer Graphics*, Vol. 18, pp. 228-241.

Saitoh, M., 2012, "A One Dimensional Lumped Parameter Model Representing Impedance Functions in General Structural Systems with Proportional Damping", *International Journal of Numerical Methods in Engineering*, Vol. 90, pp. 353-368.

Tam, N. Q., T. Violaine and F. Christophe, 2015, "The Modeling of Nonlinear Rheological Behavior and Mullin's Effect in High Damping Rubber", *International Journal of Solids and Structures*, Vol. 75-76, pp. 235-246.

Vandenbroucke, A., H. Laurent, N. A. Hocine and G. Rio, 2010, "A Hyperelasto-Visco-Hysteresis Model for an Elastomeric Behavior: Experimental and Numerical Investigations", *Computational Materials Science*, Vol. 48, pp. 495-503.

Vieira, A. C., R. M. Guedes and V. Tita, 2014, "Constitutive Modeling of Biodegradable Polymers: Hydrolytic Degradation and Time-Dependent Behavior", *International Journal of Solids and Structures*, Vol. 51, pp. 1164-1174.

Wang, L. and Y. Han, 2013, "Compressive Relaxation of the Stress and Resistance for Carbon Nanotube Filled Silicone Rubber Composite", *Composites: Part A*, Vol. 47, pp. 63-71.

Wollscheid, D. and A. Lion, 2013, "Predeformation and Frequency-Dependent Material Behavior of Filler-Reinforced Rubber: Experiments, Constitutive Modeling and Parameter Identification", *International Journal of Solids and Structures*, Vol. 50, pp. 1217-1225.

Xu, X., S. Gao, Z. Ou and H. Ye, 2018, "Mechanical Behavior of Liquid Nitrile Rubber-Modified Epoxy Resin Under Static and Dynamic Loadings: Experimental and Constitutive Analysis", *Materials (Basel)*, Vol. 11(9):1565.

Yilmaz, C., G. M. Hulbert and N. Kikuchi, 2007, "Phononic Band Gaps Induced by Inertial Amplification in Periodic Media", *Physical Review B*, Vol. 76:054309.

Yilmaz, C. and G. M. Hulbert, 2010, "Theory of Phononic Gaps Induced by Inertial Amplification in Finite Structures", *Physics Letters A*, Vol. 374, pp. 3576-3584.

Yuksel, O. and C. Yilmaz, 2015, "Shape Optimization of Phononic Band Gap Structures Incorporating Inertial Amplification Mechanisms", *Journal of Sound and Vibration*, Vol. 355, pp. 232-245.

Zhang, H., T. Lu, Q. Zhang, Y. Zhou, H. Zhu, J. Harms, X. Yang, M. Wan and M. F. Insana, 2020, “Solutions to Ramp-Hold Dynamic Oscillation Indentation Tests for Assessing the Viscoelasticity of Hydrogel by Kelvin-Voigt Fractional Derivative Modeling”, *Mechanics of Materials*, Vol. 148:103431.

Zoffoli, L., E. Corti, D. Moro, F. Ponti and V. Ravaglioli, 2017, “Zero-Dimensional Model for Dynamic Behavior of Engineered Rubber in Automotive Applications”, *72nd Conference of the Italian Thermal Machines Engineering Association*, Lecce, Italy 6-8 September, pp. 939-946.

Zrida, M., H. Laurent, G. Rio, S. Pimbert, V. Grolleau, N. Masmoudi and C. Bradai, 2009, “Experimental and Numerical Study of Polypropylene Behavior Using an Hyper-Visco-Hysteresis Constitutive Law”, *Computational Materials Science*, Vol. 45, pp. 516-527.

APPENDIX A: RUBBERS, POLYMERS AND ELASTOMERS

A.1. General Information

When nonlinear viscoelastic materials are considered, rubber is the most prominent one. Hevea Brasiliensis (rubber tree) is the source where rubber material is harvested. Crude rubber is harvested as a milky extract from rubber tree. This extract is also known as natural latex. After harvesting, the product is dried and coagulated for obtaining solid crude rubber. Natural rubber is mainly replaced by synthetic products in modern world via processing low-molecular weight monomers to create polymers. Polymers are long-chain molecules. Either natural or synthetic, crude rubbers are not good for direct usage as an end product. The material properties need to be improved by additives and heat treatment. In the modern world, crude rubber and elastomers are separated. Elastomers are basically vulcanized rubbers. Vulcanization is the heat treatment process for tying cross-linked chain molecules to each other and blocks the excessive movement of these links. Elastomers have the ability to completely regain their shape after deforming under stress. This is the essence of elastic materials. The word elastomer is generated by combining two different words, elastic and polymer. Polymers are either found in nature as biopolymers or man made after polymerization of monomers. There are two types of polymerization process, addition polymerization and condensation polymerization.

Addition polymerization is basically addition of different monomer molecules together. As an example, one of the double bonds of carbon atoms in unsaturated hydrocarbon ethylene molecule open and unite other nearby ethylene molecules to form a long chain of saturated polymer.

Condensation polymerization is a chemical reaction between molecules, and during the process, some small molecules are removed. As an example, combining diamines and dicarboxylic acids and removing water, high-molecular-weight polymer, nylon, is produced.

Considering the solid deformation properties, polymers are separated to four different types. Plastomers which are thermoplastics, elastomers which are vulcanized rubber,

thermoplastic elastomers and thermosets which are duromers are those four different polymer types. Entangled molecules of plastomers stay together by the intermolecular forces. They deform and stay as deformed till the applied force is released. This occurs due to the loose structure (Figure A.1a) of the macromolecules which can slip on each other when force is applied.

Elastomers are considered as elastic materials which have the ability to completely recover to its original shape after removing the applied force. This characteristic is a result of cross-links between the polymer chains in its macromolecules. (Figure A.1b) Cross-links between the polymer chains do not allow the chain molecules to move freely or slip on another easily. As a result of this, accumulated contrary stress provides the necessary force to complete recovery of the material shape.

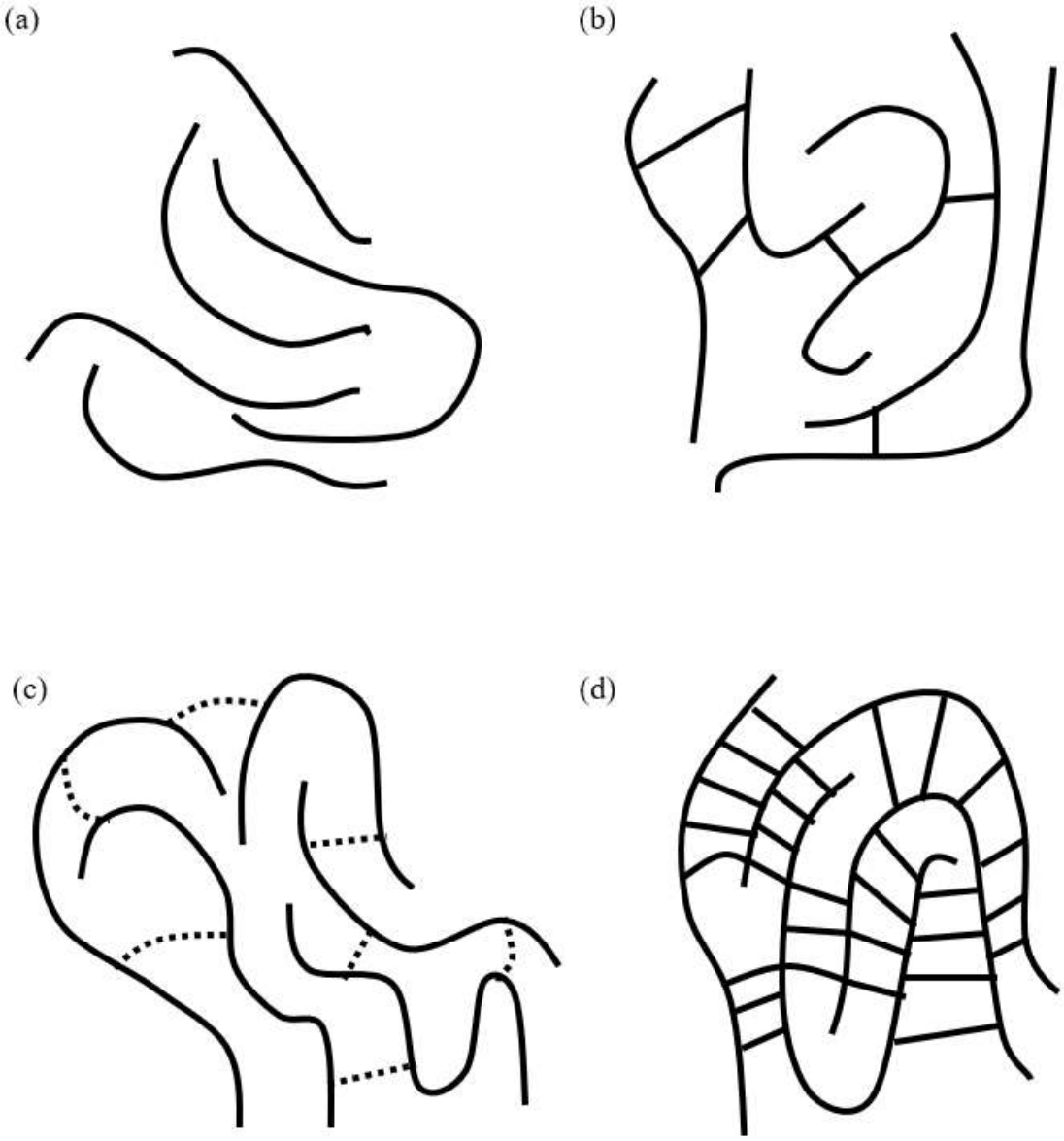


Figure A.1. Chain molecules of Different Polymers. (a) plastomers, (b) elastomers, (c) thermoplastic elastomers, and (d) thermosets (duromers).

During vulcanization process, chain molecules and broadly spread cross-links are combined. Soft crude material gains significant elastic recovery characteristic during the creation of the cross-links. For reprocessing the rubber, these created cross-links are needed to be broken. This process is called as devulcanization and the product is, reclaimed rubber.

Thermoplastic elastomers (Figure A.1c) exhibit elastic characteristics between room temperature and around 70°C. There are secondary intermolecular hydrogen bonds in thermoplastics which form additional cross-links. These additional cross-links vanish when

heated and appear when cooled. The elastic characteristics are gained again after re-appearing occurs.

Thermosets or duromers are created by a chemical process when they are heated. During this chemical process, space network molecules are created. This is similar to vulcanization process, but thermosets have tighter cross-links compared to elastomers (Figure A.1d). Thermosets are not possible to re-product since the cross-links cannot be broken by any chemical or thermal process.

Crude rubbers are the main components for creating elastomeric products. Crude rubbers are noncross-linked polymers. Creating more useful elastomeric products needs additional processes such as, compounding, forming, vulcanizing, and finishing.

Compounding is the first step for softening and mixing the crude rubber with special ingredients. Amount of those ingredients are measured and added by parts per weight. The amounts are quantified by considering the crude rubber amount in the mixture as 100 parts per weight. An example formula can be given as;

- 100 parts per weight, Crude rubber
- 50 parts per weight, Filler
- 5 parts per weight, Softener
- 5 parts per weight, Zinc Oxide
- 2 parts per weight, Sulphur
- 1 part per weight, Antioxidant
- 1 part per weight, Stearic Acid
- 1 part per weight, Accelerator

The specific functions of some ingredients are;

- Vulcanizing and curing agents, activators, and accelerators
- Plasticizers or softeners such as processing aids, extenders, and special plasticizers
- Fillers such as carbon blacks and nonblack fillers,
- Antidegradant age resistors such as protective waxes, antiozonants and antioxidants
- Special parts such as flame retardants, odorants, antistatic, blowing and coloring

Once compounding process is completed, vulcanization is considered. This process gives the elastic characteristics to the mixture. Vulcanization creates cross-links between the macromolecules with the aid of vulcanizing and curing agents.

Vulcanizing agents are used for improving the cross-link creation between polymer chains when heat is applied. For this purpose, double bonds are needed in the agent molecule, which are going to open during the process and combine nearby individual molecules together to form a chain molecule. Sulphur is one of the mostly preferred vulcanizing agents. The vulcanizing process with sulphur lasts long hours without using the accelerator agents. Accelerator agents decrease the process time from hours to minutes and even to seconds. Magnesia, litharge, and lime are the mostly used agents for vulcanization process accelerators. Stearic acid and zinc oxide is used as activators for increasing the effect of accelerators.

Plasticizers are used for modifying vulcanization process, easing the manufacturing operations, or making the product cost effective. Also, there are some costly plasticizers (ethers and esters) are used for improving the low temperature characteristics of elastomers.

Carbon blacks are created by the inadequate petroleum or natural gas combustion. The nonblack agents are silicates, calcium carbonates, clays, and fumes silicas. These fillers are used for improving the mechanical properties of the material for the final product. Abrasion resistance, tear resistance and tensile strength is increased via using fillers.

Age resistors are used for eliminating time dependent degradation and extending the operation life. Age resistors protect the elastomers from humidity, heat, sunlight, ozone, and oxygen. Antioxidants are used for protection from heat and oxidation and retards surface crack initiation when elastomers exposed to ozone. Anti-crack agents are used for crack protection under cyclic loading. There are also anti-radiation and anti-hydrolysis agents, as well.

Coloring pigments are divided into organic and inorganic groups. Generally inorganic pigments usually do not present bright colors, but they are resistive to heat and light. On the other hand, organic pigments are very effective and usually they result bright colors even small amounts are used. Organic coloring pigments are not sensitive to heat, light, and solvents.

Blowing agents are used for creating porous and sponge type product. Flame retardants such as, chlorinated hydrocarbons, antimony compounds and phosphates are used for reducing flammability. Odorants are used for changing and creating scents of the products. The most common odor is Vanillin among the other odorants. Antistatic agents such as, amides and esters are used for repelling dirt and dust for eliminating static electric discharge during usage of the product. (Khairi, 1993)

If a constant force is applied on elastomers, the strain will increase in time and will be constant after some point. This happens due to the molecular rearrangement of the material. In elastomers, if the applied force is removed after short time rather than keeping a prolonged time, the molecules tend to turn back to their original positions. According to the type of the elastomer, either the overall strain vanishes, and full recovery occurs, or it cannot fully recover and some residual strain stays. This behaviour of elastomers is known as viscoelastic creep. The term viscoelastic comes from the fact that, such materials recover since they are elastic (fully or partially), and they creep as well since they are viscous. Temperature, time, and stress are the main variables that change the characteristics of viscoelasticity of polymers and elastomers. Polymers are differed from elastic solids that, molecular chains move in Brownian motion. All together snake-like motion of the molecule chains comes from the theory of the rubber elasticity. Under applied stress, molecular chains flow and the deformation of the cross-links form contrary stress. As the applied stress is removed, full

recovery occurs. If the applied stress remains, the contrary stress increases as well and after some time (steady-state) it equals to the applied stress and the creep response completes. (Lawrence, 1974)

A.2. Copyright Details

The images that emerged within the scope of this thesis work and whose copyrights were transferred to the publishing house were used in this thesis in accordance with the "valid publishing policy for the reuse of the text and graphics produced by the author" on the website of the publisher. All figures, tables and sketches are either taken from the published journal paper of the same author of this thesis (Ozcan et al., 2020) or created by the author himself.